Electronic ISSN: 1309-0267

International Journal of Engineering & Applied Sciences

IJEAS

Volume 13, Issue 4
2021

Published by Akdeniz University

Editorial Board

(The name listed below is not Alphabetical or any title scale)

Abstracting & Indexing

IJEAS provides unique **DOI** link to every paper published.

Editorial Scope

The journal presents its readers with broad coverage across some branches of engineering and science of the latest development and application of new solution algorithms, artificial intelligent techniques innovative numerical methods and/or solution techniques directed at the utilization of computational methods in solid and nano-scaled mechanics.

International Journal of Engineering & Applied Sciences (IJEAS) is an Open Access Journal

International Journal of Engineering & Applied Sciences (IJEAS) publish original contributions on the following topics:

Numerical Methods in Solid Mechanics

Nanomechanic and applications

Microelectromechanical systems (MEMS)

Vibration Problems in Engineering

Higher order elasticity (Strain gradient, couple stress, surface elasticity, nonlocal elasticity) Applied Mathematics

CONTENTS

International Journal of Engineering & Applied Sciences (IJEAS)
Vol.13, Issue 4 (2021) 126-139
http://dx.doi.org/10.24107/ijeas.1031068
Int J Eng Appl Sci 13(4) (2021) 126-139

Artificial Neural Networks Driven Data-Based Optimization Analysis to Locate Crisis Reaction Offices for Marine Transportation in Antalya

Emre Demir [a] and Caner Akar [b]*

[a] Department of Civil Engineering, Faculty of Engineering and Natural Sciences, Antalya Bilim University
[c] Construction Technologies, Vocational School, Antalya Bilim University
[*]E-mail address: caner.akar@antalya.edu.tr[b*], emredemir07@gmail.com[a]

ORCID numbers of authors:
0000-0003-0013-4482, 0000-0003-0652-8423[*]

Received date: 01.12.2021
Accepted date: 29.12.2021

Abstract

A mishap might happen at any port along Antalya's 500-kilometer shorelines, and the counter spillage group ought to be on schedule for an intercession. The aim of this study is to decide the most appropriate areas for the counter spillage group office for Antalya's tourist ports. For this reason, Tree Seeds Algorithm (TSA), Symbiotic Organisms Search (SOS), Sooty Terns Optimization Algorithm (STOA), and Weiszfeld Algorithm (WA) optimization methods are used to track down the most advantageous area. The first three procedures are almost new and forward-thinking methods. Notwithstanding, the last one is a notable calculation for taking care of organization-based enhancement issues. This research aims to accomplish an ideal area and evaluate the exhibitions of TSA, SOS, STOA, and WA. Hence, this article offers a crisis reaction office area for oil leakage safety brought about by marine mishaps in Antalya Gulf. The originality and the main contribution of the paper to the literature is as follows: 1) for the first time, the presentations of the four optimization algorithms are analyzed and inspected together, 2) the most appropriate locations for the counter spillage group office for Antalya's ports are determined for first time in the literature.

Keywords: Transportation optimization, marine mishaps, location analysis, Antalya

1. Introduction

Marine mishaps jeopardize biological equilibrium and speed up the alteration in the wildlife at the waterfront regions antagonistically. Marine accidents or mishaps are a threat to ecological balance and tourism [1–3]. Natural habitat at the coastal areas is adversely affected due to chemical pollutions occurring near ports. The chemicals affect the environment, and the depletion of species makes fishery difficult or less economical [4–7]. Accidents or mishaps at sea put human life at risk, too. Accidents or mishaps at sea put human life at risk, too. When a spillage occurs in Antalya Gulf in Turkey, it is essential to limit its effect, so the mediation should be made as fast as expected. Antalya, a city in Turkey with almost 2,000,000 individuals living in seaside areas, has many ports utilized fundamentally for the commercial and transportation industry.

Antalya has almost two million residents and millions of tourists annually in twelve seaside districts [8, 9]. Besides the residents and the tourists, Antalya's coasts are home to countless numbers of fish and other animals [10]. Therefore, a possible accident on Antalya's five-

hundred-kilometer coastline should encounter with quick intervention. Thus, the location of an anti-leakage team for a quick response is essential. The team should be close to all the ports and closer to those with higher capacity. Ultimately, finding an optimum location of the bases for a quick-response team becomes an optimization problem. Moreover, the risk of an accident is equal to the likelihood of the accident multiplied by its severity [11]. It is assumed that the risk of an accident is proportional to the port's capacity (i.e. the more ships there are, the more accidents there may be). It is also assumed that severity of an accident is proportional to the distance of the anti-leakage team. The outcome of the accident may be less severe if the intervention is made quickly and vice versa. Thus, to present the main gist of this article, a sutiable location for a counter spillage group office for Antalya's ports is required because no area has been assigned recently for this purpose.

Furthermore, the paper's originality and the main contribution to the literature can be described as follows. Firstly, in this study, finding the optimum location for an emergency response facility is processed by four optimization techniques, which are Tree Seeds Algorithm (TSA), Symbiotic Organisms Search (SOS), Sooty Terns Optimization Algorithm (STOA), and Weiszfeld Algorithm (WA). TSA, SOS, and STOA are brand new techniques for continuous optimizations, and WA is an aged but widely used technique [12–15]. Such approaches were applied to several transportation engineering problems [16–21]. However, the presentations of the four optimization algorithms are analyzed and inspected together, and their performances are compared and discussed in this paper for the first time. Secondly, for the first time in the literature for Antalya's ports, the most suitable locations for a counter spillage group office are determined. The proposed location and its spatial characteristics are also evaluated and discussed in this study.

This paper is designed as follows. Section 2 provides the optimization problem. After Section 3 offers a succinct interpretation of the methodology proposed, results and discussion are delivered in Section 4. Lastly, Section 5 deduces the article.

2. The Optimization Problem

Regional ministries fund private companies in order to deal with marine accidents. The companies appoint quick-response teams to make a quick intervention in case of a possible accident near seaports. Supposedly, the possibility and severity of an emergency on a given port are proportional to the port's capacity and distance to the emergency facility, respectively. Hence, the objective of the problem is a function of the team's distance and ports' capacity. Therefore, the objective function can be formulated as in Eq. (1).

$$Z_{objective} = \sum_{j=1}^{N_{ports}} d_j c_j \tag{1}$$

Where; N_{ports} denotes the number of ports that are in consideration, c_j represents the capacity of the port j and d_j is the Euclidian distance between the base of the anti-leakage team and the port j, $Z_{objective}$ is the objective function which is to be minimized by optimization algorithms. Antalya's thirteen touristic ports are pointed out in "Fig. 1", and the bubble sizes represent the amount of the capacities.

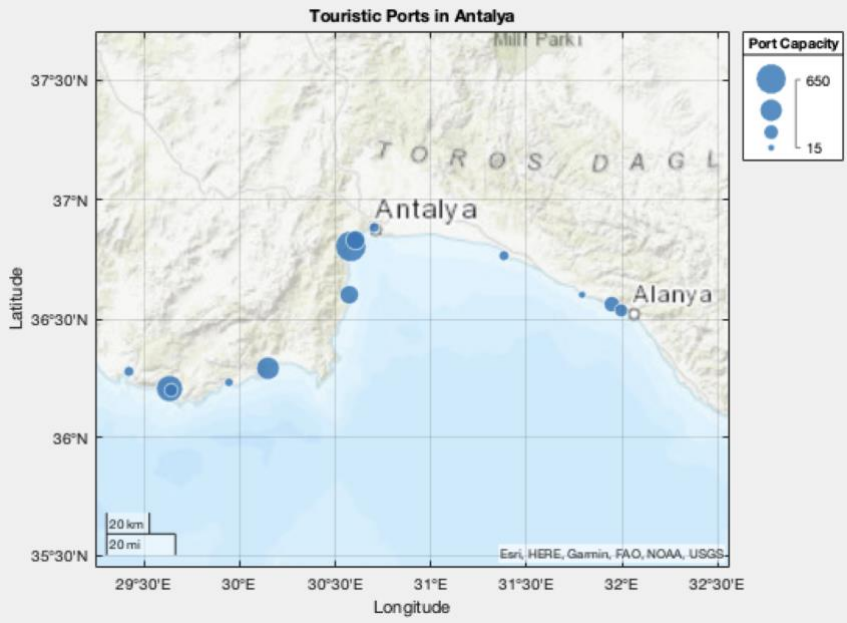

Fig. 1. Antalya's Touristic Ports

In this paper, only the touristic ports are taken into consideration. Trading ports are ignored since the shipment intensity of a trade port is not calculated according to its capacity. Like the trading ports, archeological ports are also ignored because there is no precise data about their anchoring capacity.

In this problem, the location of the marine facility can be anywhere on Antalya's coastline. Therefore, Antalya's coastline coordinates are extracted from GSHHS (A Global Self-consistent, Hierarchical, High-resolution Geography Database [22]). The coordinate data includes latitudes and longitudes of the coastline. "Fig. 2" shows the coast's GSHHS data and its approximate continuous function.

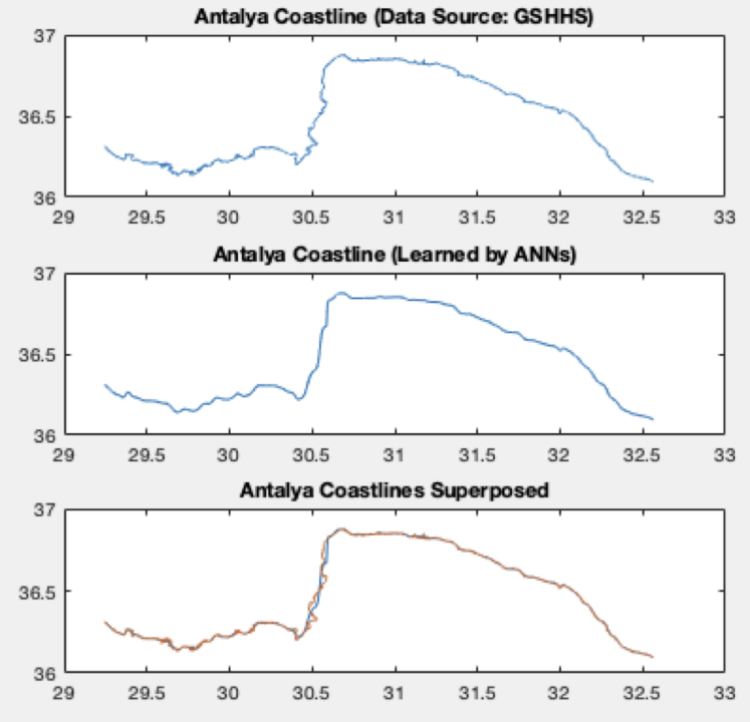

Fig. 2. Antalya's Coastline and Its Approximate Function

Artificial neural networks (ANNs) are used to get a continuous function instead of separate coordinates. Longitudes are inputs of the ANNs, and latitudes are the outputs. Supervised learning is used as one input variable and one output variable to ANNs. GSHHS data is the training data. "Fig. 3" illustrates the structure of supervised ANNs. The number of the hidden neurons is fifty, and there is a single hidden layer.

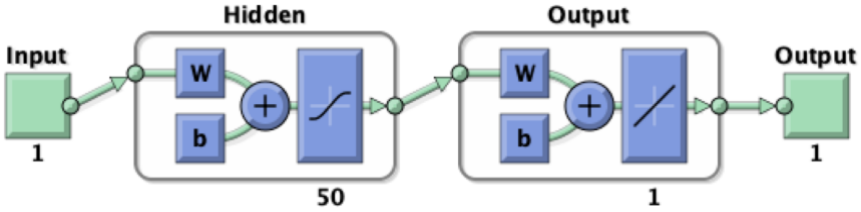

Fig. 3. Structure of the ANNs (image produced by Matlab Software)

Levenberg-Marquardt (LM) backpropagation algorithm is used as the learning algorithm of ANNs [23–27]. In the learning stage, the network's output is compared with the latitude of the training data, and ANNs adjust the weights accordingly. Training stops after reaching desired proximity. More importantly, the mean squared error of the network is 8.0848°e-04 (2.9105 seconds). It takes 182 iterations for the LM algorithm to finish the learning process. The purpose of using ANNs is to obtain a continuous function that will calculate the latitude of any longitude on Antalya's coastline. It is assumed that the facility is on the coast; therefore, a possible facility's latitude is calculated as a function of its longitude. The flowchart of the optimization problem can be seen in Fig. 4.

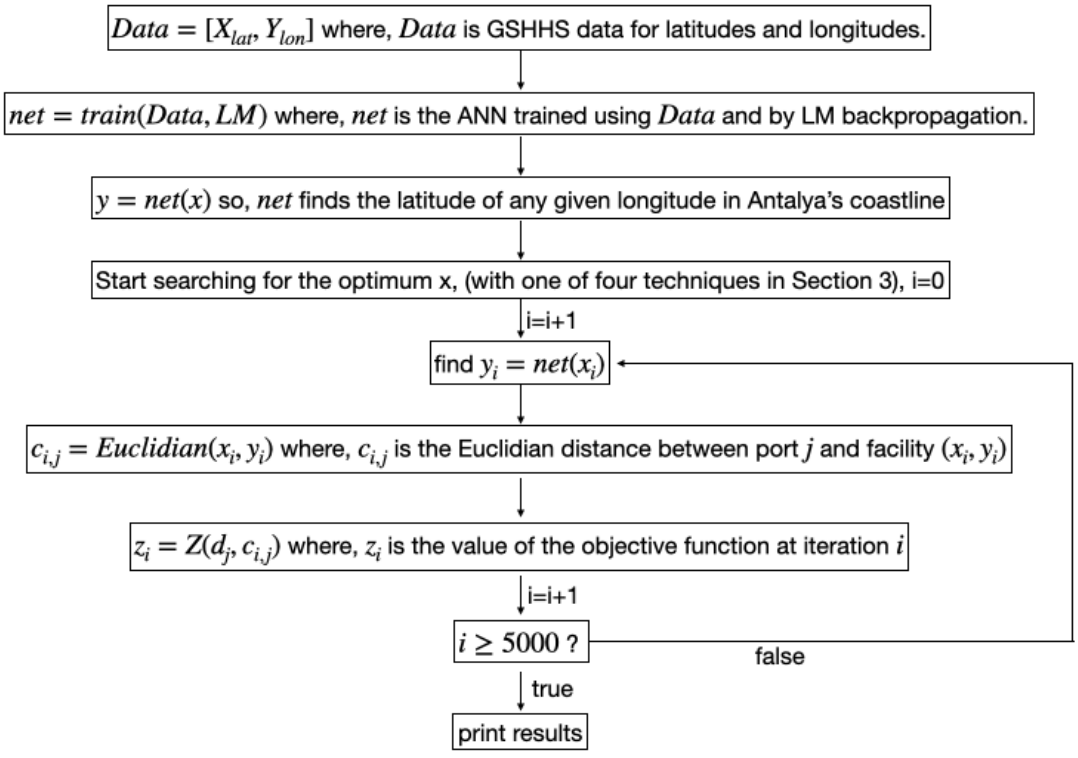

Fig. 4. Flowchart of the Optimization Problem

3. Methodology

3.1. Tree Seeds Algorithm (TSA)

Trees reproduce through their seeds in their natural environment. Seeds can reach far distances with probabilistic effects like animals and winds. In nature, only the seeds with high survival potential can grow up. In the TSA method, which was inspired by this natural event, trees represent solution vectors and seeds represent candidate solutions. The workflow of the TSA method in this paper is as follows [12]:

3.1.1 First step

Search parameters are defined in the initial step. The number of trees (N_{pop}) is chosen as five. The number of seeds is assigned randomly for each three and is between one and three. In other words, the minimum number of seeds per tree ($seed_{min}$) is one and the maximum number of seeds per tree ($seed_{max}$) is three. Initial trees and initial seeds are selected randomly. Search Tendency (ST) is a parameter adjusting the probabilistic spread rate of seeds and is chosen as 0.8. The number of maximum iterations ($maxiter$) is chosen as five thousand and it defines the maximum number of seeds that can be produced during the optimization process.
The vector of initial solutions includes a vector of initial longitudes that may be optimal for a marine facility. In this study, latitudes are dependent on the longitudes, because of the continuous function described in Section 2. Therefore, the initial solutions are produced randomly.

3.1.2 Second step

In this step, seeds are produced for each tree. The number of candidate solutions (N_{seeds}) is between $seed_{min}$ and $seed_{max}$. Each seed is produced by the formula below:

$$\begin{aligned} &if\ rand(1) < ST\ then\ S_{i,j} = T_i + \big(1 - 2 \cdot rand(1)\big) \cdot (T_{best} - S_{i,j}) \\ &if\ rand(1) \geq ST\ then\ S_{i,j} = T_i + \big(1 - 2 \cdot rand(1)\big) \cdot (T_i - S_{i,j}) \\ &i \in 1,2,\dots,N_{pop};\ j \in 1,2,3 = N_{seeds} \end{aligned} \tag{2}$$

Where $S_{i,j}$ represents seed j of tree i, T_i is tree i, T_{best} shows the best solution among the trees, $rand(1)$ is a function producing a random number between 0 and 1. As seen in Eq. (2) each seed is produced by its tree depending on the possibility of the random integer being higher or lower than ST. Kiran argues that higher values of ST lead to better local search and faster convergence, whereas lower values of ST lead to better global search.

3.1.3 Third step

At the final step, produced seeds are compared with their belonging trees. A seed, which is better than its tree and other seeds, replaces its belonging tree. Steps 2 and 3 continue until the number of produced seeds exceeds maximum iterations.

3.2. Symbiotic Organisms Search (SOS)

Similar to TSA, another brand-new and keen metaheuristic optimization algorithm is SOS. This algorithm simulates the method of interaction of animals between each other [13]. The term symbiotic stands for the relationship of animals to survive in nature. Three main relationships are inspired by the SOS algorithm. These relationships are mutualism, commensalism, and parasitism. Mutualism is when both of the interacting animals benefit from the relationship. Commensalism is when one of the animals benefits while the other is neutral and parasitism is when one animal benefits while the other animal is harmed. In the current optimization problem, SOS parameters are adapted as follows:

- Organism: candidate marine facility longitude
- Ecosystem: vector of candidate solutions (organisms)
- Survival fitness: objective function (fitness is higher when the objective function is lower)
- Mutualism: changing two of the organisms in a positive manner (their fitness value will increase)
- Commensalism: selecting two candidate solutions and positively changing one candidate solution while leaving the other candidate neutral
- Parasitism: changing a candidate solution and replacing another solution with the changed one

3.2.1 First step

Vector of initial solutions is selected randomly just like it is done in the TSA method. Initial solutions vector X consists of 5 candidates ($N_{pop} = 5$).

3.2.2 Second step (mutualism)

Two solutions are randomly selected from the pool and these solutions are updated as follows:

$$\begin{aligned} X_i^{new} &= X_i + rand(1) \cdot \left(X_{best} - round\left(1 + rand(1)\right) \cdot \frac{X_i + X_j}{2}\right) \\ X_j^{new} &= X_j + rand(1) \cdot \left(X_{best} - round\left(1 + rand(1)\right) \cdot \frac{X_i + X_j}{2}\right) \\ i, j &\in 1, 2, \dots, N_{pop} \end{aligned} \tag{3}$$

Where X_i and X_j represent randomly selected candidate solutions, X_i^{new} and X_j^{new} show updated versions of the selected solutions, X_{best} is the best solution in the ecosystem. Updated solutions replace their previous versions depending on their fitness value. This phenomenon is presented in Eq. (4,5).

$$if\ Z(X_i^{new}) < Z(X_i)\ then\ X_i = X_i^{new} \tag{4}$$

$$if\ Z(X_j^{new}) < Z(X_j)\ then\ X_j = X_j^{new} \tag{5}$$

3.2.3 Third step (commensalism)

In the commensalism phase, a randomly selected organism (with index i) is updated with another randomly selected organism (with index j). This phenomenon is represented by Eq. (6).

$$X_i^{new} = X_i + (1 - 2 \cdot rand(1)) \cdot \left(X_{best} - X_j\right) \tag{6}$$

The updated solution replaces its old version depending on their fitness power as indicated by Eq. (4).

3.2.4 Fourth step (parasitism)

A random solution (with index i) is chosen as the parasite. The parasite replaces another randomly selected solution (with index j) depending on their fitness values. This phenomenon is presented by Eq. (7).

$$if\ Z(X_i) < Z(X_i)\ then\ X_j = X_i \tag{7}$$

Steps among 2 and 4 continue until maximum iterations are reached. $maxiter$ is set to five thousand in order to get a comparison between performances of TSA, SOS, and STOA.

3.3. Sooty Terns Optimization Algorithm (STOA)

STOA is a bio-inspired optimization tool simulating migration and attacking behavior or sooty terns [14]. Sooty terns are seabirds and generally hunt as a group in nature. Seasonal movement of the birds to find locations with more prey is called migration and their hunting event is called attacking behavior. During migration, birds start from different initial locations to avoid collusion and travel through the fittest bird's direction. When sooty terns start attacking, they move in a spiral curve. The phenomenon described above is implemented to the current problem as follows:

- Sooty tern: candidate solution
- Group of sooty terns: vector of candidate solutions
- Fittest bird: solution with the lowest objective function value
- Migration and attacking behavior: updating the solution vector in order to reach the optimum solution

3.3.1 Migration behavior

$$\overrightarrow{C_{st}} = S_A \cdot \overrightarrow{P_{st}}(i) \tag{8}$$

Where, $\vec{C}_{st}$ is the position and it should not collide with another search agent, S_A is used to compute new search agents, $\vec{P}_{st}(i)$ is the candidate solution i $(i = 1,2, \dots, N_{pop})$ in the solution vector $\vec{P}_{st}$. N_{pop} is taken as 5, so the iterations start with 5 initial solutions.

$$S_A = C_f - (j \cdot C_f / Maxiter) \tag{9}$$

Where C_f adjusts S_A to avoid the collision, as j is the current iteration. Eq. (8,9) are here to avoid collusion, with Eq. (10) candidate solutions approach towards the best solution in the pool.

$$\overrightarrow{M_{st}} = 0.5 \cdot rand(1) \cdot (\overrightarrow{P_{bst}} - \overrightarrow{P_{st}}(i)) \tag{10}$$

In the formula above, $\overrightarrow{M_{st}}$ indicates different positions of the solutions, $\overrightarrow{P_{bst}}$ is the best solution in the pool.

3.3.2 Attacking behavior

Sooty terns start their hunt after taking their positions, Eq. (11) shows how the vector of solutions is updated to get better solutions during the ongoing iterations.

$$\overrightarrow{P_{st_{new}}} = \left(\overrightarrow{C_{st}} + \overrightarrow{M_{st}}\right) \cdot \sin(rand(1) \cdot 2 \cdot \pi) + \overrightarrow{P_{st_{old}}} \tag{11}$$

3.4. Weiszfeld Algorithm (WA)

In 1937, WA was first founded by a mathematician [15]. It is an old but valuable algorithm for location analysis problems. The main reason to include WA in this study is to compare the performances of TSA, SOS, and STOA with an older method like WA. The standard version of WA is adopted in this study as in Eq. (12):

$$X_{k+1} = \frac{\sum_{j=1}^{N_{ports}} \frac{w_j \cdot X_k}{d_j}}{\sum_{j=1}^{N_{ports}} \frac{w_j}{d_j}} \tag{12}$$

Where, X_k is the current value of the possible optimum longitude of the marine facility, X_{k+1} is the longitude of the facility in the next iteration, w_j is the weight (anchorage capacity) of the port j and d_j is Euclidean distance between port j and the current location of the facility (note that the latitude of the facility can be calculated by the ANN as a function of its longitude as described in Section 2). Maximum iterations are set to five thousand similar to TSA and SOS methods. WA is a successful algorithm for optimizing the task in this research, however it fails to address the spatial difficulties such as mountainous terrains because it uses the great-circle distance for the application [28].

3.5. Parameters Selection

Metaheuristic optimization techniques are known to be dependent on parameter tuning. In the TSA method, ST is a parameter between 0 and 1. Smaller values of ST parameter lead to better global search while higher values lead to better local search. In this problem ST is taken as 0.8. And the number of trees is 5 (N_{pop}=5). SOS method is not heavily dependent on the parameters selected. The number of organisms is 5 (N_{pop}=5). In the STOA method, C_f parameter is used to avoid collusion between the solutions. C_f is taken as 0.1 and the number of birds is 5 (N_{pop}=5). The parmeters are presented in "Table 1". In the WA method, no parameter has been used as described in Section 3.4.

Table 1. Selected Parameters

Method	N_{pop}	Parameter
TSA	5	ST = 0.8
SOS	5	-
STOA	5	C_f = 0.1

4. Results and Discussions

The marine facility location for the emergency problem presented in Section 2 is solved by using three optimization techniques described in Section 3. All four algorithms are run five times in order to see if the initial solutions, which are randomly selected, will impact on the results. The first algorithm, namely TSA, converged to the same optimal solution in each run

regardless of the assigned initial solution. The convergence history of the iterations in the TSA method is shown in “Fig. 5”. The x-axis of the figure is drawn on the logarithmic scale because most of the change in the best candidate solution is made at the beginning of the run.

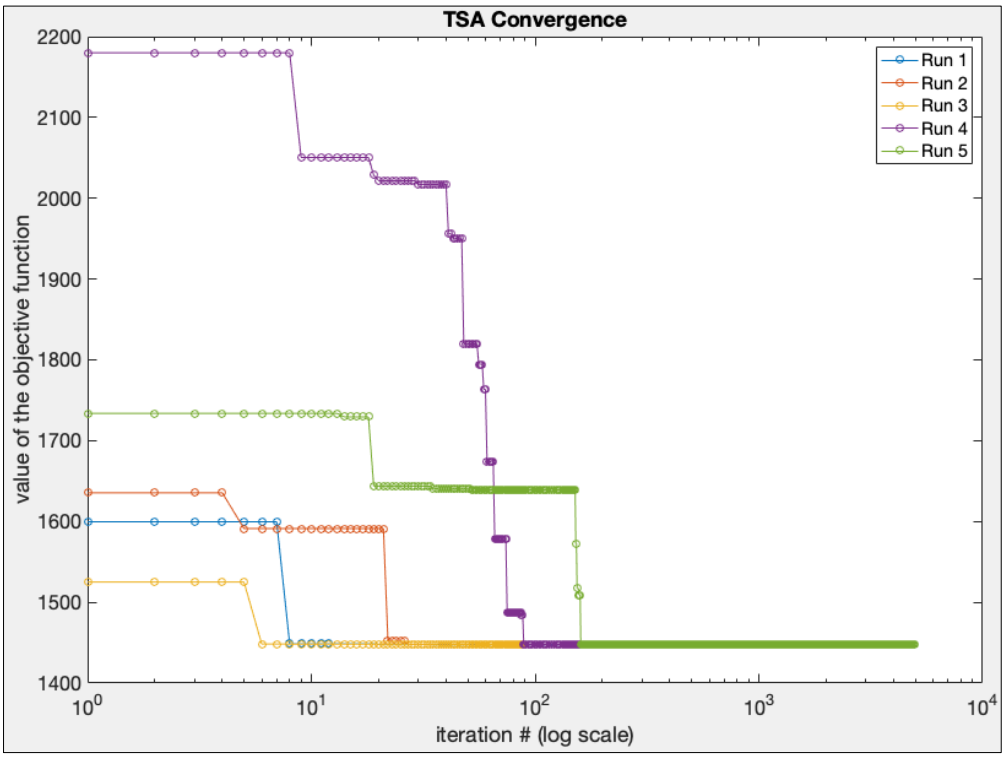

Fig. 5. Convergence of TSA Method

SOS algorithm converges to the same point regardless of the initial solutions. However, the coordinates found by SOS are different from the coordinates found by TSA and STOA methods. The convergence of the SOS algorithm is shown in “Fig. 6”, below.

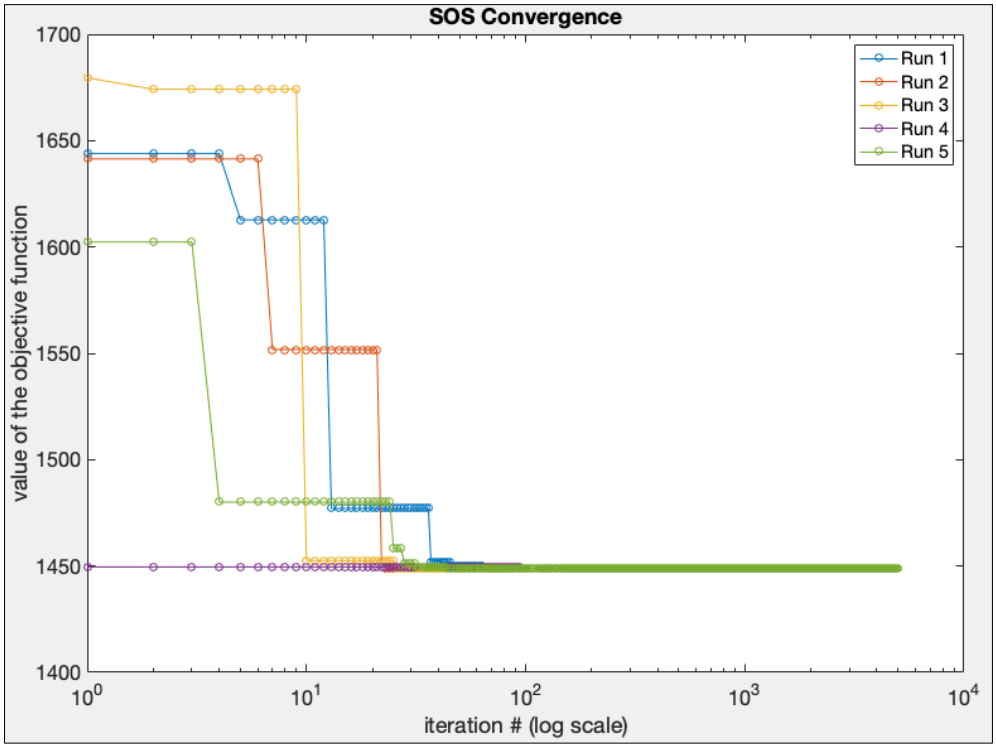

Fig. 6. Convergence of SOS Algorithm

STOA found a slightly different coordinate from the coordinate found by TSA. However, these two techniques produced similar results. Like the other four algorithms, STOA converges to the same coordinate at each of the five runs.

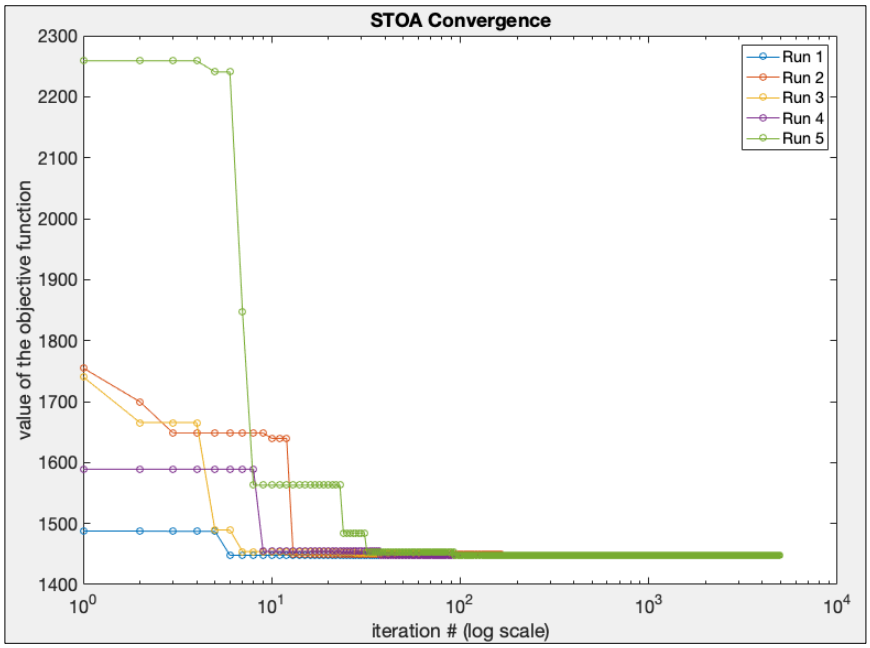

Fig.7. Convergence of STOA Method

WA seems to have lower performance in this problem because the value of the objective function is higher than the first two algorithms. The converged coordinate in WA is the same regardless of the initial solutions assigned. WA convergence is shown in "Fig. 8". In WA, the coded algorithm replaces x_{i-1} value with x_i, even if the z_i is higher than z_{i-1} (where, x_i is the longitude of the facility and z_i is the corresponding value of the objective function at iteration

i). Thus, fluctuations occur in the search history, as shown in "Fig 8.". The location found by WA, shown in "Fig 9.d", is the coordinates at the iteration with the lowest z in the search history.

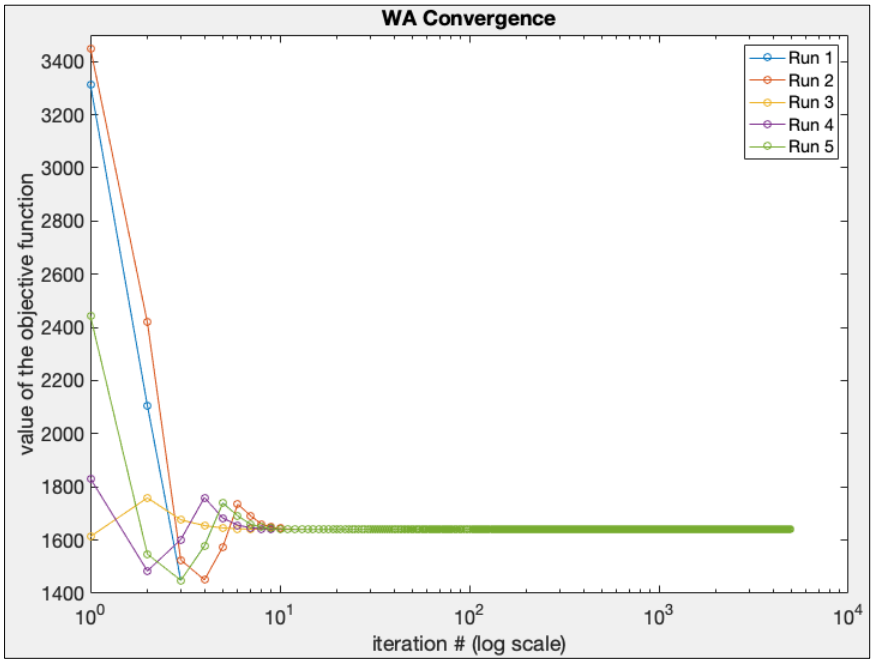

Fig. 8. Convergence of WA Method

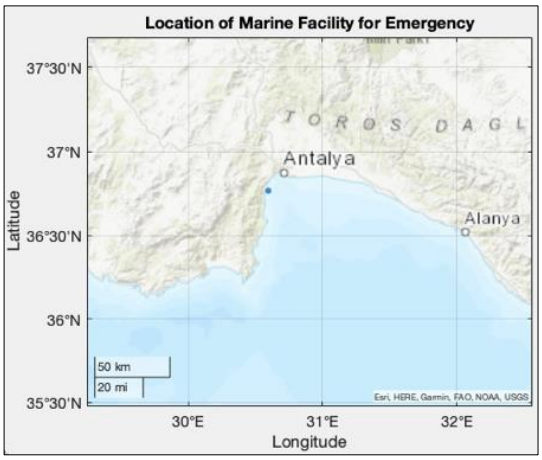

a) Optimum Location by TSA

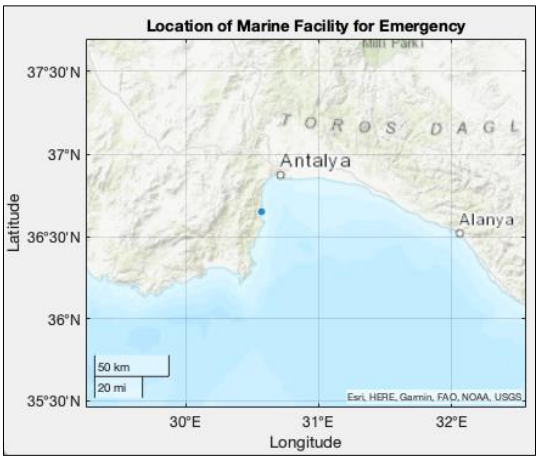

b) Optimum Location by SOS

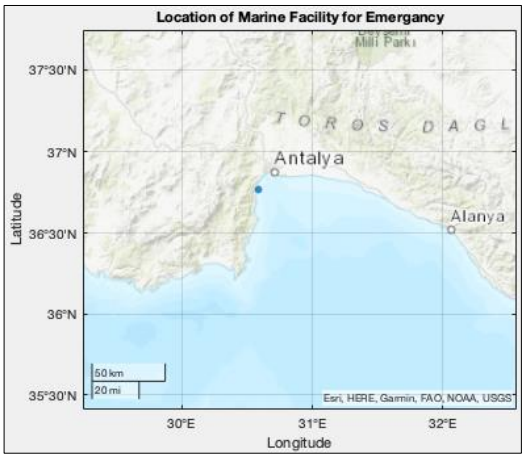

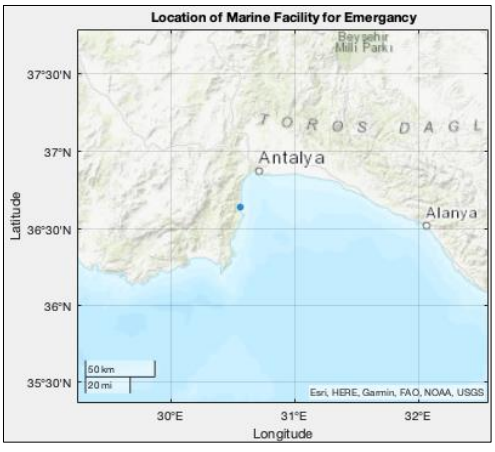

c) Optimum Location by STOA d) Optimum Location by WA

Fig. 8. Optimum Location of Single Marine Facility for Emergency

Table 2. Coordinates of the Marine Facility for Emergency

Method	Latitude	Longitude	Objective Value
TSA	36.7689°	30.5914°	1447.1
SOS	36.6559°	30.5689°	1448.9
STOA	36.7686°	30.5914°	1447.2
WA	36.6443°	30.5622°	1448.4

Table 2 presents the optimum locations found by four algorithms and the respective values of the objective functions. Please note that lower values of the objective function are desired. It is seen that TSA gives the best location among the four methods. TSA reached an objective function value of 1447.1, SOS reached an objective function value of 1448.9, STOA's objective function was 1447.2 in value and WA reached an objective function value of 1448.4. The location found by TSA (36.7689°N, 30.5914°E), which can be shown in "Fig. 7", seems to be more optimal. STOA's location (36.7686°N, 30.5914°E) is very close to TSA with a slight difference in latitudes and it can be considered inside of the error margin of the continuous function driven by ANN. The location that is found by SOS (36.6559°N, 30.5689°E) is near the location found by TSA. The difference in the latitudes between these two points is 0.0225° which is higher than the mean squared error of the continuous function of the coastline (8.0848°e-04), so the difference between TSA and SOS performances is meaningful. Therefore, performances of TSA and SOS are similar, yet TSA has slightly better performance for this problem.

WA proposed a location on the western side of the region with a higher objective value, thus WA has a lower performance. In addition, the location sits on a concave-shaped coast which signs that the algorithm is trapped at a local minimum. In WA type of optimization algorithms, the shape of the function does matter in reaching the global minimum/maximum. The interesting part of the WA result is that the algorithm proposes the same location regardless of the initial location it started from, similar to the other two algorithms.

5. Conclusions and Further Study

Human life is endangered when accidents or disasters occur at sea. When a leak occurs in Turkey's Antalya Gulf, it is critical to limit the damage, thus the mediation should happen as soon as possible. If the intervention is made quickly, the accident's consequence may be less severe, and vice versa. To summarize the significant point of this article, an appropriate location for a counter spillage group office for Antalya's ports is desired, as no area has been designated for this intent lately.

Moreover, the following is a description of the paper's uniqueness and the main contribution to the literature. To begin, four optimization strategies, TSA, SOS, STOA, and WA were used in this study to determine the best placement for an emergency response center. In addition, several other transportation engineering challenges were tackled using these four approaches. However, for the first time in this study, the presentations of the four optimization techniques were studied and scrutinized simultaneously. Later, their performances were compared and discussed. Second, the ideal locations for a counter spillage group office were selected for the

first time in the literature for Antalya's ports. In addition, this study evaluated and discussed the suggested location and its spatial characteristics.
As a result, the brand-new techniques TSA, SOS, and STOA seem to perform well for this problem. However, the standard version of WA provided a similar solution to other techniques applied in this study. Moreover, TSA and STOA determined the same location for the crisis reaction office area, while SOS and WA suggested slightly different locations. Furthermore, TSA produced the best performance among all methods performed in the article.
A similar study may be done on different regions in a country or the world. The performances of the algorithms may be different on different coastlines. The results of these studies may be compared with the actual locations of the emergency facilities or may give an idea of location determination for facilities yet to be placed. Further studies may also be done using up-to-date coastal navigation techniques instead of Euclidean distance to determine the distance between a crisis reaction office area and a port. Logically, the use of navigation techniques may have an impact on the result. Another way for a further study would be using statistical data in determining the possibility of an accident at a given port. In this study, it is assumed that this possibility is proportional to ports' capacity. The use of statistical data may lead to more specific results.

References

[1] Atherton, T., Wilks, J., Health and safety in Australian marine tourism: A social, medical and legal appraisal. *Journal of Tourism Studies*, 5(2), 2-16, 1994.

[2] Bentley, T., Page, S., Meyer, D., Chalmers, D., Laird, I., How safe is adventure tourism in New Zealand? An exploratory analysis. *Applied ergonomics*, 32(4), 327-338, 2001.

[3] Yang, E.C.L., Sharif, S.P., Khoo-Lattimore, C., Tourists' risk perception of risky destinations: The case of Sabah's eastern coast. *Tourism and Hospitality Research*, 15(3), 206-221, 2015.

[4] Carpenter, S.R., Stanley, E.H., Vander Zanden, M.J., State of the world's freshwater ecosystems: physical, chemical, and biological changes. *Annual review of Environment and Resources*, 36, 75-99, 2011.

[5] Barbier, E.B., Burgess, J.C., Folke, C., *Paradise Lost?: the ecological economics of biodiversity* (Vol. 2), Routledge, 2019.

[6] Ficke, A.D., Myrick, C.A., Hansen, L.J., Potential impacts of global climate change on freshwater fisheries. *Reviews in Fish Biology and Fisheries*, 17(4), 581-613, 2007.

[7] Lafferty, K.D., Harvell, C.D., Conrad, J.M., Friedman, C.S., Kent, M.L., Kuris, A.M., ... Saksida, S.M., Infectious diseases affect marine fisheries and aquaculture economics. *Annual review of marine science*, 7, 471-496, 2015.

[8] Akis, A., The effects of mass tourism: A case study from Manavgat (Antalya–Turkey). *Procedia-Social and Behavioral Sciences*, 19, 289-296, 2011.

[9] Ozdemir, B., Aksu, A., Ehtiyar, R., Çizel, B., Çizel, R.B., İçigen, E.T., Relationships among tourist profile, satisfaction and destination loyalty: Examining empirical evidences in Antalya region of Turkey. *Journal of Hospitality Marketing & Management*, 21(5), 506-540, 2012.

[10] de Meo, I., Miglietta, C., Mutlu, E., Deval, M.C., Balaban, C., Olguner, M.T., Ecological distribution of demersal fish species in space and time on the shelf of Antalya Gulf, Turkey. *Marine Biodiversity*, 48(4), 2105-2118, 2018.

[11] Gul, M., Ak, M.F., A comparative outline for quantifying risk ratings in occupational health and safety risk assessment. *Journal of Cleaner Production*, 196, 653-664, 2018.

[12] Kiran, M.S., TSA: Tree-seed algorithm for continuous optimization. *Expert Systems with Applications*, 42(19), 6686-6698, 2015.

[13] Cheng, M.Y., Prayogo, D., Symbiotic organisms search: a new metaheuristic optimization algorithm. *Computers & Structures*, 139, 98-112, 2014.

[14] Dhiman, G., Kaur, A., STOA: a bio-inspired based optimization algorithm for industrial engineering problems. *Engineering Applications of Artificial Intelligence*, 82, 148-174, 2019.

[15] Weiszfeld, E., Sur le point pour lequel la somme des distances de n points donnés est minimum. *Tohoku Mathematical Journal, First Series*, 43, 355-386, 1937.

[16] Aydoğdu, İ., Comparison of metaheuristics on multi objective (cost&C0 2) optimization of RC cantilever retaining walls. *Pamukkale University Journal of Engineering Sciences*, 23, 2017.

[17] Demir, E., Havalimanlarında kalkış öncesi, acil durumlarda, yardım alınabilecek en uygun lokasyonun Weber problemine uyarlanarak belirlenmesi. *Türk Coğrafya Dergisi*, 70, 81-85, 2018.

[18] Demir, E., Kockal, N.U., Iterative methodology on locating a cement plant. *Journal of Inequalities and Applications*, 2019, 1-8, 2019.

[19] Uzun, B., Civalek, O., Aydogdu, I., Optimum design of nano-scaled beam using the social spider optimization (SSO) algorithm. *Journal of Applied and Computational Mechanics*, 2019.

[20] Demir, E., Aydoğdu, İ., Transportation Path Assignment Within the Airports in Turkey. In *International Conference on Harmony Search Algorithm*, Springer, Singapore, pp 207-217, 2020

[21] Demir, E., Trafik Verilerine Göre Afetlerde Bölgesel Hizmet Verebilecek İdeal Havalimanı Önerileri. *Doğal Afetler ve Çevre Dergisi*, 7, 101-109, 2021.

[22] Wessel, P. and Smith, W. H., A global, self-consistent, hierarchical, high-resolution shoreline database. *Journal of Geophysical Research: Solid Earth*, *101*(B4), 8741-8743, 1996.

[23] Moré, J.J., The Levenberg-Marquardt algorithm: implementation and theory. In *Numerical analysis* (pp. 105-116). Springer, Berlin, 1978.

[24] Ranganathan, A., The levenberg-marquardt algorithm. *Tutoral on LM algorithm*, 11(1), 101-110, 2004.

[25] Marquardt, D., An Algorithm for Least-Squares Estimation of Nonlinear Parameters, *SIAM Journal on Applied Mathematics*, 2, 431-441, 1963.

[26] Hagan, M.T., Menhaj, M.B., Training feedforward networks with the Marquardt algorithm. *IEEE transactions on Neural Networks*, 5(6), 989-993, 1994.

[27] Hagan, M.T., Demuth, H.B., Beale, M.H., *Neural Network Design*, PWS Publishing, 1996.

[28] King, T., Soltys, M., Minimum Path Star Topology Algorithms for Weighted Regions and Obstacles. *arXiv preprint arXiv:2109.06944*, 2021.

International Journal of Engineering & Applied Sciences (IJEAS)
Vol.13, Issue 4 (2021) 140-154
http://dx.doi.org/10.24107/ijeas.1033802
Int J Eng Appl Sci 13(4) (2021) 140-154

Dynamic Loads and Different Soil Characteristics Examination on Optimum Design of Cantilever Retaining Walls Utilizing Harmony Search Algorithm

Esra Uray [a], Serdar Çarbaş [a,b]*

[a] KTO Karatay University, Konya, Türkiye
[b] Karamanoglu Mehmetbey University, Karaman, Türkiye
E-mail address: esra.uray@karatay.edu.tr[a*], scarbas@kmu.edu.tr[b]

ORCID numbers of authors:
0000-0002-1121-2880[a], 0000-0002-3612-0640[b]

Received date: 07.12.2021
Accepted date: 29.12.2021

Abstract

Optimum the cantilever retaining wall design for different soils and dynamic earthquake effects is presented here. In the investigation of optimum wall design-based metaheuristic, the harmony search algorithm was considered for different design cases which include five soil and two earthquake characteristics. Earthquake characteristics of mild and severe were obtained regarding two locations which was selected from Turkey Earthquake Risk Map. For selected two locations and local soil classes, map spectral acceleration coefficients were utilized defined in Turkish Building Earthquake Code-2018. Sliding, overturning, and bearing capacity safety factors were taken as design constraints for checking stability criteria of the cantilever retaining wall which is given in Turkish Building Earthquake Code-2018. Since the cost-based wall weight of the optimization problem was taken as the objective function, obtained optimum wall dimensions which are discrete design variables were compared in terms of different design cases. It is seen that the wall dimensions increase in order to meet the design criteria in case of the earthquake load increases when the obtained optimum design by the optimization analyzes are examined. Another result obtained for the same earthquake zone is that the wall dimensions and therefore the cost mostly increase in weak quality soils.

Keywords: Cantilever retaining wall optimum design; Seismic design; Harmony search algorithm; Turkish Building Earthquake Code-2018; TBEC-18

1. Introduction

Retaining structures which is satisfied the stability between two different soil levels have a widespread application in geotechnical engineering, especially in safe transportation on highways or railways and construction in deep excavations as shoring. In the design of the cantilever retaining wall, which is one of the retaining structures, parameters like soil properties, groundwater condition, occurred lateral loads with the effect of static and dynamic, soil stratification, construction time, building usage purpose, and so on should be considered. In traditional cantilever wall design that stability criteria like safety factors of sliding, overturning, bearing capacity, etc. are calculated according to pre-dimensions of the wall, until suggested safety factors in literature are satisfied stability analyses continue [1]. Because conducting design by considering many parameters and design criteria like the above mentioned is challenging, the design of the retaining wall turns into a complex engineering design problem. Instead of traditional design based on run-error method, which is time-consuming and

economical solution is not guaranteed, algorithm-based methods which enable to obtain the optimum solution of the retaining wall in a short time are widely used today in the solution of complex engineering design problems.

Another criterion is whether economic and environmentally friendly design is obtained optimum wall designs among vast combinations cluster formed by wall dimensions. The construction of the minimum weight retaining wall with optimum dimensions not only causes less cost but also provides less carbon dioxide emissions due to the required fewer materials. In the study conducted by Uray et.al. [2], a pre-dimension guide of cantilever retaining wall which gives safe and optimum designs was presented with harmony search optimization algorithm based.

Optimum designs of cantilever retaining walls have been acquired by many researchers utilizing metaheuristic optimization algorithms inspired by nature [3–10]. The dynamic load effect in cantilever retaining wall design is a situation that should be considered for designs to be made in earthquake zones. In the design of retaining walls, many studies have been conducted in which the design criteria specified in the Turkish Building Earthquake Code-2018 [11] were taken into account for the earthquake effect [12–15] and stability verifications for control the design criteria by considering the retaining wall-soil interaction in the earthquake effect are given in these studies. It is possible to meet studies in the literature that present optimum design of retaining walls by considering dynamic earthquake loads [16–21]. Harmony search optimization algorithm is an alternative manner obtaining optimum designs of retaining walls as it is seen from to an extensive literature review about reinforced concrete structural design optimization was given in the study conducted by Afzal et.al. [22]. In the study by Kalyoncuoğlu [23], that the acceleration records measured in different soil types subject to the same earthquake load were examined, having a different dynamic reaction considering each soil type within itself has been reported. For this reason, this study is aimed to investigate the effect of different soil types on the optimum structure design in regions with different earthquake effects.

In this study, the optimum design of the cantilever retaining wall for two different earthquake zones by regarding map spectral acceleration coefficients, S_S (for 0.25 and 1.50) and five local soil classes (ZA, ZB, ZC, ZD and ZE) selected from the Turkey Earthquake Hazard Map (TERM) [24] was investigated utilizing the harmony search algorithm presented by Geem et. al. [25]. In order to obtain optimum wall designs that ensure the stability of the cantilever retaining wall, the design criteria specified in the Turkish Building Earthquake Code-2018 (TBEC-18) [11] were taken into account. Obtained optimum designs of cantilever retaining walls for the different cases have been evaluated in terms of soil properties and earthquake effects by considering the cost.

2. Design of Cantilever Retaining Wall under Static and Dynamics Loads

2.1. Turkish Building Earthquake Code-2018

In cantilever retaining wall design, stability criteria like sliding and overturning of the wall, and carrying loads transfers from to wall to the soil through wall foundation should be satisfied under the effects of static and dynamic loads. While the static effect is occurred by lateral soil loads, surcharge loads, and so on, earthquakes cause dynamic loads owing to soil-structure interaction (Fig.1). For safe design, the safety factors of sliding, overturning, and bearing

capacity obtained according to the loads that the wall is exposed to should be greater than the safety factor accepted in the literature [1]. In this study, the investigation of the optimum cantilever retaining wall (CRW) design is performed by considering the Turkish Building Earthquake Code-2018 (TBEC-18) [11].

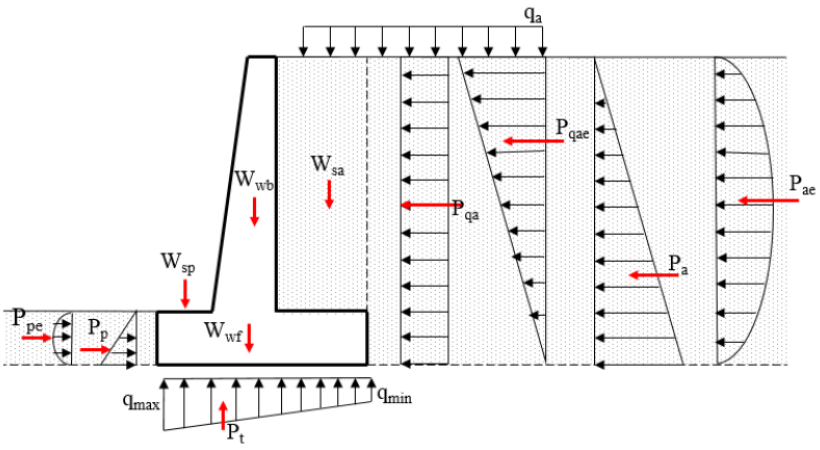

Fig.1. Acting static and dynamic loads on the cantilever retaining wall [14]

Since dynamic loads due to earthquake effect are transmitted to the wall through the soil, soil characteristics and location of the site where construct the wall are important determining of dynamic effects. The earthquake effect is affected by the horizontal (k_h) and vertical (k_v) acceleration coefficients on the wall (Eq.1).

$$k_h = \frac{0.4S_{DS}}{r} \qquad k_v = 0.5k_h \tag{1}$$

Here, while S_{DS} is defined as design spectral response acceleration at short periods, r is a coefficient based on the type of the wall and allowable displacement. In the optimization analyses, the r coefficient was taken as 1.5 from TBDY-2018 for the retaining structure, which was designed taking into account the allowable displacement after the earthquake, so as not to damage the structural functions.

Total soil pressure resultant which is included static and dynamic loads acting on the wall is calculated by using Eq. 2.

$$P_t = K(1 \mp k_v)(\frac{1}{2}\gamma^* H^2 + qH) + P_{water} + \Delta P_{water} \tag{2}$$

Here, K is the total (static+dynamic) soil pressure coefficient which is included active (K_a) or passive (K_p) cases, q is the surcharge load, H is the wall height, γ^* is the typical unit weight, P_{water} and ΔP_{water} show the resultant static and dynamic water pressures. K_a and K_p coefficients are calculated with the formulations given in TBEC-18.

The sliding safety factor of CRW under the effect of static loading is determined by using Eq.3. Here, H_s is the stem height of the wall, D_b is the wall foundation thickness, P_{as} is the active horizontal soil force in case of static loading, P_{ps} is the passive soil force along with the foundation depth, B is the wall foundation width.

$$F_{ss} = \frac{(\Sigma V \tan(2/3\phi_t) + 2/3 c_t B + P_{ps})}{P_{ash}}$$
$$P_{as} = K_a \left[q(H_s + D_b) + 0.5\gamma_d (H_s + D_b)^2 \right] \quad P_{ash} = P_{as}\cos\beta \quad P_{asv} = P_{as}\sin\beta \tag{3}$$
$$P_{ps} = 0.5 K_p \gamma_d D_b{}^2 + 2c_d \sqrt{K_p} D_b \qquad \Sigma V = W_{wb} + W_{wf} + W_{sa} + W_{sp} + P_{asv}$$

According to TBEC-18 the design horizontal force (V_{th}) acting on the foundation base should be less than the sum of the design frictional resistance (R_{th}) and the design passive resistance (R_{pt}) weighted by 0.3, in order to ensure the sliding safety factor of CRW under the effect of dynamic earthquake load (Eq.4).

$$V_{th} \le R_{th} + 0.3R_{pt} \qquad V_{th} = P_{ash} + \Delta P_{aeh} + \sum V k_h$$
$$\Delta P_{ae} = P_t - P_{as} \quad \Delta P_{aeh} = \Delta P_{ae}\cos\beta \quad \Delta P_{aev} = \Delta P_{ae}\sin\beta$$
$$P_t = K(1 \pm k_v)\left[\frac{1}{2}\gamma^* H^2 + qH \right] + P_{su} + \Delta P_{su} \quad R_{th} = \frac{P_{tv}\tan\delta}{\gamma_{Rh}}_{(drained)} \tag{4}$$
$$R_{th} = \frac{A_c c_u}{\gamma_{Rh}}_{(undrained\ cohesionless)} \qquad R_{pt} = \frac{R_{pk}}{\gamma_{Rp}} \qquad R_{pk} = K_p(1-k_v)(0.5\gamma D^2)$$

The overturning safety factor used for static loading is given by Eq.5.

$$F_{ds} = \frac{\Sigma M_r}{\Sigma M_o} \quad \Sigma M_r = \Sigma W_i x_i + P_{asv} B \quad \Sigma M_o = 0.5 K_a \left[q(H+D)^2 \cos\beta + \gamma_d (H+D)^3 / 3 \right] \tag{5}$$

Verification of overturning of cantilever retaining wall under dynamic effect is done by Eq.6.

$$\gamma_{Rdev} = \frac{R_{dev}}{E_{dev}} \ge 1.3 \tag{6}$$

Here, R_{dev} is the sum of the moments resisting overturning and E_{dev} is the sum of the moments trying to overturn.

In case of static loading, in the determination of bearing capacity, the maximum stress (q_{max}) on the foundation soil must be less than the allowable safe foundation soil bearing capacity (q_a) and the minimum stress (q_{min}) must be greater than zero (Eq.7)

$$q_{\max} \le q_a \quad q_a = \frac{q_u}{3} \quad q_{\min} \ge 0 \quad q_{\substack{\max \\ \min}} = \frac{\Sigma V}{B}\left(1 \pm \frac{6e}{B}\right) \quad e = \frac{B}{2} - \frac{\Sigma M_r - \Sigma M_o}{\Sigma V} \tag{7}$$

The ultimate soil bearing capacity, q_a, is obtained by dividing the calculated foundation soil bearing capacity (q_u) by a certain safety factor [1]. The foundation soil bearing capacity (q_u) can be determined using the overall bearing capacity proposed by Meyerhof [26]. In case of loading involving earthquake effect, the bearing capacity verification should meet the criteria given in Eq.8.

$$q_o \leq q_t \quad q_t = \frac{q_k}{\gamma_{Rv}} \tag{8}$$

Here, q_o is the foundation base pressure formed by the vertical load, shear force and moment effects at the foundation level, and γ_{Rv} is the strength coefficient for the foundation overflow force given in TBEC-2018. Considered input parameters have been tabulated in Table 1 for optimization of CRW design

Table 1. Input parameters for optimization analyses of CRW

Input parameters	Symbol	Value	Unit
Stem height	H	6	m
Surcharge load	q	0	kPa
Backfill slope	β	0	°
Undrained shear strength of base soil	c_u	250	kPa
Unit weight of base soil	γ_b	19	kPa
Cohesion of base soil	c’	70	kPa
Internal friction angle of the base soil	$Ø_b$	25	°
Cohesion of backfill soil	c_r	0	kPa
Depth of soil in front of the wall	D_f	1.5	m
Sliding and overturning safety factors	SF_{ss} and SF_{so}	1.50	–
The factor of safety for bearing capacity	SF_{sb}	3.00	-
Unit weight of concrete	γ_c	24	kPa

2.2. Design Cases

In this study, optimum design of CRW has been investigated for selected two locations from Turkey Earthquake Risk Map (TERM) [24] which is show in Fig.2.

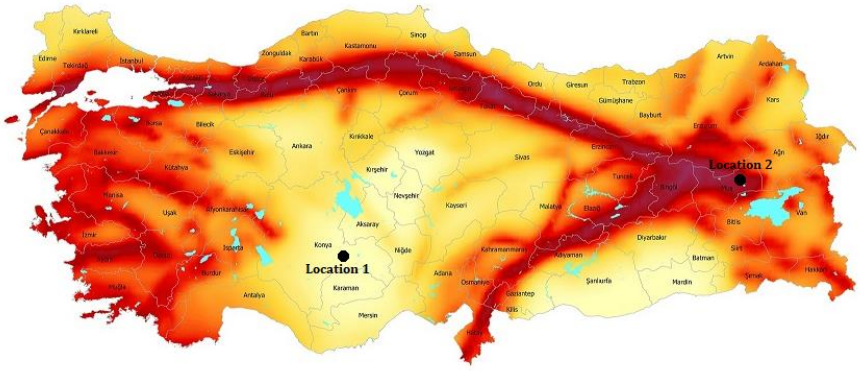

Fig.2. Selected locations from Turkey Earthquake Hazard Map (TERM) [24]

Design cases of different type of earthquake have been formed by using earthquake effect information for location 1 and location 2 obtained from TERM and local soil effect coefficients for the short period region (Fs) in TBEC-18. For the earthquake soil motion level DD-2, the seismicity of the region has been taken into account in the effect of earthquake loading on the CRW. For effect of severe earthquake and mild earthquake on the wall, the map spectral

acceleration coefficients (Ss) have been taken as 1.50 and 0.25, respectively. Different design cases are demonstrated in Table 2.

Table 2. Design cases

Case	1	2	3	4	5	6	7	8	9	10
Soil class	ZA	ZB	ZC	ZD	ZE	ZA	ZB	ZC	ZD	ZE
$Ø_r$ (°)	28	30	34	36	38	28	30	34	36	38
γ_r (kN/m^3)	16	17	18	19	20	16	17	18	19	20
F_S	0.8	1	1.2	0.9	0.8	2.4	1.6	1.3	0.9	0.8
S_{DS}	1.2	1.5	1.8	1.35	1.2	0.6	0.4	0.325	0.225	0.2
S_S	0.25	0.25	0.25	0.25	0.25	1.50	1.50	1.50	1.50	1.50

3. Optimum Design of Cantilever Retaining Wall

3.1. Harmony Search Algorithm

Recently, heuristic methods have been widely used in solving complex optimization problems encountered in the field of engineering. Heuristic methods are algorithms that produce solutions to optimization problems by making use of the solutions produced by nature in the face of difficult problems. The harmony search algorithm was first developed by Geem et al. (2001) [25] and based on the principle of finding the best harmony during music performance. Harmony search algorithm is a more advantageous algorithm than other heuristic methods because of its simple algorithm, it gives results in a reasonable time when the number of iterations is high, it can be used for continuous or discrete variables, and it reaches the global solution without getting stuck with local solutions in the optimization process.

The steps of the harmony search algorithm are given below.

Step 1: In the harmony search algorithm, the algorithm parameters that control the solution process are started. A valid range of values is defined for each design variable in the optimum design problem. By taking these values, a design pool is created for the design variables of the algorithm. Then, the number of solution vectors of the memory matrix (HMS), the memory matrix consideration ratio (HMCR), the adjustment ratio (PAR) between the two values, and the maximum number of iterations of the stopping criterion are selected in this step.

Step 2: The harmony memory matrix (HM) is initialized. Initial values are assigned to the harmony memory matrix. Each row of this matrix contains values randomly selected from the design pool, containing possible solutions for a particular design variable. Here N corresponds to the number of design variables and the number of rows in the HMS memory matrix. In the harmony memory matrix, the solution vectors are ordered from the minimum to the maximum with the values of the objective functions. Here, not only the possible solution vectors, but also the solution values with small inconveniences are included in the solution matrix.

Step 3: A new harmony memory matrix is developed. In the harmony search method, the creation of a new solution vector is controlled by the two main parameters of this method

(HMCR and PAR). HMCR is a probability value that directs the algorithm to either the harmony memory or the entire set of values to select a value for a design variable. Sometimes, when the design variable is selected from the harmony memory, it is checked whether this variable replaces its nearest upper and lower neighbors. The aim here is to make a more detailed search by providing transitions around a current solution. This phenomenon in the harmony search method is known as the adjustment (PAR) between two values.

Step 4: The harmony memory matrix is updated. After obtaining new values for each design variable, the objective function value is calculated for the new solution vector. If this value is better than the worst harmonic vector value in the harmony memory matrix, it is included in the matrix and the worst value is removed from the matrix.

Step 5: Repeat Step 3 and Step 4 until the maximum number of cycles, which is the termination criterion, is reached.

In the optimization implementation of the harmony search algorithm for the cantilever retaining wall, HMS, HMCR, and PAR algorithm parameters values have been taken as 20, 0.90, and 0.35, respectively [25,27]. The process of reaching the optimum value for each design case has been completed by operating 30,000 maximum iterations that the result did not change with the continued analyzes. Each process with 30,000 iterations has been repeated for 30 independent runs. Deb's rules have been employed in evaluating solutions that have a constraint violation [28].

3.2. Definition of Optimization Problem

In the optimum design of CRW, the top stem width (X_1), the toe extension (X_2), the bottom stem width (X_3), the heel extension (X_4) and base thickness (X_5) of the wall have been considered as design variables. Because of the design parameters corresponds to the dimensions of CRW, these values and their intervals have been selected as discrete values. The lower and upper limits of the design variables shown in Figure 3 are given in Table 3.

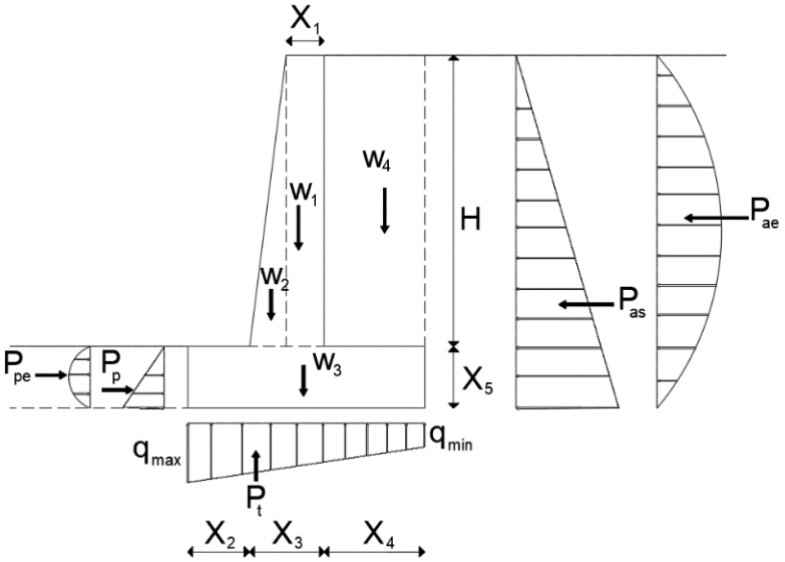

Fig. 3. CRW optimum design problem with design variables and acting loads on the wall [20,21]

Table 3. Discrete design variable values for CRW

Design variable	Lower limit	Upper limit	Increment
X_1	0.30m	0.60m	2cm
X_2	0.30m	3.00m	5cm
X_3	0.30m	0.60m	2cm
X_4	0.30m	3.00m	5cm
X_5	0.50m	1.00m	2cm

The design constraints used to meet the stability criteria of the wall in the optimization analyses in terms of obtaining both safe and optimum design are given in Table 4.

Table 4. Considering constraints in optimization analyses

Constraint	Mathematical definition
Sliding check for static case	$g_x(1) = 1 - F_{ss}/1.50 \le 0$
Overturning check for static case	$g_x(2) = 1 - F_{ds}/1.50 \le 0$
Bearing capacity check for static case	$g_x(3) = 1 - \frac{q_u}{3q_{\max}} \le 1 \qquad g_x(4) = \frac{6e}{X_2 + X_3 + X_4} \le 1$
Sliding check for dynamic case	$g_x(5) = \mathrm{V_{th}}/(\mathrm{R_{th}} + 0.30\mathrm{R_{pt}}) - 1 \le 0$
Overturning check for dynamic case	$g_x(6) = 1 - \frac{R_{dev}}{1.3E_{dev}} \le 0$
Bearing capacity check for dynamic case	$g_x(7) = 1.4q_0 / q_u - 1 \le 0$
Geometric 1	$g_x(8) = \frac{(X_2 + X_3)}{(X_2 + X_3 + X_4)} - 1 \le 0$
Geometric 2	$g_x(9) = X_1 / X_3 - 1 \le 0$

The objective function considered in the investigation of the minimum wall cost based on the wall weight is given in Equation 9.

$$f_{\min} = (W_1 + W_2 + W_3)\gamma_c c_c \tag{9}$$

4. Results of Optimization Analyses

Investigation of the cantilever retaining wall (CRW) optimum design for different soil classes (ZA, ZB, ZC, ZD, ZE) and earthquake loads (Ss=0.25, 1.50) have been performed via HSA. Obtained optimum designs for ten design cases and design variables tabulated in Table 1 and Table 3, respectively have been presented in this section.

After the optimization algorithm of HSA was operated with 30 independent runs, the optimum designs were obtained the most minimum objective function value among all runs. Obtained CRW designs which are satisfied design constraints for all runs are showed in Fig.4 for S_S=0.25 and in Fig.5 for S_S=1.50. X_1, X_2, X_3, X_4 and X_5 wall dimensions and the wall weights have been compared in terms of different design cases.

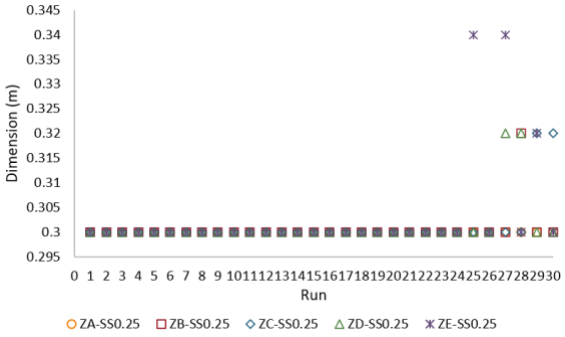

(a)

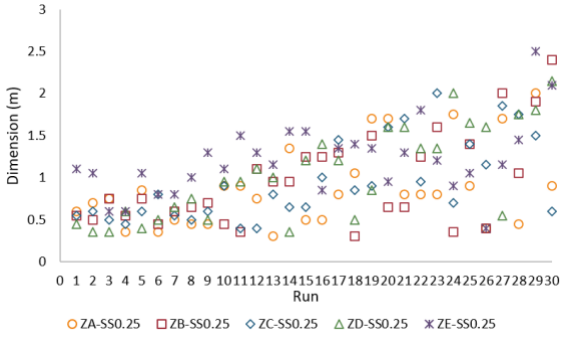

(b)

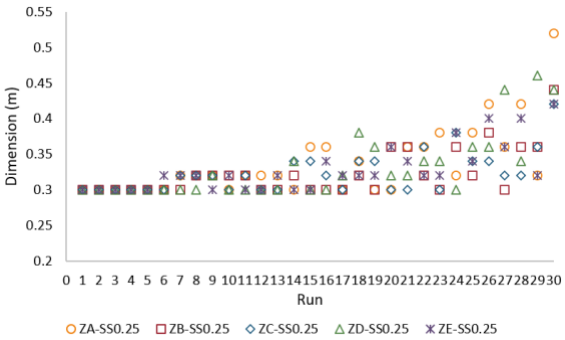

(c)

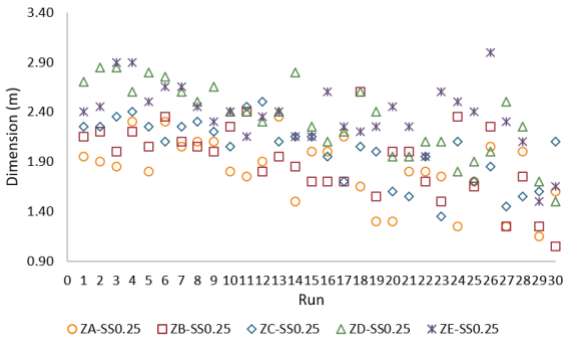

(d)

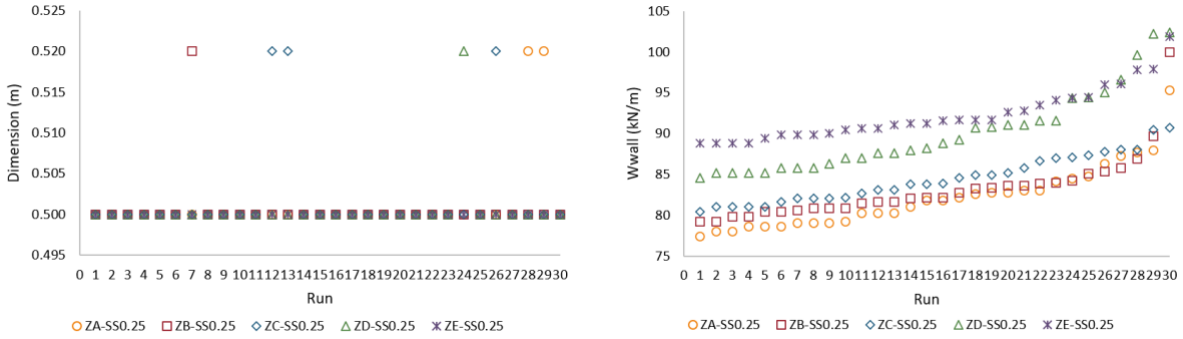

(e) (f)

Fig.4. Results of optimization analyses for case S_S=0.25: (a) X_1; (b) X_2; (c) X_3; (d) X_4; (e) X_5; (f) W_{wall}

It has been observed from Fig.4(a) and Fig.5(a), there was no significant change in the top stem width (X_1) values, even if the soil properties and earthquake effect changed. Similar linear behavior like X_1 has been seen for the base thickness (X_5) in Fig.4(e) and Fig.5(e). When the graphs, which are given in Fig.4 (b) and Fig.4 (d) for toe extension (X_2) and heel extension (X_4), respectively have been examined, it has been seen that the wall dimensions are mostly changeable in soils with different properties and effects of distinctive earthquake loads. Although X_4 has changing ground characteristics like X_2 and differing behavior under earthquake effect, it is observed that the wall weight has been boosted with decreasing X_4 values and increasing X_2 values. The bottom stem width (X_3) values have changeable behavior for different design cases. For X_2 and X_4, there is a more linear variation in Fig.5(c) than in Fig.4(c) in terms of different soil environment and different earthquake effects. It is observed that each wall dimension has almost same value in case of Ss=1.5 and ZC which exposed to larger earthquake effect than the other design cases. According to Fig.5(f), it is concluded that more different wall design satisfying design constraints has not been found due to obtaining same wall weight.

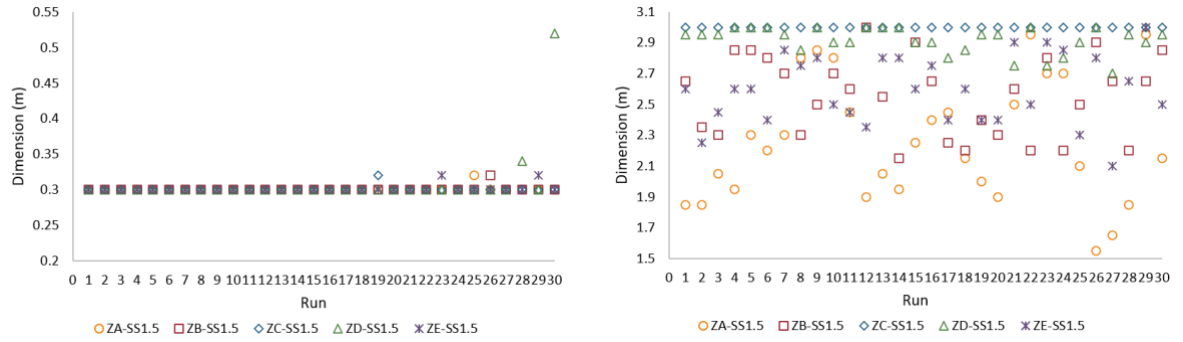

(a) (b)

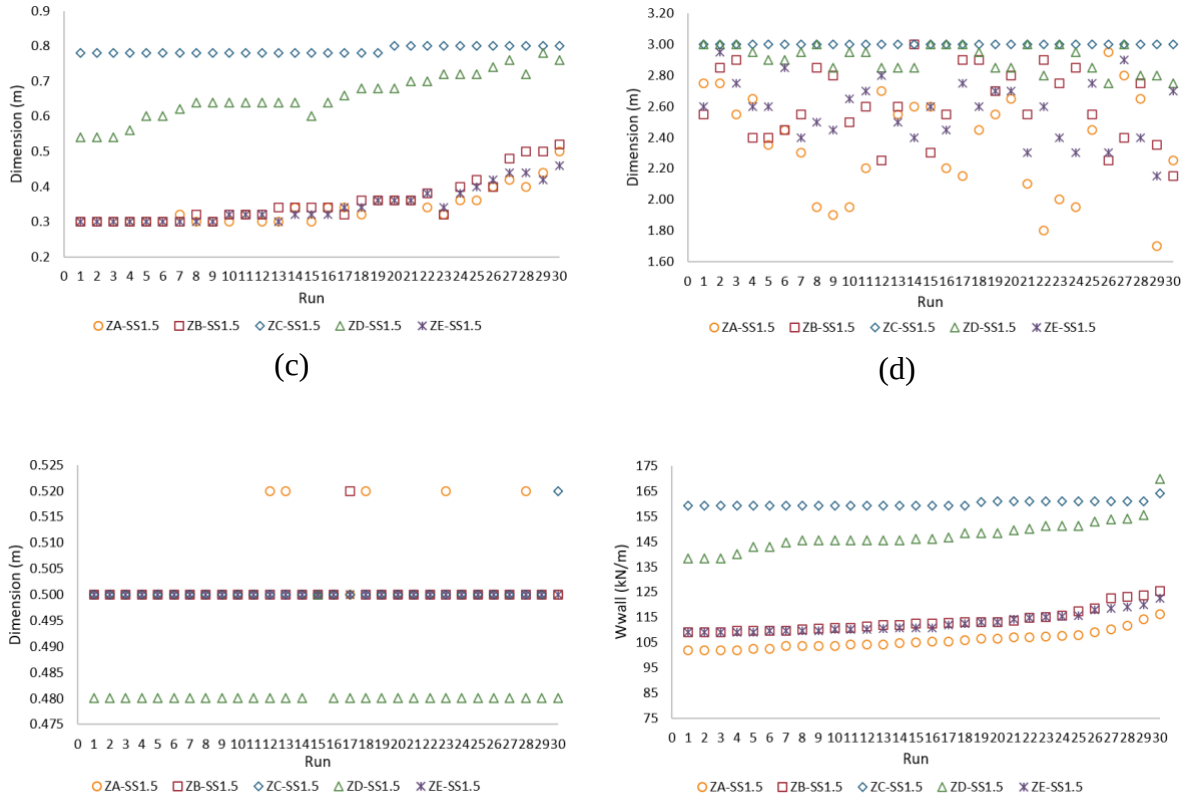

Fig.5. Results of optimization analyses for case S_S=1.50: (a) X_1; (b) X_2; (c) X_3; (d) X_4; (e) X_5; (f) W_{wall}

The optimum designs which provide all the constraints and have the most minimum objective function value are given in Fig.6 for the wall weight, cost, and dimensions. In the optimization analyses, since the feasible design were not obtained for Ss=1.50 and ZC design case, the results of the feasible design for the design case considering Ød=40° have been presented. It is due to the dynamic effect being much for Ss=1.50 and ZC design case.

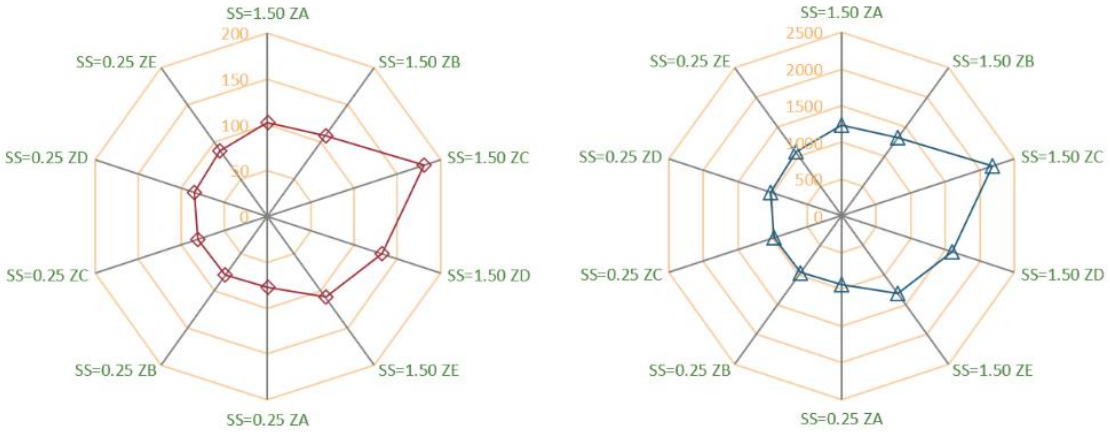

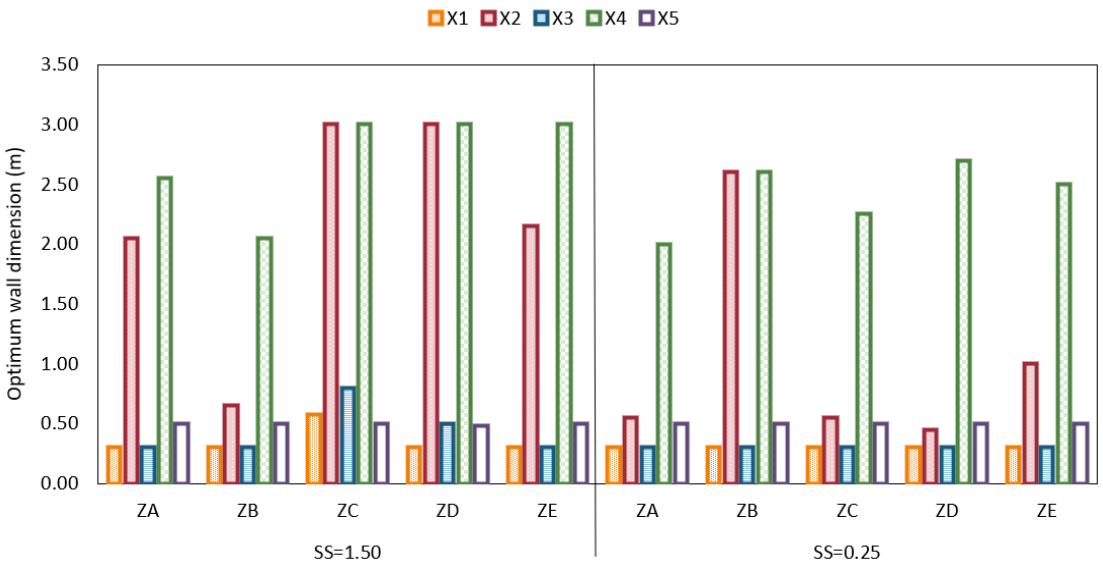

(c)

Fig.6. Optimum CRW designs for difeerent soil classes and SS values: (a) Weight (kN/m); (b) Cost (TL/m); (c) Wall dimesions

According to Fig.6 (a) and (b), it is seen that the wall costs in the case with a strong earthquake effect (S_S=1.50) increase compared to the case with less earthquake effect (S_S=0.25) in terms of different earthquake zones and soils. Providing the stability criteria for dynamic loading, which considers the effect on the wall in case of the earthquake, is possible by increasing the wall dimensions. When the results are evaluated in terms of different soil properties, it is observed that the cost increases from good quality soil to poor quality soil (from ZA to ZE) for Ss=0.25, while a similar trend is observed from ZA to ZC for Ss=1.50. It was observed in Fig.6 (b) that there was a 36% change between the maximum and minimum costs for Ss=1.50 and 12% for Ss=0.25. When the wall dimensions given in Fig.6 (c) are examined considering all design cases which are included different soil properties and earthquake effects, no significant change is observed in the values the top stem width (X_1), the bottom stem width (X_3), and base thickness (X_5). It is seen that the major change of wall dimensions has occurred in the toe extension (X_2) and the heel extension (X_4) of the wall base, especially in SS=1.50 and ZC-ZD design cases.

Iteration graphs of optimization analyses for case S_S=0.25 and S_S=1.50 have been demonstrated in Fig.7 and Fig.8, respectively. Design constraints of the optimum designs for CRW design which provide stability criteria are given in Table 5.

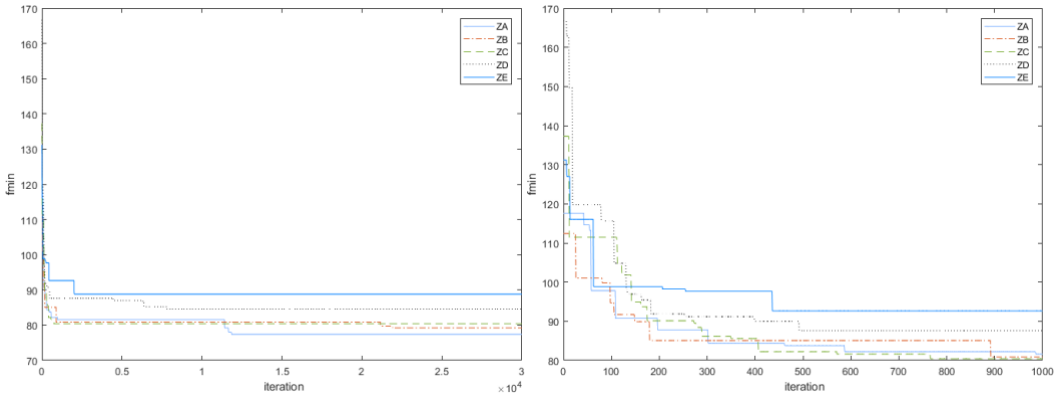

Fig.7. Iteration history graphs for S_S=0.25: (a) Weight (kN/m); (b) Cost (TL/m); (c) Wall dimesions

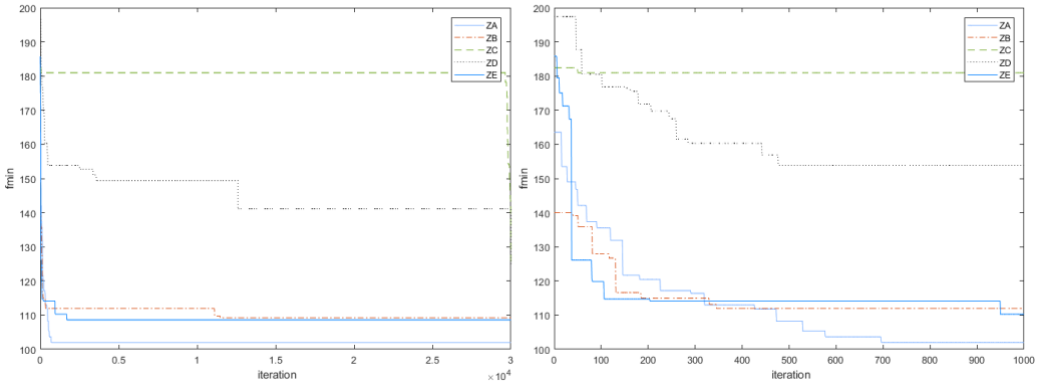

Fig.8. Iteration history graphs for S_S=1.50: (a) Weight (kN/m); (b) Cost (TL/m); (c) Wall dimesions

Table 5. Constraints values of optimum designs

S_S	1.50					0.25				
Constraint	ZA	ZB	ZC	ZD	ZE	ZA	ZB	ZC	ZD	ZE
g1(x)	-0.56	-0.625	-1.49	-0.636	-0.369	-0.014	-0.003	-0.004	-0.004	-0.01
g2(x)	-3.18	-3.563	-7.40	-4.093	-2.568	-0.601	-0.62	-0.62	-0.73	-0.88
g3(x)	-17.25	-53.36	-172.84	-30.66	-19.69	-10.37	-3.93	-9.91	-2.14	-3.60
g4(x)	-1.39	-1.549	-1.80	-1.592	-1.194	-0.024	-0.07	-0.004	-0.01	-0.32
g5(x)	-0.72	-0.726	-0.70	-0.710	-0.734	-0.811	-0.81	-0.79	-0.77	-0.76
g6(x)	-0.004	-0.005	-0.001	-0.005	-0.005	-0.306	-0.29	-0.13	-0.12	-0.02
g7(x)	-0.97	-0.986	-0.99	-0.974	-0.980	-0.985	-0.96	-0.98	-0.94	-0.95
g8(x)	-0.52	-0.473	-0.442	-0.462	-0.550	-0.702	-0.68	-0.72	-0.78	-0.65
g9(x)	0.000	0.000	-0.615	-0.400	0.000	0.000	0.000	0.000	0.000	0.000

5. Discussion

The results obtained for the optimal design of the CRW by using HSA have been compared with the studies in the literature, which is presented with different heuristic optimization algorithms for the same optimization problem as this study. While the modified artificial bee colony algorithm (MABC) study has more minimum wall weight and cost, the particle swarm optimization (PSO) study has almost the same values by comparison with optimum designs with HSA according to results of optimum CRW design obtained by considering the MABC [20] and the particle swarm optimization (PSO) [21] for the same design cases. It has been observed similarly that the optimum design that provides the design constraints for Ød=34° in

the case of ZC and SS=1.5 could not be obtained, due to the large impacting earthquake load and different soil characteristics.

The optimum weight of the cantilever retaining wall by HSA has been obtained as W_{wall} = 59.4kN/m for $Ø_r$ =40° and γ_r=18kN/m^3 with considering static load case in another literature study [29]. For the same design case, the optimum wall weight has been obtained as 181kN/m with considering dynamic loads in this study ($Ø_r$=40° and γ_r=18kN/ m^3). This result shows that wall weight accordingly wall dimension has increased in order to provide design criteria (constraints) for additional loads like dynamic effect. That's why optimization analyses in this kind of design problem may be an alternative manner for obtaining more economic design in the wall design.

6. Conclusions

In this study, the harmony search algorithm (HSA) has been utilized in order to obtain the optimum design of the cantilever retaining wall (CRW) and the minimum wall weight for different design cases. Besides, the effect of different soil properties and earthquake loads on the wall weight and wall dimensions have been investigated.

According to the optimization analyzes results, when the map spectral acceleration coefficient (Ss) taken from TERM and expressing the seismicity effect of the region is 1.50, it is seen that the CRW design has the highest cost for ZC type soil from among the design situations. Another remarkable result is that ZD and ZE, which have worse soil properties than ZC, have lower costs under the same earthquake effect. Since the characteristics of the earthquake wave that occurred in the earth and transmitted to the structure through the soil changes depending on the different soil properties, and the dynamic earthquake behavior should be evaluated within its specific structure in the designs to be made in different soil environments. As a result, obtaining larger dimensions due to safely meet the loads caused by the earthquake effect in the structure has been shown that performing optimization analyses based on heuristic algorithms is important for the most economical and safe design in the current design cases.

It has been concluded that HSA is an alternative method in obtaining CRW optimum design which is a complex engineering design problem with many unknowns under effect both static and dynamic loads. For different design cases which included many design parameters, the heuristic optimization algorithms can be utilized safely and effectively in the examination of parameter effects on the target goals like cost, design criteria, and so on.

References

[1] Das Braja M. S.K., Principles of Foundation Engineering (9th Edition). Cengage Learning, 2017

[2] Uray, E., Tan, Ö., Çarbaş, S., Erkan, H., Metaheuristics-based pre-design guide for cantilever retaining walls, *Teknik Dergi*, 32, 2021. doi:10.18400/tekderg.561956

[3] Carbas, S., Toktas, A., Ustun, D.editors, Nature-Inspired Metaheuristic Algorithms for Engineering Optimization Applications. Springer Singapore, 2021. doi:10.1007/978-981-

33-6773-9

[4] Uray, E., Carbas, S., Erkan, I.H., Tan, O., Parametric investigation for discrete optimal design of a cantilever retaining wall, *Challenge Journal of Structural Mechanics*, 5, 108, 2019. doi:10.20528/cjsmec.2019.03.004

[5] Kalemci, E.N., İkizler, S.B., Dede, T., Angın, Z., Design of reinforced concrete cantilever retaining wall using Grey wolf optimization algorithm, *Structures*, 23, 245–53, 2020. doi:10.1016/j.istruc.2019.09.013

[6] Temür, R., Bekdas¸ G., Teaching learning-based optimization for design of cantilever retaining walls, *Structural Engineering and Mechanics*, 57, 763–83, 2016

[7] Akin, A., Saka, M.P., Optimum design of concrete cantilever retaining walls using the harmony search algorithm, *Civil-Comp Proceedings*, 93, 1–21, 2010. doi:10.4203/ccp.93.130

[8] Temur, R., Bekdas, G., Temür, R., Bekdaş, G., Teaching Learning-Based Optimization for Design of Cantilever Retaining Walls Design and analysis of nonlinear structural systems View project Teaching learning-based optimization for design of cantilever retaining walls, *Structural Engineering and Mechanics*, 57, 763–83, 2016. doi:10.12989/sem.2016.57.4.763

[9] Dağdeviren, U., Kaymak, B., Investigation of parameters affecting optimum cost design of reinforced concrete retaining walls using artificial bee colony algorithm, *Journal of the Faculty of Engineering and Architecture of Gazi University*, 33, 239–53, 2018. doi:10.17341/gazimmfd.406796

[10] Gandomi, A.H., Kashani, A.R., Zeighami, F., Retaining wall optimization using interior search algorithm with different bound constraint handling, *International Journal for Numerical and Analytical Methods in Geomechanics*, 41, 1304–31, 2017. doi:10.1002/NAG.2678

[11] T.C. Resmi Gazete., Turkish Building Earthquake Code (Türkiye Bina Deprem Yönetmeliği)-2018 (TBEC-18). 2018

[12] Arslan, Ö., Keskin, I., Ateş, A., Farklı deprem yüklerinin betonarme konsol bir istinat duvarının maliyetine etkisinin analizi, *Anadolu Üniversitesi Bilim ve Teknoloji Dergisi - B Teorik Bilimler*, 6, 28–35, 2018. doi:10.20290/aubtdb.497527

[13] Bilgin, H., İstinat duvarlarının dinamik ve statik yükler altındaki davranışının analizi. Karadeniz Teknik University, Department of Civil Engineering, Master Thesis, 2006

[14] Dalyan, İ., Akın, M., Akbay Arama Z., Betonarme istinat duvarlarının geoteknik tasarımında etkili parametrelerin 2018 Türkiye Bina Deprem Yönetmeliği'ne göre değerlendirilmesi, *Türk Deprem Araştırma Dergisi*, 2, 176–92, 2020. doi:10.46464/tdad.80428

[15] Yıldırım, İ.Z., İstinat duvarlarının tasarımında deprem etkilerinin incelenmesi. İstanbul Teknik University, Department of Civil Engineering, Master thesis, 2004

[16] Aydogdu, I., Cost optimization of reinforced concrete cantilever retaining walls under

seismic loading using a biogeography-based optimization algorithm with Levy flights, *Taylor & Francis*, 49, 381–400, 2017. doi:10.1080/0305215X.2016.1191837

[17] Kayhan, A., Demir, A., Statik ve dinamik yüklere maruz betonarme konsol istinat duvarlarının diferansiyel gelişim algoritması ile optimum tasarımı, *Pamukkale Üniversitesi Mühendislik Bilimleri Dergisi*, 24, 403–12, 2018. doi:10.5505/pajes.2017.04834

[18] Ravichandran, N., Wang, L., Rahbari, P., Juang, C.H., Robust design optimization of retaining wall backfilled with shredded tire in the face of earthquake hazards, *Bulletin of Engineering Geology and the Environment*, 80, 1351–63, 2021. doi:10.1007/s10064-020-02038-9

[19] Kaveh, A., Akbari, H., Hosseini, S.M., Plasma generation optimization for optimal design of reinforced concrete cantilever retaining wall structures, *Iranian Journal of Science and Technology - Transactions of Civil Engineering*, 2021. doi:10.1007/s40996-020-00566-8

[20] Uray, E., Çıtırık, B.N., Modifiye Yapay Arı Kolonisi Algoritması ile konsol dayanma duvarının Türkiye Bina Deprem Yönetmeliği 2018'e göre optimum tasarımı, *Avrupa Bilim ve Teknoloji Dergisi*, 26, 61–7, 2021. doi:10.31590/ejosat.948040

[21] Uray, E., Çarbaş, S., Parçacık Sürü Optimizasyonu ile konsol dayanma duvarının Türkiye Bina Deprem Yönetmeliği-2018'e göre optimum tasarımı. In: Özkaya U, editor. 1st Int. Conf. Appl. Eng. Nat. Sci., 2021. doi:ISBN: 978-625-00-0389-3

[22] Afzal, M., Liu, Y., Cheng, J.C.P., Gan, V.J.L., Reinforced concrete structural design optimization: A critical review, *Journal of Cleaner Production*, 260, 120623, 2020. doi:10.1016/J.JCLEPRO.2020.120623

[23] Kalyoncuoğlu, Ü.Y., Depreme dayanıklı yapılanma için zemin sınıfları ve ivme tepkileri (Tayvan örneği), *Süleyman Demirel Üniversitesi Fen Bilimleri Enstitüsü Dergisi*, 10, 428–36, 2006

[24] TDTH., Turkey Earthquake Hazard Map (TERM) (Türkiye Deprem Tehlike Haritaları), 2018. https://tdth.afad.gov.tr/TDTH/main.xhtml

[25] Geem, Z., Kim, J., Loganathan, G., A new heuristic optimization algorithm: harmony search, *Simulation*, 76, 60–8, 2001. doi:10.1177/003754970107600201

[26] Meyerhof, G.G., Some recent research on the bearing capacity of foundations, *Canadian Geotechnical Journal*, 1, 16–26, 1963. doi:10.1139/t63-003

[27] Lee, K., Geem, Z., A new meta-heuristic algorithm for continuous engineering optimization: harmony search theory and practice, *Computer Methods in Applied Mechanics and Engineering*, 194, 3902–33, 2005. doi:10.1016/j.cma.2004.09.007

[28] Deb, K., An efficient constraint handling method for genetic algorithms, *Computer Methods in Applied Mechanics and Engineering*, 186, 311–38, 2000. doi:10.1016/S0045-7825(99)00389-8

[29] Uray, E., Çarbaş, S., Erkan, İ.H., Tan, Ö., Parametric investigation for discrete optimal design of a cantilever retaining wall, *Challenge Journal of Structural Mechanics*, 5, 108, 2019. doi:10.20528/cjsmec.2019.03.004

International Journal of Engineering & Applied Sciences (IJEAS)
Vol.13, Issue 4 (2021) 155-165
http://dx.doi.org/10.24107/ijeas.1036574
Int J Eng Appl Sci 13(4) (2021) 155-165

Examination of How Size-Effect Modifies the Stiffness and Mass Matrices of Nanotrusses/Nanoframes

Hayri Metin Numanoğlu

[a] *Giresun University, Civil Engineering Department, Division of Mechanics, Giresun, Turkey*
[*] *E-mail address*: metin_numanoglu@hotmail.com

ORCID number of author:
0000-0003-0556-7850

Abstract

The effect of the nonlocal parameter on the free vibration analysis of nano scaled trusses and frames is examined. Accordingly, firstly, the axial and bending vibrations of the nano scaled longitudinal element are formulated. Simple rod and Euler-Bernoulli assumptions are considered for axial and bending vibrations, respectively. Finite element matrices are obtained by applying the average weighted residue to the nonlocal equation of motion for free vibration. These matrices are combined according to the freedoms of longitudinal element and the matrix displacement method is explained for structures consisting of discrete longitudinal elements. It is discussed how the classical stiffness and mass matrices are modified by the atomic parameter.

Keywords: Mass matrix, matrix displacement method, nanoframe, nanotruss, nonlocal free vibration, stiffness matrix.

1. Introduction

The fact that nano scaled materials play a role in today's modern applications such as biosensors, resonators, transistors, gas sensors, nanocantilever, microcircuits, medicine, and dental has increased the importance of investigation on their mechanical properties as well as the physical, electrical, optical, and thermal properties of these materials. One-dimensional materials such as carbon nanotubes, boron nitride nanotubes, silica carbide nanotubes, metallic nanowires, and two-dimensional materials such as graphene, borophene, silicene are encountered in today's modern applications. In the investigation of mechanical behavior of such materials, because of expensiveness, high specialization requirement, high computational volume, long and inefficient processes, the studies based molecular dynamics simulation have led researchers to use mechanical structure models known from solid mechanics. It is a well-known result of scientific studies that models based classical physics theories do not give accurate results. Therefore, researchers have efforted to explain the mechanical behavior of nano scaled structures by combining these models with higher-order continuum formulations such as nonlocal elasticity, modified couple stress elasticity, modified strain gradient elasticity, doublet mechanics, surface energy.

When studies on the mechanics of nano scaled structures are examined, it can be observed that the nonlocal elasticity theory has been investigated more intensively than other higher-order continuum mechanics theories. Mechanical structure models such as rod [1-11] and beam [12-25] form the basis of studies in the nonlocal mechanics of nanostructures. Also, recently, studies

that mention mechanical analyses with nonlocal elasticity of discrete structures such as truss and frame [26-28] have entered the scientific literature.

Analytical methods such as double integration, separation of variables and series expansion have been able to solve some problems in solid mechanics [29-34]. However, reasons such as the inclusion of some parameters (elastic foundation/medium, thermal/hygrothermal environment, electro-magnetic environment, functionally grading, etc.) to the problem or the complication of boundary conditions may make the using of analytical methods in the problem impossible. Therefore, the using of numerical methods has gained importance in the solution of solid mechanics problems [35-39]. Moreover, the using of the finite element method in solid mechanics problems involving nonlocal elasticity is available in the scientific literature [2-4,10,11,17-26,40,41].

How the nonlocal parameter affects the classical elasticity solution in mechanical analysis of nano scaled truss and frame structures is discussed in this current study. It is planned that to scrutinize the nonlocal parameter on the matrices in the study [26] where vibration analyses of nanotrusses and nanoframes were given in detail. Firstly, the stiffness and mass matrices of nonlocal axial and bending vibrations of nano scaled longitudinal element are obtained using the weighted residue method. Then, stiffness and mass matrices are presented for nonlocal free vibration analysis of discrete structural models formed by axial or bending members by matrix displacement method. Finally, the effect of nonlocal parameter on the matrices of nanostructure is discussed.

2. Nonlocal Equation of Motions and Application of Average Weighted Residue

For vibration analysis of discrete structures consisting of nano scaled longitudinal elements, firstly, the axial and bending vibrations of the longitudinal element should be investigated. The free vibration equations are solved by the average weighted residue defined below:

$$\mathrm{I} = \int_0^L h \cdot R \mathrm{d}x \tag{1}$$

where I, h, and R define the average weighted residue, weighting function, and residue, respectively. L is length of the longitudinal element. According to method, the average weighted residue should be equal to 0. The residue is the equation to be solved, namely, the equation of motion. On the other hand, weighting function is $h = \phi^{\mathrm{T}}$ and ϕ is a shape function. The shape functions are written as follow for axial and bending vibrations, respectively:

$$\phi_a = \left\{1-\xi \quad \xi\right\} \tag{2}$$

$$\phi_b = \left\{1-3\xi^2+2\xi^3 \quad L\left(-\xi-2\xi^2+\xi^3\right) \quad 3\xi^2-2\xi^3 \quad L\left(-\xi^2+\xi^3\right)\right\} \tag{3}$$

where $\xi = x/L$ is called as nondimensional longitudinal coordinate.

2.1. Axial Vibration

The equation of motion of nonlocal free axial vibration for nano scaled structures according to the simple (without shear effect) rod formulation is as [3,30]:

$$EA\frac{\partial^2 u}{\partial x^2}-\rho A\frac{\partial^2 u}{\partial t^2}+\left(e_0 a\right)^2\rho A\frac{\partial^4 u}{\partial x^2\partial t^2}=0 \tag{4}$$

where E, A, and ρ state the modulus of elasticity, area of cross-section, and mass of unit volume, respectively. e_0 is atomic material constant and a is characteristic internal length. Also, u means the axial motion. Total partial integration of the average weighted residue can be reached:

$$\int_0^L\left[-EA\frac{\partial h}{\partial x}\frac{\partial u}{\partial x}-\rho Ah\frac{\partial^2 u}{\partial t^2}-\left(e_0 a\right)^2\rho A\frac{\partial h}{\partial x}\frac{\partial^3 u}{\partial x\partial t^2}\right]\mathrm{d}x=0 \tag{5}$$

In order to rearrange Eq. (5), the axial motion and its kinematic relation should be defined:

$$u=\phi\mathbf{u}\,,\quad \frac{\partial u}{\partial x}=\mathrm{D}^{\mathrm{k}}u=\mathbf{B}\mathbf{u}\,,\quad \frac{\partial^2 u}{\partial t^2}=\phi\ddot{\mathbf{u}} \tag{6}$$

where $\mathbf{u}$ is axial motion vector of end freedoms of longitudinal element. Additionally, D^{k} is kinematic operator ($\mathrm{D}^{\mathrm{k}}\phi=\mathbf{B}$). After Eq. (6) is replaced into Eq. (5), the following definitions can be made:

$$K=\int_0^L EA\left(\mathbf{B}^{\mathrm{T}}\mathbf{B}\right)\mathrm{d}x=\frac{EA}{L}\begin{bmatrix}1 & -1\\ -1 & 1\end{bmatrix} \tag{7}$$

$$M_c=\int_0^L \rho A\left(\phi^{\mathrm{T}}\phi\right)\mathrm{d}x=\frac{\rho AL}{6}\begin{bmatrix}2 & 1\\ 1 & 2\end{bmatrix} \tag{8}$$

$$M_{nl}=\int_0^L \left(e_0 a\right)^2\rho A\left(\mathbf{B}^{\mathrm{T}}\mathbf{B}\right)\mathrm{d}x=\frac{\left(e_0 a\right)^2\rho A}{L}\begin{bmatrix}1 & -1\\ -1 & 1\end{bmatrix} \tag{9}$$

where K is axial stiffness matrix. M_c and M_{nl} explain the classical and nonlocal mass matrices, respectively.

2.2. Bending Vibration

The equation of motion of nonlocal free bending vibration is expressed as [30]:

$$EI\frac{\partial^4 w}{\partial x^4}+\rho A\frac{\partial^2 w}{\partial t^2}+\left(e_0 a\right)^2\rho A\frac{\partial^4 w}{\partial x^2\partial t^2}=0 \tag{10}$$

In which, I is moment of inertia and w is transverse motion. Similar to axial vibration, the average weighted residue result is rewritten as follow:

$$\int_0^L\left[-EI\frac{\partial^2 h}{\partial x^2}\frac{\partial^2 w}{\partial x^2}-\rho Ah\frac{\partial^2 w}{\partial t^2}-\left(e_0 a\right)^2\rho A\frac{\partial h}{\partial x}\frac{\partial^3 w}{\partial x\partial t^2}\right]\mathrm{d}x=0 \tag{11}$$

Also, transverse motion and its kinematic relations are presented as:

$$w = \phi \mathbf{w}\,,\quad \frac{\partial w}{\partial x} = \mathrm{D}^{\mathrm{k}} w = \mathbf{B}\mathbf{w}\,,\quad \frac{\partial^2 w}{\partial x^2} = \mathbf{B}'\mathbf{w}\,,\quad \frac{\partial^2 w}{\partial t^2} = \phi \ddot{\mathbf{w}} \tag{12}$$

Substituting Eq. (12) into Eq. (11) yields the following bending stiffness matrix *K*, classical mass matrix M_c, and nonlocal mass matrix M_{nl}, respectively [26]:

$$K = \int_0^L EA\left(\mathbf{B}'^{\mathrm{T}}\mathbf{B}'\right)\mathrm{d}x = \frac{EI}{L^3}\begin{bmatrix} 12 & 6L & -12 & 6L \\ 6L & 4L^2 & -6L & 2L^2 \\ -12 & -6L & 12 & -6L \\ 6L & 2L^2 & -6L & 4L^2 \end{bmatrix} \tag{13}$$

$$M_c = \int_0^L \rho A\left(\phi^{\mathrm{T}}\phi\right)\mathrm{d}x = \frac{\rho AL}{420}\begin{bmatrix} 156L & 22L^2 & 54L & -13L^2 \\ 22L^2 & 4L^3 & 13L^2 & -3L^3 \\ 54L & 13L^2 & 156L & -22L^3 \\ -13L & -3L^3 & -22L^2 & 4L^3 \end{bmatrix} \tag{14}$$

$$M_{nl} = \int_0^L \left(e_0 a\right)^2 \rho A\left(\mathbf{B}^{\mathrm{T}}\mathbf{B}\right)\mathrm{d}x = \frac{\left(e_0 a\right)^2 \rho A}{30L}\begin{bmatrix} 36 & 3L & -36 & 3L \\ 3L & 4L^2 & -3L & -L^2 \\ -36 & -3L & 36 & -3L \\ 3L & -L^2 & -3L & 4L^2 \end{bmatrix} \tag{15}$$

3. Nonlocal Matrix Displacement Formulation

To constitute the vibration formulation of the structures consisting of discrete members, the stiffness and mass matrices of the element that makes a positive α angle with the horizontal in the general axes should be determined. The detail of this process can be found in [26]. Accordingly, the stiffness and mass matrices are transformed from the global axes to the local axes.

The transformation matrices for discrete structures under axial effects only (nanotrusses) and both axial and bending effects (nanoframes) are as follows, respectively:

$$T_a = \begin{bmatrix} \cos\alpha & \sin\alpha & 0 & 0 \\ -\sin\alpha & \cos\alpha & 0 & 0 \\ 0 & 0 & \cos\alpha & \sin\alpha \\ 0 & 0 & -\sin\alpha & \cos\alpha \end{bmatrix} \tag{16}$$

$$T_b = \begin{bmatrix} \cos\alpha & \sin\alpha & 0 & 0 & 0 & 0 \\ -\sin\alpha & \cos\alpha & 0 & 0 & 0 & 0 \\ 0 & 0 & 1 & 0 & 0 & 0 \\ 0 & 0 & 0 & \cos\alpha & \sin\alpha & 0 \\ 0 & 0 & 0 & -\sin\alpha & \cos\alpha & 0 \\ 0 & 0 & 0 & 0 & 0 & 1 \end{bmatrix} \tag{17}$$

3.1. Nonlocal Matrices of Nanotrusses

Since the axial discrete member has not a stiffness in the perpendicular direction to the element, the inputs of the matrix in Eq. (7) constitute only the axial freedoms of discrete member. However, due to Newton's second law, since the mass constitute the acceleration of the motion in the axial and transverse freedoms, the matrices calculated in Eqs. (8) and (9) determine the inputs of discrete member in both axial both and transverse directions [26].

The stiffness and mass matrices in the local axes are calculated as follows [26]:

$$K_e = T_a^{\mathrm{T}} K T_a =$$
$$\begin{bmatrix} \cos\alpha & -\sin\alpha & 0 & 0 \\ \sin\alpha & \cos\alpha & 0 & 0 \\ 0 & 0 & \cos\alpha & -\sin\alpha \\ 0 & 0 & \sin\alpha & \cos\alpha \end{bmatrix} \times \frac{EA}{L} \begin{bmatrix} 1 & 0 & -1 & 0 \\ 0 & 0 & 0 & 0 \\ -1 & 0 & 1 & 0 \\ 0 & 0 & 0 & 0 \end{bmatrix} \times \begin{bmatrix} \cos\alpha & \sin\alpha & 0 & 0 \\ -\sin\alpha & \cos\alpha & 0 & 0 \\ 0 & 0 & \cos\alpha & \sin\alpha \\ 0 & 0 & -\sin\alpha & \cos\alpha \end{bmatrix}$$
$$= \frac{EA}{L} \begin{bmatrix} \cos^2\alpha & \cos\alpha\sin\alpha & -\cos^2\alpha & -\cos\alpha\sin\alpha \\ \cos\alpha\sin\alpha & \sin^2\alpha & -\cos\alpha\sin\alpha & -\sin^2\alpha \\ -\cos^2\alpha & -\cos\alpha\sin\alpha & \cos^2\alpha & \cos\alpha\sin\alpha \\ -\cos\alpha\sin\alpha & -\sin^2\alpha & \cos\alpha\sin\alpha & \sin^2\alpha \end{bmatrix} \tag{18}$$

$$M_e = T_a^{\mathrm{T}} \left(M_c + M_{nl} \right) T_a =$$
$$\begin{bmatrix} \cos\alpha & -\sin\alpha & 0 & 0 \\ \sin\alpha & \cos\alpha & 0 & 0 \\ 0 & 0 & \cos\alpha & -\sin\alpha \\ 0 & 0 & \sin\alpha & \cos\alpha \end{bmatrix} \times \left(\frac{\rho AL}{6} \begin{bmatrix} 2 & 0 & 1 & 0 \\ 0 & 2 & 0 & 1 \\ 1 & 0 & 2 & 0 \\ 0 & 1 & 0 & 2 \end{bmatrix} + \frac{\left(e_0 a\right)^2 \rho A}{L} \begin{bmatrix} 1 & 0 & -1 & 0 \\ 0 & 1 & 0 & -1 \\ -1 & 0 & 1 & 0 \\ 0 & -1 & 0 & 1 \end{bmatrix} \right) \times$$
$$\begin{bmatrix} \cos\alpha & \sin\alpha & 0 & 0 \\ -\sin\alpha & \cos\alpha & 0 & 0 \\ 0 & 0 & \cos\alpha & \sin\alpha \\ 0 & 0 & -\sin\alpha & \cos\alpha \end{bmatrix} = \rho AL \begin{bmatrix} \frac{1}{3} + \frac{\left(e_0 a\right)^2}{L^2} & 0 & \frac{1}{3} + \frac{\left(e_0 a\right)^2}{L^2} & 0 \\ 0 & \frac{1}{3} + \frac{\left(e_0 a\right)^2}{L^2} & 0 & \frac{1}{6} - \frac{\left(e_0 a\right)^2}{L^2} \\ \frac{1}{6} - \frac{\left(e_0 a\right)^2}{L^2} & 0 & \frac{1}{3} + \frac{\left(e_0 a\right)^2}{L^2} & 0 \\ 0 & \frac{1}{3} + \frac{\left(e_0 a\right)^2}{L^2} & 0 & \frac{1}{3} + \frac{\left(e_0 a\right)^2}{L^2} \end{bmatrix} \tag{19}$$

The vibration of the nanotruss is solved by the eigenvalue formulation as follow:

$$\det\left(\sum_{i=1}^{ne}\left[K_e\right]^*_{n\times n}-\omega_n^2\sum_{i=1}^{ne}\left[M_e\right]^*_{n\times n}\right)=0 \tag{20}$$

where $\left[K_e\right]^*$ and $\left[M_e\right]^*$ represent the reduced total stiffness and mass matrices, respectively. Also, *n* is degree of freedom of discrete system. ω_n denotes the natural frequency.

3.2. Nonlocal Matrices of Nanoframes

Because bending discrete members have freedoms in the axial direction, too, the stiffness and mass matrices in the global axes can be assembled by considering Eqs. (7)-(9) and (13)-(15) [26]:

$$K=\begin{bmatrix} \frac{EA}{L} & 0 & 0 & -\frac{EA}{L} & 0 & 0 \\ 0 & \frac{12EI}{L^3} & -\frac{6EI}{L^2} & 0 & -\frac{12EI}{L^3} & -\frac{6EI}{L^2} \\ 0 & -\frac{6EI}{L^2} & \frac{4EI}{L} & 0 & \frac{6EI}{L^2} & \frac{2EI}{L} \\ -\frac{EA}{L} & 0 & 0 & \frac{EA}{L} & 0 & 0 \\ 0 & -\frac{12EI}{L^3} & \frac{6EI}{L^2} & 0 & \frac{12EI}{L^3} & \frac{6EI}{L^2} \\ 0 & -\frac{6EI}{L^2} & \frac{2EI}{L} & 0 & \frac{6EI}{L^2} & \frac{4EI}{L} \end{bmatrix} \tag{21}$$

$$M_c=\frac{\rho AL}{420}\begin{bmatrix} 140 & 0 & 0 & 70 & 0 & 0 \\ 0 & 156 & 22L & 0 & 54 & -13L \\ 0 & 22L & 4L^2 & 0 & 13L & -3L^2 \\ 70 & 0 & 0 & 140 & 0 & 0 \\ 0 & 54 & 13L & 0 & 156 & -22L \\ 0 & -13L & -3L^2 & 0 & -22L & 4L^2 \end{bmatrix} \tag{22}$$

$$M_{nl}=\left(e_0a\right)^2\rho AL\begin{bmatrix}\frac{1}{L} & 0 & 0 & -\frac{1}{L} & 0 & 0\\ 0 & \frac{6}{5L} & \frac{1}{10} & 0 & -\frac{6}{5L} & \frac{1}{10}\\ 0 & \frac{1}{10} & \frac{2L}{15} & 0 & -\frac{1}{10} & -\frac{L}{30}\\ -\frac{1}{L} & 0 & 0 & \frac{1}{L} & 0 & 0\\ 0 & -\frac{6}{5L} & -\frac{1}{10} & 0 & \frac{6}{5L} & -\frac{1}{10}\\ 0 & \frac{1}{10} & -\frac{L}{30} & 0 & -\frac{1}{10} & \frac{2L}{15}\end{bmatrix} \tag{23}$$

The stiffness and mass matrices of the bending discrete member are expressed as:

$$K_e=T_b^{\mathrm{T}}KT_b=\left[k_{ij}\right]_{6\times6} \tag{24}$$

$$M_e=T_b^{\mathrm{T}}\left(M_c+M_{nl}\right)T_b=\left[m_{ij}\right]_{6\times6} \tag{25}$$

The components of the stiffness matrix are calculated as follows:

$$\begin{gathered}k_{11}=k_{44}=\frac{EA}{L}\cos^2\alpha+\frac{12EI}{L^3}\sin^2\alpha,\ \ k_{12}=k_{45}=\left(\frac{EA}{L}-\frac{12EI}{L^3}\right)\cos\alpha\sin\alpha,\\ k_{13}=k_{16}=-\frac{6EI}{L^2}\sin\alpha,\ k_{14}=-\frac{EA}{L}\cos^2\alpha-\frac{12EI}{L^3}\sin^2\alpha,\\ k_{15}=k_{24}=\left(-\frac{EA}{L}+\frac{12EI}{L^3}\right)\cos\alpha\sin\alpha,\ \ k_{22}=k_{55}=\frac{EA}{L}\sin^2\alpha+\frac{12EI}{L^3}\cos^2\alpha,\\ k_{23}=k_{26}=\frac{6EI}{L^2}\mathrm{c},\ \ k_{25}=-\frac{EA}{L}\sin^2\alpha-\frac{12EI}{L^3}\cos^2\alpha,\ \ k_{33}=k_{66}=\frac{4EI}{L},\\ k_{34}=k_{46}=\frac{6EI}{L^2}\sin\alpha,\ \ k_{35}=k_{56}=-\frac{6EI}{L^2}\cos\alpha,\ \ k_{36}=\frac{2EI}{L}\end{gathered} \tag{26}$$

Additionally, the components of the mass matrix can be given as:

$$\begin{gathered}m_{11}=m_{44}=\left(\frac{\rho AL}{3}+\frac{\left(e_0a\right)^2\rho A}{L}\right)\cos^2\alpha+\left(\frac{13\rho AL}{35}+\frac{6\left(e_0a\right)^2\rho A}{5L}\right)\sin^2\alpha,\\ m_{12}=m_{45}=\left(-\frac{4\rho AL}{105}-\frac{\left(e_0a\right)^2\rho A}{5L}\right)\cos\alpha\sin\alpha,\ \ m_{13}=\left(-\frac{11\rho AL^2}{210}-\frac{\left(e_0a\right)^2\rho A}{10}\right)\sin\alpha,\\ m_{14}=\left(\frac{\rho AL}{6}-\frac{\left(e_0a\right)^2\rho A}{L}\right)\cos^2\alpha+\left(\frac{9\rho AL}{70}-\frac{6\left(e_0a\right)^2\rho A}{5L}\right)\sin^2\alpha,\\ m_{15}=m_{24}=\left(\frac{4\rho AL}{105}+\frac{\left(e_0a\right)^2\rho A}{5L}\right)\cos\alpha\sin\alpha,\ \ m_{16}=\left(\frac{13\rho AL^2}{420}-\frac{\left(e_0a\right)^2\rho A}{10}\right)\sin\alpha,\end{gathered}$$

$$m_{22}=m_{55}=\left(\frac{\rho AL}{3}+\frac{6\left(e_0a\right)^2\rho A}{5L}\right)\cos^2\alpha+\left(\frac{13\rho AL}{35}+\frac{\left(e_0a\right)^2\rho A}{L}\right)\sin^2\alpha\,,$$

$$m_{23}=\left(\frac{11\rho AL^2}{210}+\frac{\left(e_0a\right)^2\rho A}{10}\right)\cos\alpha\,,$$

$$m_{25}=\left(\frac{9\rho AL}{70}-\frac{6\left(e_0a\right)^2\rho A}{5L}\right)\cos^2\alpha+\left(\frac{\rho AL}{6}-\frac{\left(e_0a\right)^2\rho A}{L}\right)\sin^2\alpha\,,$$

$$m_{26}=\left(-\frac{13\rho AL^2}{420}+\frac{\left(e_0a\right)^2\rho A}{10}\right)\cos\alpha\,,\quad m_{33}=m_{66}=\frac{\rho AL^3}{105}+\frac{2\left(e_0a\right)^2\rho AL}{15}\,,$$

$$m_{34}=\left(-\frac{13\rho AL^2}{420}+\frac{\left(e_0a\right)^2\rho A}{10}\right)\sin\alpha\,,\quad m_{35}=\left(\frac{13\rho AL^2}{420}-\frac{\left(e_0a\right)^2\rho A}{10}\right)\cos\alpha\,,$$

$$m_{36}=-\frac{\rho AL^3}{140}-\frac{\left(e_0a\right)^2\rho AL}{30}\,,\quad m_{46}=\left(\frac{11\rho AL^2}{210}+\frac{\left(e_0a\right)^2\rho A}{10}\right)\sin\alpha\,,$$

$$m_{56}=\left(-\frac{11\rho AL^2}{210}-\frac{\left(e_0a\right)^2\rho A}{10}\right)\cos\alpha \tag{27}$$

Free vibration frequencies of nanoframes are also calculated as in Eq. (20).

4. Discussions

The solution based on matrix displacement method for the nonlocal free dynamics of nano scaled truss and frame structures is mentioned. According to this, the stiffness and mass matrices of the nanostructure members are achieved. When obtained expressions are investigated, it is understood that the stiffness matrices are not affected by the nonlocal parameter, and additionally, the nonlocal parameter is included in the inputs of the mass matrix. The reason for this is the nonlocal parameter is only added as a multiplier to the mass of unit length (ρA) in the equations of motion which the average weighted residue is applied.

5. Conclusions

While studies dealing with the nonlocal mechanics of nanostructures with continuous system models such as beams and rods are numerous, studies on the mechanical analysis of nano scaled structures with discrete models are quite limited. This current study is explained the stiffness and mass matrices in the matrix displacement formulation given for the dynamic analysis of nano scaled trusses and frames are modified how by the nonlocal parameter.

In the nonlocal free dynamic analysis of nanotrusses and nanoframes, the fact that the stiffness matrices are the same as the classical elasticity and the mass matrix increases, shows that the classical natural frequencies will be a decrease due to the nonlocal parameter in the dynamic analysis of the nanostructures consisting of discrete members [26]. Therefore, since the response of the structure to dynamic excitations will decrease, this case should be taken into account in the design of the engineering system where nanostructures may take part.

References

[1] Aydogdu, M., Axial vibration of the nanorods with the nonlocal continuum rod model. *Physica E: Low-dimensional Systems and Nanostructures*, 41, 861-864, 2009.

[2] Adhikari, S., Murmu, T., McCarthy, M.A., Dynamic finite element analysis of axially vibrating nonlocal rods. *Finite Elements in Analysis and Design*, 630, 42-50, 2013.

[3] Demir, Ç., Civalek, Ö., Torsional and longitudinal frequency and wave response of microtubules based on the nonlocal continuum and nonlocal discrete models. *Applied Mathematical Modelling*, 37, 9355-9367, 2013.

[4] Lim, C.W., Islam, M.Z., Zhang, G., A nonlocal finite element method for torsional statics and dynamics of circular nanostructures. *International Journal of Mechanical Sciences*, 94-95, 232-243, 2015.

[5] Zhu, X., Li, L., On longitudinal dynamics of nanorods. *International Journal of Engineering Science*, 120, 129-145, 2017.

[6] Numanoğlu, H.M., Akgöz, B., Civalek, Ö., On dynamic analysis of nanorods. *International Journal of Engineering Science*, 130, 33-50, 2018.

[7] Karlicic, D.Z., Ayed, S., Flaieh, E., Nonlocal axial vibration of the multiple Bishop nanorod system. *Mathematics and Mechanics of Solids*, 24, 1668-1691, 2018.

[8] Nazemnezhad, R., Kamali, K., Free axial vibration analysis of axially functionally graded thick nanorods using nonlocal Bishop's theory. *Steel and Composite Structures*, 28, 749-758, 2018.

[9] Bao, S., Cao, J., Wang, S., Vibration analysis of nanorods by the Rayleigh-Ritz method and truncated Fourier series. *Results in Physics*, 12, 327-334, 2019.

[10] Numanoğlu, H.M., Civalek Ö., On the torsional vibration of nanorods surrounded by elastic matrix via nonlocal FEM, *International Journal of Mechanical Sciences*, 161-162, 105076, 2019.

[11] Civalek, Ö., Numanoğlu, H.M., Nonlocal finite element analysis for axial vibration of embedded Love–Bishop nanorods. *International Journal of Mechanical Sciences*, 188, 105939, 2020.

[12] Reddy, J.N., Nonlocal theories for bending, buckling and vibration of beams. *International Journal of Engineering Science*, 45, 288-307, 2007.

[13] Benzair, A., Tounsi, A., Besseghier, A., Heireche, H., Moulay, N., Boumia, L., The thermal effect on vibration of single-walled carbon nanotubes using nonlocal Timoshenko beam theory. *Journal of Physics D: Applied Physics*, 41, 225404, 2008.

[14] Thai, H.T., A nonlocal beam theory for bending, buckling and vibration of nanobeams. *International Journal of Engineering Science*, 52, 56-64, 2012.

[15] Askari, H., Esmailzadeh, E., Zhang, D., Nonlinear vibration analysis of nonlocal nanowires. *Composites Part B: Engineering*, 67, 607-613, 2014.

[16] Mercan, K., Numanoğlu, H.M., Akgöz, B., Demir, C., Civalek, Ö., Higher-order continuum theories for buckling response of silicon carbide nanowires (SiCNWs) on elastic matrix. *Archive of Applied Mechanics*, 87, 1797-1814, 2017.

[17] Eltaher, M.A., Alshorbagy, A.E., Mahmoud, F.F., Vibration analysis of Euler–Bernoulli nanobeams by using finite element method. *Applied Mathematical Modelling*, 37, 4787-4797, 2013.

[18] Eptaimeros, K.G., Koutsoumaris, C.C., Tsamasphyros, G.J., Nonlocal integral approach to the dynamical response of nanobeams. *International Journal of Mechanical Sciences*, 115-116, 68-80, 2016.

[19] Civalek, Ö., Demir, C., A simple mathematical model of microtubules surrounded by an elastic matrix by nonlocal finite element method. *Applied Mathematics and Computation*, 289, 335-352, 2016.

[20] Numanoğlu, H.M., Uzun, B., Civalek, Ö., Derivation of nonlocal finite element formulation for nano beams. *International Journal of Engineering and Applied Sciences*, 10, 131-139, 2018.

[21] Numanoğlu, H.M., Mercan, K, Civalek, Ö., Finite element model and size-dependent stability analysis of boron nitride and silicon carbide nanowires/nanotubes. *Scientia Iranica Transactions A: Civil Engineering*, 26, 2079-2099, 2019.

[22] Numanoğlu, H.M., Thermal vibration of zinc oxide nanowires by using nonlocal finite element method. *International Journal of Engineering and Applied Sciences*, 12, 99-110, 2020.

[23] Numanoğlu, H.M., Ersoy, H., Civalek, O., Ferreira, A.J.M., Derivation of nonlocal FEM formulation for thermo-elastic Timoshenko beams on elastic matrix. *Composite Structures*, 273, 114292, 2021.

[24] Ersoy, H, Numanoğlu, H.M., Akgöz, B., Civalek Ö., A new eigenvalue problem solver for thermo-mechanical vibration of Timoshenko nanobeams by an innovative nonlocal finite element method. *Mathematical Methods in the Applied Sciences*, 2021.

[25] de Sciarra, F.M., Finite element modelling of nonlocal beams. Physica E: Low-Dimesional Systems and Nanostructures, 59, 144-149, 2014.

[26] Numanoğlu, H.M., Civalek Ö., On the dynamics of small-sized structures, *International Journal of Engineering Science*, 145, 103164, 2019.

[27] Hozhabrossadati, S.M., Challamel, N., Rezaiee-Pajand, M., Sani, A.A., Free vibration of a nanogrid based on Eringen's stress gradient model. *Mechanics Based Design of Structures and Machines*, 2020.

[28] Russillo, A.F., Failla, G., Alotta, G., de Sciarra, F.M., Barretta, R., On the dynamics of nano-frames. *International Journal of Engineering Science*, 160, 103433, 2021.

[29] Numanoğlu, H.M., Mercan, K., Civalek, Ö., Frequency and mode shapes of Au nanowires using the continuous beam models. *International Journal of Engineering and Applied Sciences*, 9, 55-61, 2017.

[30] Numanoğlu, H.M., Nanoyapıların Kiriş ve Çubuk Modellerinin Yerel Olmayan Elastisite Teorisi Kullanılarak Titreşim Analizi. BSc. Thesis, Akdeniz University, Antalya, 2017.

[31] Numanoğlu, H.M., Civalek, Ö., Elastic beam model and bending analysis of silver nanowires. *International Journal of Engineering and Applied Sciences*, 10, 13-20, 2018.

[32] Numanoğlu, H.M., Ersoy, H, Akgöz, B., Civalek Ö., Small size and rotary inertia effects on the natural frequencies of carbon nanotubes. *Curved and Layered Structures*, 5, 273-279, 2018.

[33] Akgöz, B., Civalek Ö., Vibrational characteristics of embedded microbeams lying on a two-parameter elastic foundation in thermal environment. *Composites Part B: Engineering*, 150, 68-77, 2018.

[34] Akgöz, B., Civalek, Ö., Investigation of size effects on static response of single-walled carbon nanotubes based on strain gradient elasticity. *International Journal of Computational Methods*, 9, 1240032, 2012.

[35] Civalek, Ö., Kiracioglu, O., Free vibration analysis of Timoshenko beams by DSC method. *International Journal for Numerical Methods in Biomedical Engineering*, 26, 1890-1898, 2010.

[36] Mercan, K., Demir, Ç., Civalek, Ö., Vibration analysis of FG cylindrical shells with power-law index using discrete singular convolution technique. *Curved and Layered Structures*, 3, 82-90, 2016.

[37] Dastjerdi, S., Akgöz, B., Civalek, Ö., On the effect of viscoelasticity on behavior of gyroscopes. *International Journal of Engineering Science*, 149, 103236, 2020.

[38] Civalek, Ö., Dastjerdi, S., Akbaş, Ş.D., Akgöz, B., Vibration analysis of carbon nanotube-reinforced composite microbeams. *Mathematical Methods in the Applied Sciences*, 2021.

[39] Dastjerdi, S., Akgöz, B., New static and dynamic analyses of macro and nano FGM plates using exact three-dimensional elasticity in thermal environment. *Composite Structures*, 192, 626-641, 2018.

[40] Uzun, B, Numanoğlu, H.M., Civalek, Ö., Definition of length-scale parameter in Eringen's nonlocal elasticity via nolocal lattice and finite element formulation. *International Journal of Engineering and Applied Sciences*, 10, 264-275, 2018.

[41] Numanoğlu, H.M., Dynamic analysis of nano continuous and discrete structures based on nonlocal finite element formulation (NL-FEM). MSc. Thesis, Akdeniz University, Antalya, 2019, (In Turkish).

International Journal of Engineering & Applied Sciences (IJEAS)
Vol.13, Issue 4 (2021) 166-178
http://dx.doi.org/10.24107/ijeas.1037908
Int J Eng Appl Sci 13(4) (2021) 166-178

Optimum Design of Reinforced Concrete T-Beam Considering Environmental Factors via Flower Pollination Algorithm

Aylin Ece Kayabekir [a], Gebrail Bekdaş [b], Sinan Melih Nigdeli [c]*

[a] Istanbul Gelişim University, Civil Engineering Department, 34310 Avcılar, Istanbul/Tukey
[b,c] Istanbul University-Cerrahpaşa, Civil Engineering Department, 34320 Avcılar, Istanbul/Tukey
[*]E-mail address: melihnig@iuc.edu.tr

ORCID numbers of authors:
0000-0003-3592-4564[a], 0000-0002-7327-9810[b], 0000-0002-9517-7313[c]

Received date: 17.12.2021
Accepted date: 29.12.2021

Abstract

The minimum cost designs may be costly for the environment. In that case, the cost is not only a single objective in the design of structures. In that situation, CO_2 emission minimization can be considered in the optimum design. In this study, reinforced concrete (RC) T-beams were optimized via flower pollination algorithm for the environmental factor minimizing the CO_2 emission of the materials. The investigation was done for 4 cases of CO_2 emission values and these cases were compared with 5 cases of the cost ratios of concrete and steel. Due to this investigation, it was found that CO_2 emission optimization is effective in the reduction of the CO_2 emission value by 4.5% compared to cost optimization. If the ratios of CO_2 emission and the cost of steel per concrete are different, the optimum design variables and objectives are different. Also, the use of recycled steel is %.30.24 more effective on the reduction of CO_2 emission and saving the planet.

Keywords: Metaheuristic; Carbon Minimization; Cost Optimization; Eco-friendly design; Minimum carbon emission.

1. Introduction

Due to a shortage of resources and sustainability, engineering design must be eco-friendly. In structural engineering, choosing eco-friendly or recycled material can play an important role. For the design of steel structures, the eco-friendliest material can be chosen, and it is optimum in minimization of CO_2 emission if it has the same strength as the one with a higher emission value. Also, optimization can be done if the strengths are different for the steel types to find a design that has low CO_2 emissions.

The optimization is more challenging for RC structures. For RC structures, two materials such as concrete and steel are used to provide a design in required ductility. These materials have different costs and different CO_2 emissions. Also, the design is constrained by the factors given in design regulations. These problems can be only optimized via numerical iterations and the best way to apply numerical iteration systematically, effectively, and rapidly is through the usage of metaheuristic methods.

To reach the optimum solution of RC members, various metaheuristic algorithms have been employed. The genetic algorithm that uses the factors such as mutation, crossover, reproduction [1-2] was used in the optimum design of RC beams with rectangular cross-section [3], RC continuous beams [4], RC biaxial columns [5-6], RC frames [6] and RC T-beams [7]. Also, hybrid methods that combines GA with sequential quadratic programming [8], simulating annealing [9-10] and Hook and Jeeves method [11-12] were used to optimize RC members.

Harmony Search (HS) that imitates the musical performances and uses the harmony memory of musicians was also employed in many cost optimization methods for T-beams [13], slender columns [14-15], shear walls [16], frames [17-19] and retaining walls [20-21].

The number of metaheuristic-based cost optimization studies for RC members shows a great increase in the last decade and several examples are as follows.

An artificial bee colony algorithm was employed to optimize RC continuous beams by modifying the algorithm by Jahjouh et al. [22]. Nigdeli et al. [23] proposed a HS-based methodology for bi-axial loading of RC columns. Bat algorithm [24] and teaching-learning-based optimization (TLBO) [25] were employed for the optimum design of RC columns. Swarm intelligence was also used in the optimum design of RC members by Esfandiary et al. [26] and Chutani and Singh [27]. Kayabekir et al. employed the single-phase and parameter-free Jaya algorithm (JA) to optimize T-beams [28]. Also, Kayabekir et al. [29] evaluated four metaheuristics including HS, TLBO, JA, and Flower pollination algorithm (FPA) for the optimum design of RC T-beams, and Kayabekir and Nigdeli [30] statistically compared these algorithms according to methods such as one-way ANOVA, independent samples t-test, Friedman ranking, post-hoc Bonferroni test. By employing FPA, RC footings [31], RC cantilever retaining walls [32], and 3D RC frames [33] were optimized.

Generally, the objective function is the cost minimization, but optimization studies related with CO_2 emission minimization have been conducted. These studies include optimization of RC frames via simulated annealing [34], RC columns via GA [35], RC frames via big-bang big crunch algorithm (BB-BC) [36], precast-prestressed concrete U beam road bridges via hybrid glowworm swarm algorithm [37], post-tensioned concrete box-girders via HS [38], RC footings via BB-BC [39], RC cantilever solider piles via HS [40], RC retaining walls via HS [41], and concrete-filled steel tubular columns via spider and HS algorithms [43-43].

In the present study, the T-beam optimization is presented via FPA for CO_2 minimization. The results were compared with cost optimization results ad multiple cases of cost ad CO_2 ratios steel and concrete is investigated.

2. Flower Pollination Algorithm Optimization Procedure

The principles of the flower pollination algorithm optimization process were first introduced by Xin-She Yang in 2012 [44]. In this algorithm, Yang expressed his observations of the pollination characteristics of flowering plants with mathematical equations and then developed an algorithm including these equations to perform the optimum search process.

According to this; similar to the pollination process inspired by the algorithm, two different processes called global and local pollination are applied probabilistically in the optimization process. Global pollination is the pollination process of flowers through a carrier (such as wind, and various living things), and it is expressed in the algorithm as follows.

$$x_i^{t+1} = x_i^t + r1 \cdot (x_b^t - x_i^t) \tag{1}$$

Local pollination, on the other hand, refers to the pollination process carried out by the flower itself and was expressed by Yang as follows.

$$x_i^{t+1} = x_i^t + r2 \cdot \left(x_j^t - x_k^t\right) \tag{2}$$

In the equations, x_i^{t+1} is the new solution generated from the x_i^t solution, x_b^t is the best existing solution, x_j^t and x_j^t are two randomly selected solutions from the exiting solutions, r1 is the levy flight and r2 is a randomly generated decimal number between 0 and 1.

The application of the equations for optimum design of the reinforced concrete T-beam (Fig. 1) and processes of FPA can be summarized in five steps. The flowchart of the optimization is given as Fig. 2.

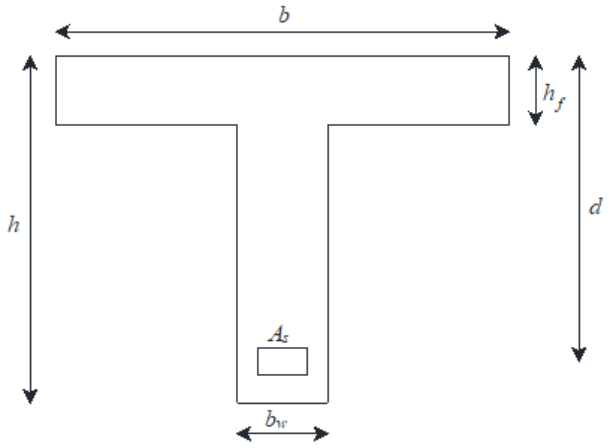

Fig. 1. Cross-section of T-shaped beam [29]

The first step is the stage where the problem is defined. At this stage, the data defined for the problem are the design constants, the lower and upper limits of the design variables, the FPA algorithm parameters, the number of solution vectors (pn), the switch probability (sp), and the maximum number of iterations as the stopping criterion. The definitions of design constants and variables and their values used in the numerical example are taken from Fedghouche and Tiliouine [7] and presented in Tables 1 and 2, respectively. The Eurocode 2 [45] regulation and the technical constraints that the section must provide are defined in Table 3.

Table 1. The design constants

Symbol	Definition	Value
f_{ck}	Characteristic compressive strength for concrete	20 MPa
f_{cd}	Allowable compressive strength for concrete	11.33 MPa
f_{yd}	Characteristic yield strength of reinforcement	348 MPa
ρ_{max}	The maximum reinforcement ratio	0.04
ρ_{min}	The minimum reinforcement ratio	0.0013
L	The length of the beam	20 m
E_s	Young's elastic modules for steel	200000 MPa
M_{Ed}	The ultimate bending moment capacity	4.991 N.m

V_{Ed}	The ultimate bending moment capacity	1.039 N
C_s /C_c	The ratio for unit steel and concrete costs	5, 10, 20, 30, 36
$C_{s,co2}$ /$C_{c,co2}$	The ratio for unit steel and concrete costs	0.95, 10, 15, 20

In the second step, the initial solution matrix is constructed. The design variables are generated randomly within the minimum ($x_{i,min}$) and maximum ($x_{i,max}$) ranges defined in the first step and recorded in this matrix (Eq. (3)).

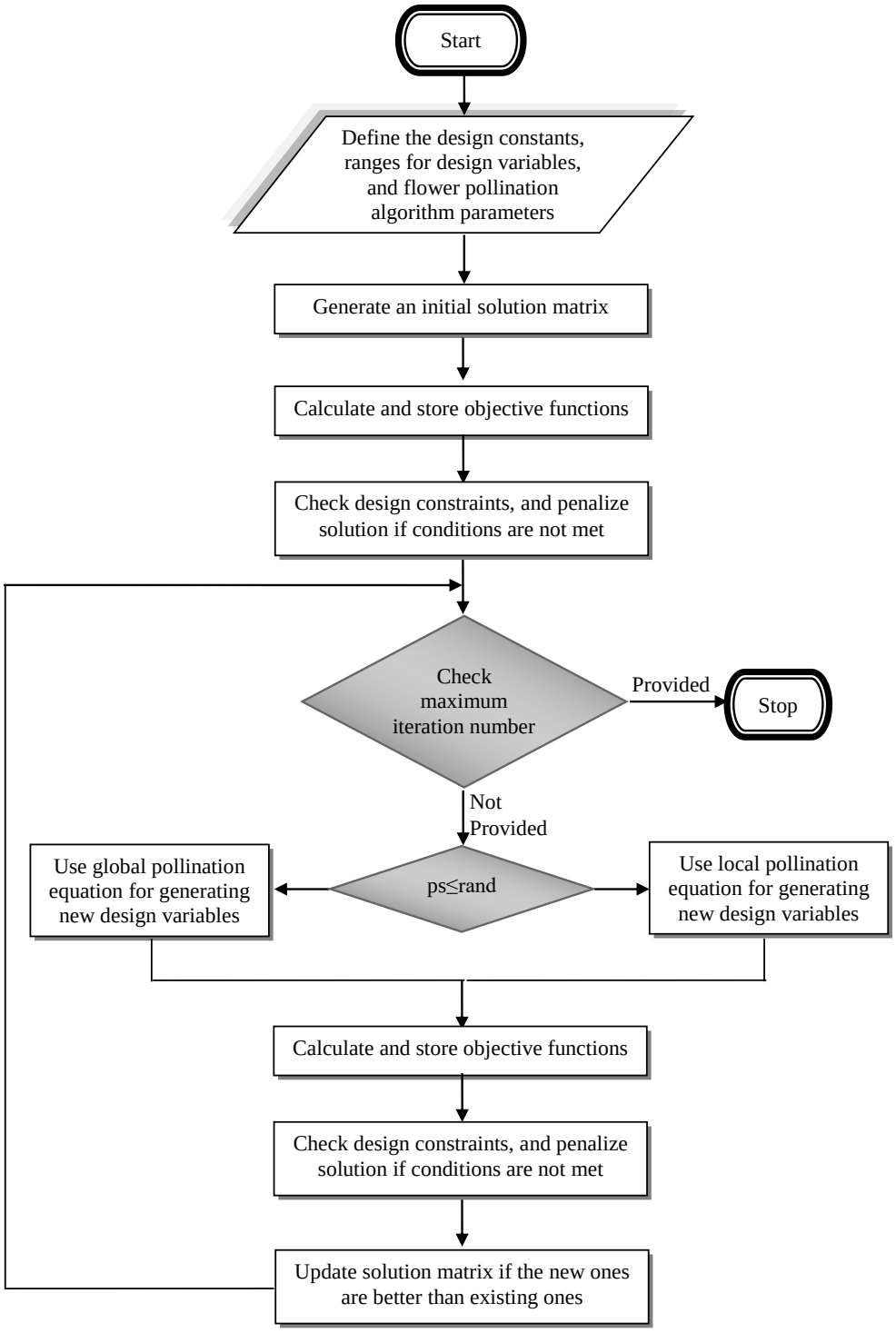

Fig. 2. Flowchart of the optimization process

$$x_i = x_{i,min} + r3 \cdot \left(x_{i,max} - x_{i,min}\right) \tag{3}$$

Table 2. Ranges of design variables

Symbol	Definition	Minimum	Maximum
b	Effective with of compressive flange [mm]	b_w	min $[0.2L + b_w, 8h_f]$
b_w	Web width [mm]	0.2d	0.4d
h	Height [mm]	L/16	2.0
h_f	Flange depth [mm]	0.15	d
d	Effective depth [mm]	0.9h	
d_s	Cover of reinforcements [mm]	0.1h	
A_s	Area of reinforcing steel [mm^2]	0	0.1

Table 3. The design constraints

$\omega(1 - 0.5\omega) \leq 0.392$
$0.0035(0.8 - \omega)/\omega \geq f_{yd}/E_s$
$\rho_{min} \leq \rho \leq \rho_{max}$
$M_{Ed} \leq M_{Ed1}$
$V_{Ed} \leq V_{Rd\,max}$

After the design variables are determined, beam reinforced concrete designs are performed for each solution (from first to pn number of solutions) in the initial solution matrix. The reinforced concrete design must satisfy the Eurocode 2 [45] regulation constraints presented in Table 3 calculated based on Eqs. (4)-(9) for the situation without shear reinforcement optimization as presented in Fedghouche and Tiliouine [7].

$$\omega = (f_{yd}/f_{cd})(A_s/b_w d) - (b - b_w)h_f/(b_w d) \tag{4}$$

$$\rho = A_s/(b_w d) \tag{5}$$

$$M_{Ed1} = f_{cd}(b - b_w)h_f\left(d - 0.50h_f\right) + f_{cd}b_w d^2\omega(1 - 0.5\omega) \tag{6}$$

$$V_{Rd\,max} = \nu_1 f_{cd} b_w z/(tan(45) + cot\,(45)) \tag{7}$$

$$\nu_1 = 0.6(1 - f_{ck}/250) \tag{8}$$

$$z = 0.9d \tag{9}$$

Finally, in this step, the total CO_2 emission value for each beam design is calculated and stored as the corresponding solution. This expression is the objective function of the optimization problem. If constraints are provided in the design, the solution is evaluated by subjecting the objective function of the design to a process called penalty. In the literature, various penalty

methods are depending on the problem. In this study, equating the objective function to a high value (10^6) was applied.

$$f_{co2}(x) = \mathrm{C}_{c,co2} b_w d + \mathrm{C}_{c,co2}(b - b_w)h_f + (\mathrm{C}_{s,co2}/\mathrm{C}_{c,co2})A_s \quad (10)$$

For the compared cases for cost optimization, the objective function as the total beam cost is shown in Eq. (11).

$$f_{cost}(x) = \mathrm{C}_c b_w d + \mathrm{C}_c(b - b_w)h_f + (\mathrm{C}_s/\mathrm{C}_c)A_s \quad (11)$$

In the third step, the new solutions are derived. According to the algorithm rules, one of the global (Eq. (1)) or local (Eq. (2)) pollination equations is used to generate a new solution. The value of switch probability (sp) is used for the global and local pollination probabilistic selection. According to this; if the randomly generated number between 0 and 1 is less than the sp value, new solutions are generated according to global pollination, otherwise, local pollination rules are applied.

In the fourth step, old and new solutions are compared. The objective functions of each solution are compared, in case the new solution is better (the objective function is lower), the existing solution is deleted and the values of the new solution are saved instead. Otherwise, the existing solution is preserved.

In the last step, the stopping criterion is checked. New solution generation and comparison processes (steps 3 and 4) are repeated until the criterion is determined in the first step as the maximum number of iterations are met.

3. Numerical Examples

For the T-beam given in Figure 1, the analysis was carried out by the numerical values of the design constants, design constraints, and design variable limits given in Section 2. Analysis with the objective function of the total beam cost was also performed simultaneously to compare with the optimization results for CO_2 emission.

As it is known, unit costs of concrete and steel vary in different parts of the world. To take this situation into account, 5 different steel and concrete unit cost ratios were taken into account in the analysis. Information on these cases is presented in Table 4.

Table 4. Cases for Cost optimization

Case No	1	2	3	4	5
C_s /C_c	36	30	20	10	5

A similar situation is seen in unit carbon emission rates. In addition to many factors such as the materials and additive rates in the concrete content and the production method, the recycled material content of the steel, even the region where the materials are produced affects the unit carbon emission rates of these materials. To take these variations into account, studies in the literature were examined and carbon emission ratios were determined for four different steel and concrete units [34, 46]. The carbon emission rates in question are shown in Table 5. Case 6 shows the value for the use of recycled steel.

Table 5. Cases for CO_2 optimization

Case No	6	7	8	9
$C_{s,co2}$ /$C_{c,co2}$	0.95	10	15	20

The optimum results for these cases are given in Tables 6 and 7. In addition to the optimum results of the design variables, the carbon emission and total cost values for the relevant cases are presented in the tables to examine the cost-carbon emission relationship.

Table 6. Optimum results for cost optimization

Design variables	Case 1	Case 2	Case 3	Case 4	Case 5
b (m)	1.137640	1.155663	1.229911	1.330057	1.378292
b_w (m)	0.304351	0.298164	0.291116	0.278516	0.272245
h (m)	1.690838	1.656469	1.617309	1.547309	1.512473
d (m)	1.521755	1.490822	1.455578	1.392578	1.361225
h_f (m)	0.150000	0.150000	0.153739	0.166323	0.172287
A_s (m^2)	0.011414	0.011870	0.012071	0.012442	0.012651
ω	0.487053	0.530813	0.534350	0.534348	0.534351
$f_{cost}(x)$	0.999034	0.929226	0.809488	0.687166	0.624400
$C_{s,co2}$ /$C_{c,co2}$=0.95	0.598984	0.584411	0.579538	0.574569	0.573162
$C_{s,co2}$ /$C_{c,co2}$=10	0.702278	0.691832	0.688780	0.687166	0.687656
$C_{s,co2}$ /$C_{c,co2}$=15	0.759346	0.751180	0.749134	0.749375	0.750912
$C_{s,co2}$ /$C_{c,co2}$=20	0.827828	0.822398	0.821559	0.824025	0.826819

Table7. Optimum results for CO_2 optimization

Design variables	Case 6	Case 7	Case 8	Case 9
b (m)	1.382218	1.327519	1.278476	1.217860
b_w (m)	0.271727	0.278872	0.285113	0.292575
h (m)	1.509592	1.549286	1.583961	1.625415
d (m)	1.358633	1.394358	1.425565	1.462873
h_f (m)	0.172777	0.165940	0.159810	0.152232
A_s (m^2)	0.012669	0.012430	0.012239	0.012032
ω	0.534351	0.534351	0.534345	0.534351
$f_{co2}(x)$	0.573080	0.687161	0.748787	0.821529
C_s /C_c=5	0.624391	0.625010	0.626393	0.629018
C_s /C_c=10	0.687737	0.687161	0.687590	0.689178
C_s /C_c=20	0.814431	0.811463	0.809984	0.809497

C_s/C_c=30	0.941124	0.935765	0.932378	0.929817
C_s/C_c=36	1.01714	1.010347	1.005815	1.002009

4. Discussion of The Results

As seen in Fig. 3, by the increase of the cost of steel bars concerning the cost of concrete, the cross-section dimensions are increasing in size for b_w, h_f, and d. In that case, the area of rebar is approximately reduced by 1 dm^2. The increase in the flange of the beam also results in the increase of rebar for equilibrium. In that case, h is optimally chosen to be increased to reduce the amount of rebar that has a high cost. The optimization methodology can decide it and it shows a relationship with the theory of RC design.

As seen from Fig. 3, the reduction of cost ratio of steel per column reduces the total optimum cost. For Case 1 to 5, a significant difference for CO_2 emission is not seen if $C_{s,co2}/C_{c,co2}$ is bigger than 10, but the CO_2 emission for Case 5 is 4.5% better than Case 1 if $C_{s,co2}/C_{c,co2}$=0.95.

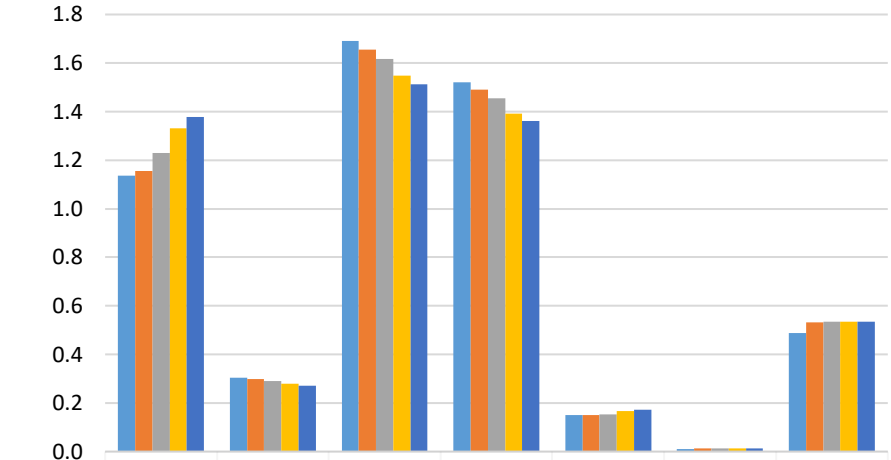

	b (m)	bw (m)	h (m)	d (m)	hf (m)	As (m2)	ω
Case 1	1.137640	0.304351	1.690838	1.521755	0.150000	0.011414	0.487053
Case 2	1.155663	0.298164	1.656469	1.490822	0.150000	0.011870	0.530813
Case 3	1.229911	0.291116	1.617309	1.455578	0.153739	0.012071	0.534350
Case 4	1.330057	0.278516	1.547309	1.392578	0.166323	0.012442	0.534348
Case 5	1.378292	0.272245	1.512473	1.361225	0.172287	0.012651	0.534351

Fig. 3. Design variables for the cost optimization

As seen in Fig. 5, the increase of $C_{s,co2}/C_{c,co2}$ shows the same increases and decreases as cost optimization for the cross-section dimensions. Fig. 6 shows the CO_2 emission and cost concerning different cost ratios. In CO_2 minimization, it is possible to find solutions with lower CO_2 emissions than the results found via cost optimization. For cost optimization results of Case 5, the gap between CO_2 values for cost and CO_2 optimization closes.

In CO_2 optimization, Case 6 has a marginal $C_{s,co2}/C_{c,co2}$ ratio that can reflect a case of using recycled steel. In this case, the dimensions of b and h_f are the biggest compared to all cases. In Case 9, the costs are close to cost optimization results. This proves that cost and CO_2

optimization may have very different optimum results if $C_{s,co2}$/ $C_{c,co2}$, and C_s/ C_c are different. The use of recycled steel is 30.24% more eco-friendly comparing to Case 9.

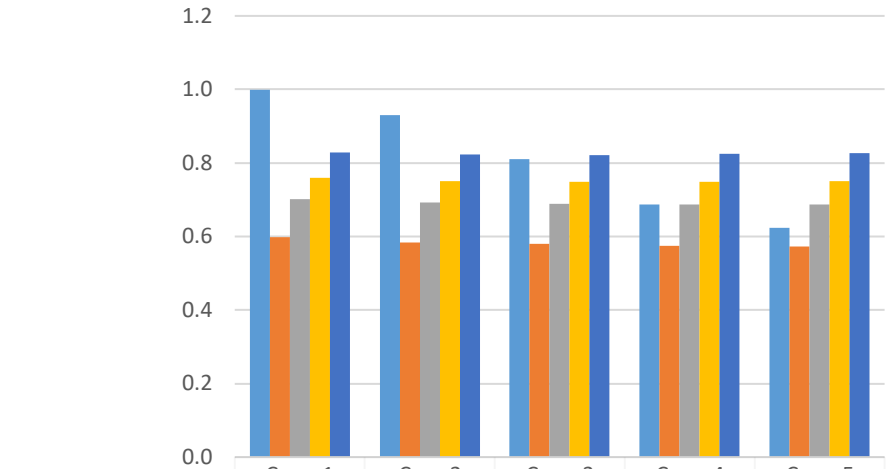

	Case 1	Case 2	Case 3	Case 4	Case 5
fcost(x)	0.999034	0.929226	0.809488	0.687166	0.624400
Cs,co2 /Cc,co2=0.95	0.598984	0.584411	0.579538	0.574569	0.573162
Cs,co2 /Cc,co2=10	0.702278	0.691832	0.688780	0.687166	0.687656
Cs,co2 /Cc,co2=15	0.759346	0.751180	0.749134	0.749375	0.750912
Cs,co2 /Cc,co2=20	0.827828	0.822398	0.821559	0.824025	0.826819

Fig. 4. Objective functions for cost optimization

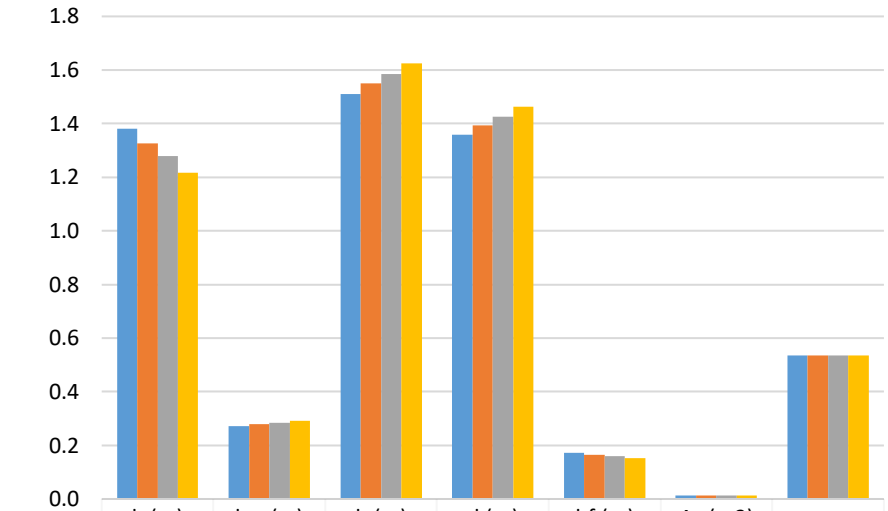

	b (m)	bw (m)	h (m)	d (m)	hf (m)	As (m2)	ω
Case 6	1.382218	0.271727	1.509592	1.358633	0.172777	0.012669	0.534351
Case 7	1.327519	0.278872	1.549286	1.394358	0.165940	0.012430	0.534351
Case 8	1.278476	0.285113	1.583961	1.425565	0.159810	0.012239	0.534345
Case 9	1.217860	0.292575	1.625415	1.462873	0.152232	0.012032	0.534351

Fig. 5. Design variables for the CO_2 optimization

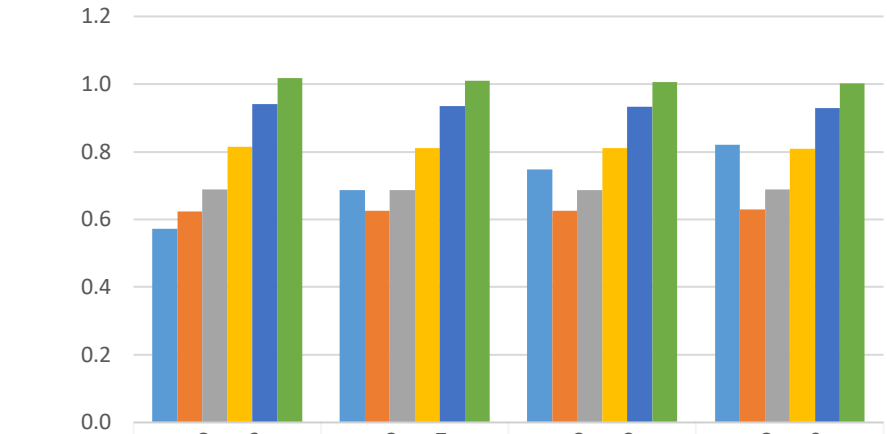

	Case 6	Case 7	Case 8	Case 9
Fx	0.573080	0.687161	0.748787	0.821529
Cs /Cc=5	0.624391	0.625010	0.626393	0.629018
Cs /Cc=10	0.687737	0.687161	0.687590	0.689178
Cs /Cc=20	0.814431	0.811463	0.809984	0.809497
Cs /Cc=30	0.941124	0.935765	0.932378	0.929817
Cs /Cc=36	1.01713989	1.010346646	1.005814598	1.002008735

Fig. 6. Objective functions for the CO_2 optimization

5. Conclusion

In the present paper, an optimization methodology for the CO_2 emission minimization of T-beams is presented. To find out the differences between CO_2 and cost optimization, both objectives are calculated for multiple cases of cost and CO_2 emission ratios of steel and concrete. According to the results, the cross-section dimensions ad steel reinforcement area shows great differences for these ratios. For both increases of cost and CO_2 emission of steel, the optimum design tends to be minimum in reinforcement area and maximum in the moment arm value by increasing the height and directly increasing the depth of T-beam.

Since the cost and CO_2 objectives are similar in form with the only difference in cost and CO_2 values of the materials, the behavior is the same in CO_2 and cost optimization. Due to that, the difference in CO_2 values for cost and CO_2 optimization are close if cost and CO_2 ratios of steel per concrete are similar as seen from the results of Case 3 and Case 9 or Case 4 and Case 7. This is not acceptable for Case 6 where recycled steel bars are used. This case has 4.5% reduced CO_2 emission concerning cost optimization and 30.24% reduced CO_2 emission compared to Case 9.

As the final remarks, CO_2 optimization may have different optimum results if C_s/ C_c and $C_{s,co2}$/ $C_{c,co2}$ are different. Also, recycled steel is very useful in the protection of the earth by conducting an optimum design.

References

[1] Goldberg, D.E.: Genetic algorithms in search, Optimization and machine learning. Boston MA: Addison Wesley, 1989.

[2] Holland, J.H.: Adaptation in Natural and Artificial Systems. Ann Arbor MI: University of Michigan Press, 1975.

[3] Coello, C. C., Hernández, F. S., Farrera, F. A., Optimal design of reinforced concrete beams using genetic algorithms. Expert systems with Applications, 12(1), 101-108, 1997.

[4] Koumousis, V. K., & Arsenis, S. J., Genetic algorithms in optimal detailed design of reinforced concrete members. Computer-Aided Civil and Infrastructure Engineering, 13(1), 43-52, 1998.

[5] Rafiq, M. Y., & Southcombe, C., Genetic algorithms in optimal design and detailing of reinforced concrete biaxial columns supported by a declarative approach for capacity checking. Computers & Structures, 69(4), 443-457, 1998.

[6] Camp, C. V., Pezeshk, S., & Hansson, H., Flexural design of reinforced concrete frames using a genetic algorithm. Journal of Structural Engineering, 129(1), 105-115, 2003.

[7] Fedghouche, F., & Tiliouine, B., Minimum cost design of reinforced concrete T-beams at ultimate loads using Eurocode2. Engineering Structures, 42, 43-50, 2012

[8] Rath, D. P., Ahlawat, A. S., & Ramaswamy, A., Shape optimization of RC flexural members. Journal of Structural Engineering, 125(12), 1439-1446, 1999.

[9] Govindaraj, V., & Ramasamy, J. V., Optimum detailed design of reinforced concrete continuous beams using genetic algorithms. Computers & structures, 84(1-2), 34-48, 2005.

[10] Lepš, M., & Šejnoha, M., New approach to optimization of reinforced concrete beams. Computers & structures, 81(18-19), 1957-1966, 2003.

[11] Sahab, M. G., Ashour, A. F., & Toropov, V. V., A hybrid genetic algorithm for reinforced concrete flat slab buildings. Computers & structures, 83(8-9), 551-559, 2005.

[12] Sahab, M. G., Ashour, A. F., & Toropov, V. V., Cost optimisation of reinforced concrete flat slab buildings. Engineering Structures, 27(3), 313-322, 2005.

[13] Bekdaş, G., & Nigdeli, S. M., Optimization of T-shaped RC flexural members for different compressive strengths of concrete. International Journal of Mechanics, 7, 109-119, 2013.

[14] Bekdas, G., & Nigdeli, S. M., The optimization of slender reinforced concrete columns. PAMM, 14(1), 183-184, 2014.

[15] Bekdaş G., & Nigdeli S.M., The Effect of Eccentricity for Optimum Compressively Loaded Reinforced Concrete Column. In 15th EU/ME Workshop: Metaheuristic and Engineering, Istanbul, Turkey, 2014.

[16] Nigdeli S.M., & Bekdaş G., Optimization of reinforced concrete shear walls using harmony search. In 11th International Congress on Advances in Civil Engineering, Istanbul, Turkey, 2014.

[17] Akin, A., & Saka, M. P., Harmony search algorithm based optimum detailed design of reinforced concrete plane frames subject to ACI 318-05 provisions. Computers & Structures, 147, 79-95, 2015.

[18] Bekdaş G., & Nigdeli S.M., Optimization of RC Frame Structures Subjected to Static Loading. 11th. World Congress on Computational Mechanics, Barcelona, Spain, 2014.

[19] Ulusoy S., Kayabekir A.E., Bekdaş G., & Nigdeli S.M., Optimum Design of Reinforced Concrete Multi-Story Multi-Span Frame Structures under Static Loads. In 8th International Conference on Environment Science and Engineering (ICESE 2018), Barcelona, Spain, 2018.

[20] Akin, A. & Saka, M.P., Optimum Detailed Design of Reinforced Concrete Continuous Beams using the Harmony Search Algorithm, In The Tenth International Conference on Computational Structures Technology, Paper 131, Stirlingshire, UK, 2010.

[21] Kayabekir, A. E., Arama, Z. A., & Bekdas, G., Effect of application factors on optimum design of reinforced concrete retaining systems. Structural Engineering and Mechanics, 80(2), 113-127, 2021.

[22] Jahjouh, M. M., Arafa, M. H., & Alqedra, M. A., Artificial Bee Colony (ABC) algorithm in the design optimization of RC continuous beams. Structural and Multidisciplinary Optimization, 47(6), 963-979, 2013.

[23] Nigdeli, S. M., Bekdas, G., Kim, S., & Geem, Z. W., A novel harmony search based optimization of reinforced concrete biaxially loaded columns. Structural Engineering and Mechanics, 54(6), 1097-1109, 2015.

[24] Bekdaş G., & Nigdeli S.M., Bat algorithm for optimization of reinforced concrete columns. In Joint Annual Meeting of GAMM and DMV, Braunschweig, Germany, 2016.

[25] Bekdaş G., & Nigdeli S.M., Optimum Design Of Reinforced Concrete Columns Employing Teaching Learning Based Optimization. In 12th International Congress on Advances in Civil Engineering, Istanbul, Turkey, 2016.

[26] Esfandiary, M. J., Sheikholarefin, S., & Bondarabadi, H. R., A combination of particle swarm optimization and multi-criterion decision-making for optimum design of reinforced concrete frames. International Journal of Optimization in Civil Engineering, 6(2), 245-268, 2016.

[27] Chutani, S., & Singh, J., Use of modified hybrid PSOGSA for optimum design of RC frame. Journal of the Chinese Institute of Engineers, 41(4), 342-352, 2018.

[28] A. E. Kayabekir, G. Bekdaş and S. M. Nigdeli, Optimum Design of T-Beams Using Jaya Algorithm in 3rd International Conference on Engineering Technology and Innovation (ICETI), Belgrad, Serbia, 2019.

[29] Kayabekir, AE, Bekdaş G, Nigdeli SM. Evaluation of Metaheuristic Algorithm on Optimum Design of T-Beams, 6th International Conference on Harmony Search, Soft Computing and Applications (ICHSA 2020), 16-17 July 2020, Istanbul, Turkey.

[30] Kayabekir, A. E., & Nigdeli, M., Statistical Evaluation of Metaheuristic Algorithm: An Optimum Reinforced Concrete T-beam Problem. In Advances in Structural Engineering—Optimization 299-310. Springer, Cham, 2021.

[31] Nigdeli, Sinan Melih, Gebrail Bekdaş, and Xin-She Yang. Metaheuristic optimization of reinforced concrete footings. KSCE Journal of Civil Engineering, 22.11(2018), 4555-4563, 2018.

[32] Mergos, P. E., & Mantoglou, F., Optimum design of reinforced concrete retaining walls with the flower pollination algorithm. Structural and Multidisciplinary Optimization, 61(2), 575-585, 2020.

[33] Mergos, P. E., Optimum design of 3D reinforced concrete building frames with the flower pollination algorithm. Journal of Building Engineering, 44, 102935, 2021.

[34] Paya-Zaforteza, I., Yepes, V., Hospitaler, A., & Gonzalez-Vidosa, F., CO2-optimization of reinforced concrete frames by simulated annealing. Engineering Structures, 31(7), 1501-1508, 2009.

[35] Park, H. S., Kwon, B., Shin, Y., Kim, Y., Hong, T., & Choi, S. W., Cost and CO2 emission optimization of steel reinforced concrete columns in high-rise buildings. Energies, 6(11), 5609-5624, 2013.

[36] Camp, C. V., & Huq, F., CO2 and cost optimization of reinforced concrete frames using a big bang-big crunch algorithm. Engineering Structures, 48, 363-372, 2013.

[37] Yepes, Víctor, José V. Martí, and Tatiana García-Segura. Cost and CO2 emission optimization of precast–prestressed concrete U-beam road bridges by a hybrid glowworm swarm algorithm. Automation in Construction, 49 (2015), 123-134, 2015.

[38] García-Segura, T., Víctor Y., Multiobjective optimization of post-tensioned concrete box-girder road bridges considering cost, CO2 emissions, and safety. Engineering Structures, 125 (2016): 325-336, 2016.

[39] Camp, C. V., and Andrew, A., CO2 and cost optimization of reinforced concrete footings subjected to uniaxial uplift. Journal of Building Engineering, 3 (2015), 171-183, 2015.

[40] Arama, Z. A., Kayabekir, A. E., Bekdaş, G., & Geem, Z. W., CO2 and cost optimization of reinforced concrete cantilever soldier piles: a parametric study with harmony search algorithm. Sustainability, 12(15), 5906, 2020.

[41] Kayabekir, A. E., Arama, Z. A., Bekdaş, G., Nigdeli, S. M., & Geem, Z. W., Eco-friendly design of reinforced concrete retaining walls: multi-objective optimization with harmony search applications. Sustainability, 12(15), 6087, 2020.

[42] Cakiroglu, C., Islam, K., Bekdaş, G., & Billah, M., CO2 Emission and Cost Optimization of Concrete-Filled Steel Tubular (CFST) Columns Using Metaheuristic Algorithms. Sustainability, 13(14), 8092, 2021.

[43] Cakiroglu, C., Islam, K., Bekdaş, G., Kim, S., & Geem, Z. W., CO2 Emission Optimization of Concrete-Filled Steel Tubular Rectangular Stub Columns Using Metaheuristic Algorithms. *Sustainability*, 13(19), 10981, 2021

[44] Yang, X. S. Flower pollination algorithm for global optimization. In International conference on unconventional computing and natural computation, Springer, Berlin, Heidelberg. 240-249, 2012

[45] EN (Veranst.): EN 1992-1-1 Eurocode 2: Design of concrete structures. Brussels : CEN, 2005

[46] Yeo, Dong Hun, and Florian A. Potra. Sustainable design of reinforced concrete structures through CO_2 emission optimization. Journal of Structural Engineering, 141(3), B4014002, 2015.

International Journal of Engineering & Applied Sciences (IJEAS)
Vol.13, Issue 4 (2021) 179-188
http://dx.doi.org/10.24107/ijeas.1036951
Int J Eng Appl Sci 13(4) (2021) 179-188

Bending Analysis of Functionally Graded Nanobeam Using Chebyshev Pseudospectral Method

Nurettin Şenyer [a], Nihat Can [b], İbrahim Keles [c]*

[a] Samsun University, Faculty of Engineering, Department of Software Engineering, Samsun, Turkey
[b] Ondokuz Mayıs University, Faculty of Engineering, Department of Mechanical Engineering, Samsun, Turkey
[c] Samsun University, Faculty of Engineering, Department of Mechanical Engineering, Samsun 55080, Turkey
[*]E-mail address: ibrahim.keles@samsun.edu.tr

ORCID numbers of authors:
0000-0002-2324-9285 [a], 0000-0002-5741-0890 [b], 0000-0001-8252-2635 [c]

Received date: 15.12.2021
Accepted date: 30.12.2021

Abstract

Static performance of functionally graded cantilever nanobeams exposed to lateral and axial loads from the end was examined by applying the Pseudospectral Chebyshev Method. A solution is given for bending analysis using Euler-Bernoulli beam theory. The nonlocal elasticity theory was first introduced by Eringen and is used to represent effect on a small scale. Using the aforementioned theory, the governing differential equations the phenomenon for functionally graded nanobeams are reproduced. It is supposed that the modulus of elasticity of the beam changes exponentially in the x-axis direction, except for the values taken as constant. The exponential change of material properties may not allow analytical problems to be solved with known methods. Therefore, numerical approach is inevitable for the solution of the problem.

Keywords: Nonlocal elasticity theory, nanobeam, Chebyshev pseudospectral method, bending analysis

1. Introduction

Functionally graded materials (FGMs) have gained wide application in different industrial areas due to varying toughness and other material properties in the form of graded functions along certain dimensions. In order to have two opposite properties such as high thermal conductivity and high thermal resistance, which are found in FGMs, in a material, a lot of research has been done in the literature for static, buckling and dynamic conditions in order to lightness, strength and durability [1,2,11–15,3–10].

With the rapid advancement of technology, FGMs have begun to be used in applied engineering fields in micro or nanoscale structures[14]. These materials, which have superior technical and physical properties, are of great importance in the pharmaceutical industry, especially with their use in electrically operated Micro-Electro-Mechanical Systems (MEMS)[16] and atomic force microscopes (AFMs) [17].

The size effect is extremely important in mechanical calculations of nano and micro-size constructions. Conventional elasticity technique cannot be used to explain the size effect since there is no material length size parameter. There are different non-traditional continuity assumptions to explain the size-dependent effect. Some of these theories include modified strain change, non-local elasticity, modified stress couple theories. Eringen [16] and Eringen and Edelen [17] first addressed the non-local elasticity principle in their research. This theory is frequently used in dissection mechanics, wave distribution, fracture mechanics, beam-type structures [18–20] and plate-type structures [21–23]. According to the non-local elasticity theory, many academic studies have been conducted in recent years. Some of these are [24–29] [8-13]. Wang et al. [30] addressed the vibration and bending problem in carbon nanotube using the beam-shell relationship and nonlocal elastic structure equations. A comprehensive analytical method for solving the fourth-order differential equation related to the bending analysis of bidirectional functional grade nanobeams obtained by Eringen's nonlocal elasticity theory is presented by Nazmul and Devnath[31]. Akgöz et al.[32] investigated the thermo-elastic vibrational behavior of thick microbeams based on elastic foundation with modified double stress theory. Dastjerdi and Akgöz[33] used 3D elasticity theory together with nonlocal theory to study the static and vibrational behavior of FG circular nanoplates. Akgöz and Civalek[34] utilized the double stress theory for the static and stability analysis of single-walled carbon nanotubes applying different theories. Different method was used for the analysis of micro- or nano-scale mechanical systems under different conditions in[35]. Civalek and Kiracioglu[36] applied the discrete singular convolution method for the numerical solution of the Timoshenko beam's equation of motion. Some studies[37,38] have established a nonlocal finite element method for thin beams.

The nonlocal parameter (e_0a) captures the small-scale effects on the response of structures in nano-size; e_0 is called the nonlocal material constant, and a is the internal scale parameter. In the previous studies related to nano functionally graded materials, the nonlocal parameter is generally assumed as a constant. A conservative estimation of the nonlocal parameter $0 < e_0a < 2$ nm for single-walled carbon nanotubes is suggested by Wang[39]. Therefore, in this study, the nonlocal parameter is taken as $e_0a = 1$ nm to investigate bending analysis on the responses of functionally graded nanobeam.

In this study, bending analysis of functionally graded cantilever nanobeams as well as extreme intense loads using modified stress couple and Pseudospectral Chebyshev Method (PCM) is discussed. A system of differential equalities is obtained with early and limit conditions. PCM with known initial conditions is used to these systems of differential equalities including non-local elasticity parameter. The precision of the proposed technique was confirmed using the literature, then the outcomes were graphically shown and discussed according to the calculations obtained.

2. Theory and Formulations

The geometric fitness condition, equilibrium equations and constitutive relations of the FG nano beam in the two-dimensional plane are as follows[40,41]

$$\frac{dw}{dx} = \varphi \tag{1}$$

$$\frac{d\varphi}{dx} = -\frac{M}{E(x)I} \tag{2}$$

$$\frac{dM}{dx} = P_1\varphi + T \tag{3}$$

$$\frac{dT}{dx} = 0 \tag{4}$$

where T and M are the shear force and the bending moment, φ and w are the slope of the FG nano beam and the lateral displacement. Also, I is moment of inertia, the elasticity modulus varies corresponding to the function given in the equation $E(x)=E_1e^{-\lambda x}$ [42], here λ is inhomogeneity parameter.

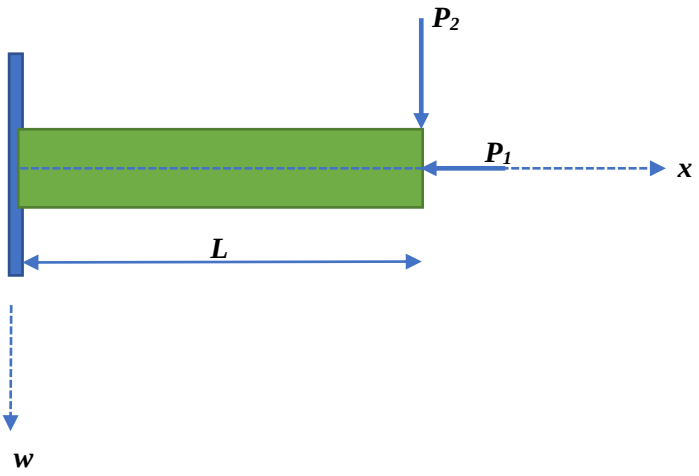

Fig. 1. Cantilever nano-beam with lateral and axial forces[32]

The final form of Eq.(2) according to the nonlocal elasticity theory takes the following form[43]

$$M - (e_0a)^2\frac{d^2M}{dx^2} = -E(x)I\frac{d^2w}{dx^2} \tag{5}$$

where a is the inner typical length, is a constant (e_0= 0.39, a=4*10^{-8} cm). Using Eq. (2), above relation takes the following form

$$M = E(x)I[1 - (e_0a)^2\frac{P_1}{E(x)I}]\frac{d\varphi}{dx} \tag{6}$$

The final form of the governing differential equations the situation is given as:[40,41]

$$\frac{d}{dx}\begin{bmatrix} w \\ \varphi \\ M \\ T \end{bmatrix} = \begin{bmatrix} 0 & 1 & 0 & 0 \\ 0 & 0 & \frac{-1}{E(x)I[1-(e_0a)^2\frac{P_1}{E(x)I}]} & 0 \\ 0 & P_1 & 0 & 1 \\ 0 & 0 & 0 & 0 \end{bmatrix}\begin{bmatrix} w \\ \varphi \\ M \\ T \end{bmatrix} \tag{7}$$

where P_1 the axial force, P_2 the side force, the inner typical length and e_0 is a constant. The primary conditions are given below;

$$w(0) = 0 \tag{8}$$

$$\varphi(0) = 0 \tag{9}$$

$$M(0) = -P_2\, L \tag{10}$$
$$T(0) = P_2 \tag{11}$$

From Eq. (7), the following expressions are obtained;

$$\frac{dw}{dx} = \varphi \tag{12}$$
$$\frac{d\varphi}{dx} = -\frac{M}{E(x)I[1-(e_0 a)^2\frac{P_1}{E(x)I}]} \tag{13}$$
$$\frac{dM}{dx} = P_1\varphi + T \tag{14}$$
$$\frac{dT}{dx} = 0 \tag{15}$$

2. Solution Procedure

This section is where PCM is applied to discretize the main equalities and boundary conditions and transform them in algebraical equalities. This model is utilized to execute the evaluation of the static performance of the FG nanobeam by reference to the work of Trefethen[44], Fornberg[45] and Gottlieb[46]. It depends on a discretization of the main equalities with respect to the spatial variable. With regard to collocation points, the initial order *(n + 1) × (n + 1)* Chebyshev differentiation matrix

$$0 = x_0 < x_1 \ldots < x_n \;\text{ with } x_j = \frac{1}{2}[1 - \cos\left(\frac{j\pi}{n}\right)] \tag{16}$$

(j = 0, 1, . . . , *n)* will be represented by *D*. First-order Chebyshev differentiation matrix D offers a very precise approximation to $V'_n(x_j), V''_n(V_j)\ldots$, simply by multiplying differential matrix with vector data:

$$\begin{bmatrix} \frac{dV_n}{dx}(x_0) \\ \frac{dV_n}{dx}(x_1) \\ \vdots \\ \frac{dV_n}{dx}(x_n) \end{bmatrix} \approx D \begin{bmatrix} V_n(x_0) \\ V_n(x_1) \\ \vdots \\ V_n(x_n) \end{bmatrix}, \quad \begin{bmatrix} \frac{d^2V_n}{dx^2}(x_0) \\ \frac{d^2V_n}{dx^2}(x_1) \\ \vdots \\ \frac{d^2V_n}{dx^2}(x_n) \end{bmatrix} \approx D^2 \begin{bmatrix} V_n(x_0) \\ V_n(x_1) \\ \vdots \\ V_n(x_n) \end{bmatrix} \tag{17}$$

Details on the calculation of the Chebyshev differentiation matrix and codes as m-files can be discovered in remarkable references, e.g. Trefethen[44].
By using the Chebyshev differential matrix, derivatives of any order can be easily discretized. The final form of Eqs. (12-15) is written in the form below:

$$L_w w = 0 \tag{18}$$

where $L_w = D - \frac{\varphi}{w}$

$$L_\varphi \varphi = 0 \tag{19}$$

where $L_\varphi = D + \dfrac{M}{\varphi\, E(x)I[1-(e_0 a)^2\dfrac{P_1}{E(x)I}]}$

$$L_M \varphi = 0 \tag{20}$$

$$L_M = D - \frac{P_1}{M}\varphi + \frac{T}{M}$$

$$L_T T = 0 \tag{21}$$

where $L_T = D$

To get the non-trivial solution, the boundary conditions (8-11) for the bending analysis are imposed on this linear system (18-21) with replacing just the initial and last row of the linear operators ($L_w; L_\varphi; L_M; L_T$) with the appropriate values and the values corresponding to the function on the right.

3. Validation of the Present Results

For the efficiency and reality of the numerical method, when the solutions are performed by taking zero instead of λ in the cantilever FG nano beam, which is taken as $E(x)=E_1e^{-\lambda x}$[42], the cantilever nano beam, which has been solved in the literature[32]will be in a homogeneous state. E_1=1 nN/m^2, e_0a=1nm, I=1 nm^4 and P_2 =1.0 nN are taken in all calculations. In Table 1, the static deviation values of the homogeneous cantilever nano beam are given by using the material properties $E(x)=E_1e^{-\lambda x}$ and taking λ=0. It has been observed that the displacement values obtained by PCM correspond exactly to the findings in the literature[32].

Table 1. Comparison of the static deflection (w) values with PCM solutions and the results in the literature [32] for a homogeneous cantilever beam

	P_2 =1.0 nN		P_2 =1.2 nN		P_2 =1.4 nN	
x	PCM	Ref. [32]	PCM	Ref. [32]	PCM	Ref. [32]
0.0	0.00017	0.00017	0.00020	0.00020	0.00024	0.00024
0.1	0.00467	0.00467	0.00561	0.00561	0.00655	0.00655
0.2	0.01846	0.01846	0.02215	0.02215	0.02585	0.02585
0.3	0.04013	0.04013	0.04816	0.04816	0.05618	0.05618
0.4	0.06828	0.06828	0.08194	0.08194	0.09560	0.09560
0.5	0.10153	0.10153	0.12183	0.12183	0.14214	0.14214
0.6	0.13846	0.13846	0.16615	0.16615	0.19384	0.19384
0.7	0.17768	0.17768	0.21322	0.21322	0.24876	0.24876
0.8	0.21780	0.21780	0.26136	0.26136	0.30492	0.30492
0.9	0.25741	0.25741	0.30890	0.30890	0.36038	0.36038
1.0	0.29513	0.29513	0.35415	0.35415	0.41318	0.41318

The tilt of the FG cantilever nanobeam and its effects on the lateral and axial forces applied to the beam are presented in Table 2. When Table 2 is analyzed, it is seen that the results in the literature are compatible with the current method.

Table 2. Comparison of the slope (φ) values for different concentrated forces with PCM solutions and the results in the literature[32]for a homogeneous cantilever beam

	P_2 =1.0 nN		P_2 =1.2 nN		P_2 =1.4 nN	
x	PCM	Ref. [32]	PCM	Ref. [32]	PCM	Ref. [32]
0.0	-0.00053	-0.00053	-0.00064	-0.00064	-0.00075	-0.00075
0.1	0.09525	0.09525	0.11431	0.11431	0.13336	0.13336
0.2	0.17895	0.17895	0.21474	0.21474	0.25052	0.25052
0.3	0.25008	0.25008	0.30010	0.30010	0.35012	0.35012
0.4	0.30822	0.30822	0.36987	0.36987	0.43151	0.43151
0.5	0.35292	0.35292	0.42350	0.42350	0.49408	0.49408

0.6	0.38372	0.38372	0.46047	0.46047	0.53721	0.53721
0.7	0.40020	0.40020	0.48023	0.48023	0.56027	0.56027
0.8	0.40189	0.40189	0.48227	0.48227	0.56264	0.56264
0.9	0.38835	0.38835	0.46603	0.46603	0.54370	0.54370
1.0	0.35915	0.35915	0.43098	0.43098	0.50281	0.50281

The bending moment of the FG cantilever nano beam and its effects on the lateral and axial forces applied to the beam are presented in Table 3. The effect of lateral and axial force on the bending moment is clearly seen when Table 3. is examined. The compatibility of the current results with the results in the literature is clearly displayed in Table 3.

Table 3. Comparison of the bending moment (M) values for different concentrated forces with PCM solutions and the results in the literature [32]for a homogeneous cantilever beam

	P_2 =1.0 nN		P_2 =1.2 nN		P_2 =1.4 nN	
x	PCM	Ref. [32]	PCM	Ref. [32]	PCM	Ref. [32]
0.0	-1,00E-05	-1,00E-05	-1,20E-05	-1,20E-05	-1,40E-05	-1,40E-05
0.1	-8,94E-06	-8,94E-06	-1,07E-05	-1,07E-05	-1,25E-05	-1,25E-05
0.2	-7,78E-06	-7,78E-06	-9,33E-06	-9,33E-06	-1,09E-06	-1,09E-06
0.3	-6,52E-06	-6,52E-06	-7,82E-06	-7,82E-06	-9,13E-06	-9,13E-06
0.4	-5,18E-06	-5,18E-06	-6,22E-06	-6,22E-06	-7,25E-06	-7,25E-06
0.5	-3,78E-06	-3,78E-06	-4,54E-07	-4,54E-07	-5,29E-06	-5,29E-06
0.6	-2,34E-06	-2,34E-06	-2,81E-06	-2,81E-06	-3,27E-06	-3,27E-06
0.7	-8,68E-08	-8,68E-08	-1,04E-06	-1,04E-06	-1,21E-06	-1,21E-06
0.8	6,14E-07	6,14E-07	7,36E-07	7,36E-07	8,59E-07	8,59E-07
0.9	2,09E-07	2,09E-07	2,51E-06	2,51E-06	2,92E-06	2,92E-06
1.0	3,54E-06	3,54E-06	4,25E-06	4,25E-06	4,96E-06	4,96E-06

4. Results and Discussion

In this study, static deflection, inclination and bending moment distributions in the beam were investigated in the static study of non-local FG nano beams subjected to end and lateral applied forces. It is assumed that the beam's modulus of elasticity changes exponentially. In addition, E_1=1 nN/m^2, e_0a=1nm, I=1 nm^4, P_1 =P_2 =1.2 nN in calculations. By applying extreme axial forces to the FG nano beam, it has been tried to obtain information about the effect of bending on its mechanical behavior. Figure 2 was created to see the effect of inhomogeneity parameter on deflection in cantilever FG nano beam subjected to end lateral and axial forces.

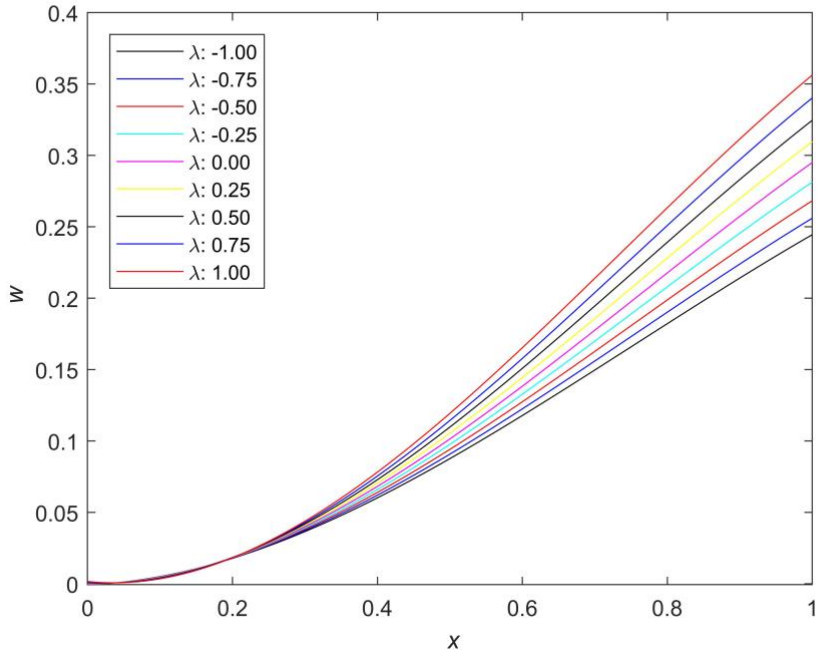

Fig. 2. Static deflection for end lateral and axial forces

When Figure 2 is examined, it is noted that the static deviation value rises with the rise in the distance from the fixed end and the static deviation rises with the rise in the inhomogeneity constraint. Figure 3 shows the impacts of end and lateral forces on the curvature of the cantilever FG nano-beam.

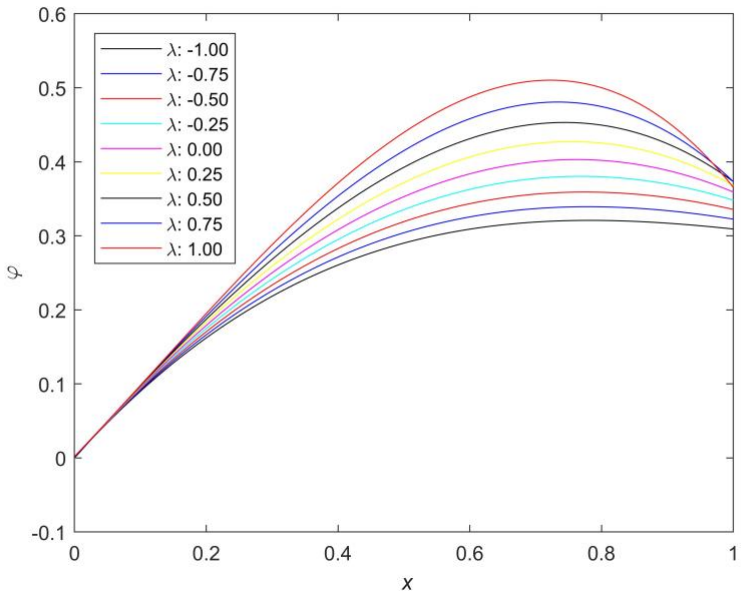

Fig. 3. Slope for end and lateral forces

Figure 3 shows the rise and decline in slope with increasing distance from the tip, emphasizing the importance of tip lateral concentrated forces. It can also be concluded that the higher values of the inhomogeneity constraint increase the slope considerably.

The impacts of end loads on the bending moment of FG cantilever nano-beams are presented in Figure 4. Again, in adding to the axial and lateral forces, the impacts of the inhomogeneity parameter on the bending moment are very clear.

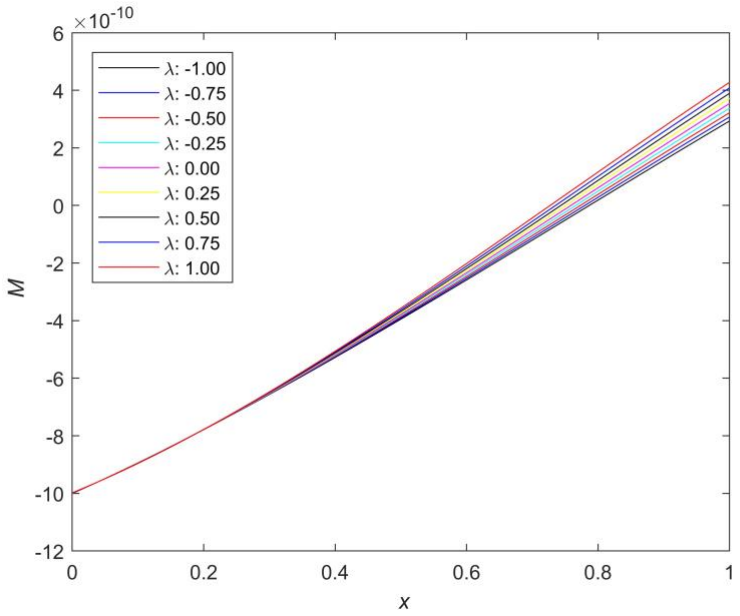

Fig. 4. Moment diagram for constant end and axial forces

5. Conclusion

In this study, it has been shown that PCM can be applied to the solution of the nonlocal primary worth problem involving homogeneous linear differential equalities. The FG nanotube was modeled as a beam with the Euler-Bernoulli theory. For the small-scale effect, the nonlocal elasticity theory is used. The results obtained and the methodology presented in this research can be used as an aid in the design and analysis of FG nanobeams. Therefore, it can be concluded:

- It has been determined that the homogeneity parameters have a strong effect on the static deflection, tilt and bending moment distribution.

- PCM has a high-level correctness rate with low computational cost due to its dense mesh structure close to the border and its rough structure towards the center points. Therefore, it can be used as a practical solution tool in solving such problems.

- It provides an effective performance when the inhomogeneity parameter is high when a functionally graded nano beam operates under the effect of end and lateral forces.

References

[1] Aydogdu, M., Taskin, V., Free vibration analysis of functionally graded beams with simply supported edges, Materials & design, 28(5), 1651-1656, 2007.

[2] Chakraborty, A., Gopalakrishnan, S., Reddy, J.N., A new beam finite element for the analysis of functionally graded materials, International journal of mechanical sciences,

45(3), 519–539, 2003.

[3] Ke, L. L., Yang, J., Kitipornchai, S., Xiang, Y., Flexural vibration and elastic buckling of a cracked Timoshenko beam made of functionally graded materials. Mechanics of Advanced Materials and Structures, 16(6), 488-502, 2009.

[4] Li, X.F., A unified approach for analyzing static and dynamic behaviors of functionally graded Timoshenko and Euler–Bernoulli beams. J Sound Vib., 318(4-5), 1210–1229, 2008.

[5] Sina, S.A., Navazi, H.M., Haddadpour, H., An analytical method for free vibration analysis of functionally graded beams, Mater Des, 30(3), 741–747, 2009.

[6] Şimşek, M., Static analysis of a functionally graded beam under a uniformly distributed load by Ritz method, Int J Eng Appl Sci., 1(3), 1–11, 2009.

[7] Şimşek, M., Dynamic analysis of an embedded microbeam carrying a moving microparticle based on the modified couple stress theory, Int J Eng Sci., 48(12), 1721–1732, 2010.

[8] Şimşek, M., Fundamental frequency analysis of functionally graded beams by using different higher-order beam theories, Nucl Eng Des., 240(4), 697–705, 2010.

[9] Şimşek, M., Vibration analysis of a functionally graded beam under a moving mass by using different beam theories, Compos Struct., 92(4), 904–917, 2010.

[10] Şimşek, M., Non-linear vibration analysis of a functionally graded Timoshenko beam under action of a moving harmonic load, Compos Struct., 92(10), 2532–2546, 2010.

[11] Şimşek, M., Kocatürk T., Akbaş Ş.D., Static bending of a functionally graded microscale Timoshenko beam based on the modified couple stress theory, Compos Struct., 95(1), 740–747, 2013.

[12] Thai, H.T., Vo, T.P., Bending and free vibration of functionally graded beams using various higher-order shear deformation beam theories, Int J Mech Sci., 62(1), 57–66, 2012.

[13] Ying, J., Lü, C.F., Chen, W.Q., Two-dimensional elasticity solutions for functionally graded beams resting on elastic foundations, Compos Struct., 84(3), 209–219, 2008.

[14] Lü, C.F., Lim, C.W., Chen, W.Q., Size-dependent elastic behavior of FGM ultra-thin films based on generalized refined theory, Int J Solids Struct., 46(5), 1176–1185, 2009.

[15] Zhong, Z., Yu, T., Analytical solution of a cantilever functionally graded beam, Compos Sci Technol., 67(3-4), 481–488, 2007.

[16] Eringen, A.C., Nonlocal polar elastic continua, Int J Eng Sci., 10(1), 1–16, 1972.

[17] Eringen, A.C., Edelen, D.G.B., On nonlocal elasticity, Int J Eng Sci., 10(3), 233–248, 1972.

[18] Aydogdu, M., A general nonlocal beam theory: its application to nanobeam bending, buckling and vibration, Phys E Low-Dimensional Syst Nanostructures, 41(9), 1651–1655, 2009.

[19] Liu, T., Hai, M., Zhao, M., Delaminating buckling model based on nonlocal Timoshenko beam theory for microwedge indentation of a film/substrate system, Eng Fract Mech., 75(17), 4909–4919, 2008.

[20] Reddy, J.N., Nonlocal theories for bending, buckling and vibration of beams, Int J Eng Sci., 45(2-8), 288–307, 2007.

[21] Narendar, S., Buckling analysis of micro-/nano-scale plates based on two-variable refined plate theory incorporating nonlocal scale effects, Compos Struct., 93(12), 3093–3103, 2011.

[22] Pradhan, S.C., Phadikar, J.K., Nonlocal elasticity theory for vibration of nanoplates, J Sound Vib., 325(1-2), 206–223, 2009.

[23] Shen, L.E., Shen, H.S., Zhang, C.L., Nonlocal plate model for nonlinear vibration of single layer graphene sheets in thermal environments, Comput Mater Sci., 48(3), 680–685, 2010.

[24] Mercan, K., Civalek, Ö., Buckling analysis of silicon carbide nanotubes (SiCNTs), Int J Eng Appl Sci., 8(2), 101–108, 2016.

[25] Mercan, K., Demir, Ç., Akgöz, B., Civalek, Ö., Coordinate transformation for sector and annular sector shaped graphene sheets on silicone matrix, Int J Eng Appl Sci., 7(2), 56–73, 2015.

[26] Mercan, K., Civalek, Ö., DSC method for buckling analysis of boron nitride nanotube (BNNT) surrounded by an elastic matrix, Compos Struct., 143(1), 300–309, 2016.

[27] Gürses, M., Akgöz, B., Civalek, Ö., Mathematical modeling of vibration problem of nano-sized annular sector plates using the nonlocal continuum theory via eight-node discrete singular convolution transformation, Appl Math Comput., 219(6), 3226–3340, 2012.

[28] Yaylı, M.Ö., Buckling analysis of a rotationally restrained single walled carbon nanotube embedded in an elastic medium using nonlocal elasticity, Int J Eng Appl Sci., 8(2), 40–50, 2016.

[29] Yaylı, M.Ö., An analytical solution for free vibrations of a cantilever nanobeam with a spring mass system, Int J Eng Appl Sci., 7(4), 10–18, 2016.

[30] Wang, Q., Shindo, Y., Nonlocal continuum models for carbon nanotubes subjected to static loading, J Mech Mater Struct., 1(4), 663–680, 2006.

[31] Nazmul, I.M., Devnath, I., Exact analytical solutions for bending of bi-directional functionally graded nanobeams by the nonlocal beam theory using the Laplace transform, Forces Mech., 1(1), 100002, 2020.

[32] Akgöz, B., Civalek, Ö., Vibrational characteristics of embedded microbeams lying on a two-parameter elastic foundation in thermal environment, Compos Part B Eng., 150(1), 68–77, 2018.

[33] Dastjerdi, S., Akgöz, B., New static and dynamic analyses of macro and nano FGM plates using exact three-dimensional elasticity in thermal environment, Compos Struct., 192(1), 626–641, 2018.

[34] Akgöz, B., Civalek, Ö., Investigation of size effects on static response of single-walled carbon nanotubes based on strain gradient elasticity, Int J Comput Methods, 9(2), 1240032, 2012.

[35] Mercan, K., Numanoglu, H.M., Akgöz, B., Demir, C., Civalek, Ö., Higher-order continuum theories for buckling response of silicon carbide nanowires (SiCNWs) on elastic matrix, Arch Appl Mech., 87(11), 1797–1814, 2017.

[36] Civalek, Ö., Kiracioglu, O., Free vibration analysis of Timoshenko beams by DSC method, Int j Numer Method Biomed Eng., 26(12), 1890–1898, 2010.

[37] Sciarra, F.M.D., Finite element modelling of nonlocal beams, Phys E., 59(1), 144–149, 2014.

[38] Nguyen, N.T., Kim, N.I., Lee, J., Mixed finite element analysis of nonlocal Euler–Bernoulli nanobeams, Finite Elem Anal Des., 106(1), 65–72, 2015.

[39] Wang, Q., Wave propagation in carbon nanotubes via nonlocal continuum mechanics, J Appl Phys., 98(12), 124301, 2005.

[40] Artan, R., Tepe, A., The initial values method for buckling of nonlocal bars with application in nanotechnology, Eur J Mech., 27(3), 469–477, 2008.

[41] Yaylı, M.Ö., Kandemir, S.Y., Bending analysis of a cantilever Nanobeam with end forces by Laplace transform, Int J Eng Appl Sci., 9(2), 103–111, 2017.

[42] Nihat, C., Kurgan, N., Hassan, A.H.A., Buckling Analysis of Functionally Graded Plates Using Finite Element Analysis, Int J Eng Appl Sci., 12(1), 43–56, 2020.

[43] Peddieson, J., Buchanan, G.R., McNitt, R.P., Application of nonlocal continuum models to nanotechnology, Int J Eng Sci., 41(3-5), 305–312, 2003.

[44] Trefethen, L.N., Spectral methods in MATLAB, volume 10 of Software, Environments, and Tools, Soc Ind Appl Math (SIAM), Philadelphia, PA 2000.

[45] Fornberg, B., A practical guide to pseudospectral methods, Cambridge university press, 1998.

[46] Gottlieb, D., The stability of pseudospectral-Chebyshev methods, Math Comput., 36(153), 107–118, 1981.

International Journal of Engineering & Applied Sciences (IJEAS)
Vol.13, Issue 4 (2021) 189-200
http://dx.doi.org/10.24107/ijeas.1041504
Int J Eng Appl Sci 13(4) (2021) 189-200

Comparative Stability Analysis of Boron Nitride Nanotube using MD Simulation and Nonlocal Elasticity Theory

Kadir Mercan [a], Ömer Civalek [b]*

[a] Department of Civil Engineering, Faculty of Architecture-Engineering, Burdur Mehmet Akif Ersoy University
[b] Research Center for Interneural Computing University, China Medical University, Taichung, Taiwan
[*]E-mail address: kmercan@mehmetakif.edu.tr [a*], civalek@yahoo.com [b]

ORCID numbers of authors:
0000-0003-3657-6274[a], 0000-0003-1907-9479[b]*

Received date: 24.12.2021
Accepted date: 31.12.2021

Abstract

Boron Nitride Nanotube (BNNT) is a promising nano sized structure with superior electrical, physical, and mechanical properties comparing to Carbon nanotube. Higher Young's modulus, oxidation resistance, hardness, corrosion resistance, durability in high temperature, piezoelectric and pyroelectric characteristics are some featured characteristics of BNNT. In this paper the critical buckling load of Boron Nitride Nanotube is investigated. Two different method is used. First Eringen's nonlocal elasticity theory is employed to obtain size-dependent critical buckling loads. Then, LAMMPS software is used to simulate molecular dynamics and obtain critical buckling loads. Zigzag (5,5) BNNT with 400 atoms is examined into MD simulation analyzes.

Keywords: BNNT, Nonlocal Elasticity Theory, LAMMPS, MD Simulation.

1. Introduction

Since more than a decade, nanoscience has gained much popularity parallel to advances in technology and shrink in size of electronic devices. Starting from 1991 by Iijima's discovery of carbon nanotube (CNT) [1], the interest to nanotubes and nano sized structures increased substantially. CNT was the first discovered nanotube and attracted great attention [2], but this outstanding nano sized material had some weak properties comparing to discovered and developed nanotubes and nano sized materials latterly. The main reason to the substantial increase in the interest and usage of nanomaterials was the extreme mechanical, electrical, and thermal properties of materials comparing to conventional materials used while these materials emerged around thirty years ago. Boron Nitride Nanotube (BNNT), Silicon Carbide Nanotube (SiCNT) are some newer types of nanotube with some advantages and disadvantages compared to CNT [3]. Comparing the mechanical properties of these three types of nanotube by checking its Young's modulus BNNT become prominent with 1.8 TPa while CNT perform 1 TPa, and SiCNT around 0.62 TPa [4, 5]. BNNT has a wide usage area since their superior electrical and mechanical properties and physical properties. Ferreira *et al.* investigated the BNNT's drug delivery capacity as nanovectors to kill cancer cells using magnetohyperthermia therapy by targeting nanbotubes to tumor areas. Results demonstrated that magnetite nanoparticles are linked to the nanotubes while coercivity and magnetization were stable after fusion to nanotube [6]. Khaleghian and Azarakhshi studied (9,9) BNNT's quantum mechanical investigation of

geometrical structure and dynamic behavior [7]. Vedaei and Nadimi studied the gas sensing properties of BNNT toward NO_2, O_2 and H_2O [8]. Ashraf *et al.* demonstrated the catalytic capabilities Cr-BNNT to oxidation of CN molecule [9]. Li *et al.* analized the stability of MoS2 sheet under uniaxial compression using MD simulation [10]. Yang *et al.* studied the critical fracture properties of arsene using MD simulation [11]. Jiang *et al.* studied the stability of blue phosphorus nanotube using MD simulation [12]. Also, Ajori *et al.* used MD simulation technique to study the buckling behavior x-graphyne based single- and multi-walled nanotubes [13]. More recently, Zhang and Zhou studied the buckling behavior of boron nanotube which compose only from boron atoms[14]. To analyze nanotubes by taking the size effect into consideration, many methods have been used such as couple stress theory [15, 16], strain gradient theory, nonlocal elasticity theory [17-22], surface elasticity theory, nonlocal surface elasticity theory [23], DSC method [24-29]. Furthermore, many research have been done studying vibration behavior of nanostructures [30-33].

2. Boron Nitride Nanotube (BNNT)

Boron Nitride Nanotube (BNNT) is not the first nanotube discovered but it is one of the most promising with superior electrical, mechanical and physical properties compared to CNT. The structure of Boron Nitride sheet is demonstrated in Figure 1. In Figure 1, blue spheres represent Boron atoms while anthracite spheres represent Nitrogen atoms. Boron and Nitrogen atoms are bonded each other in hexagonal form.

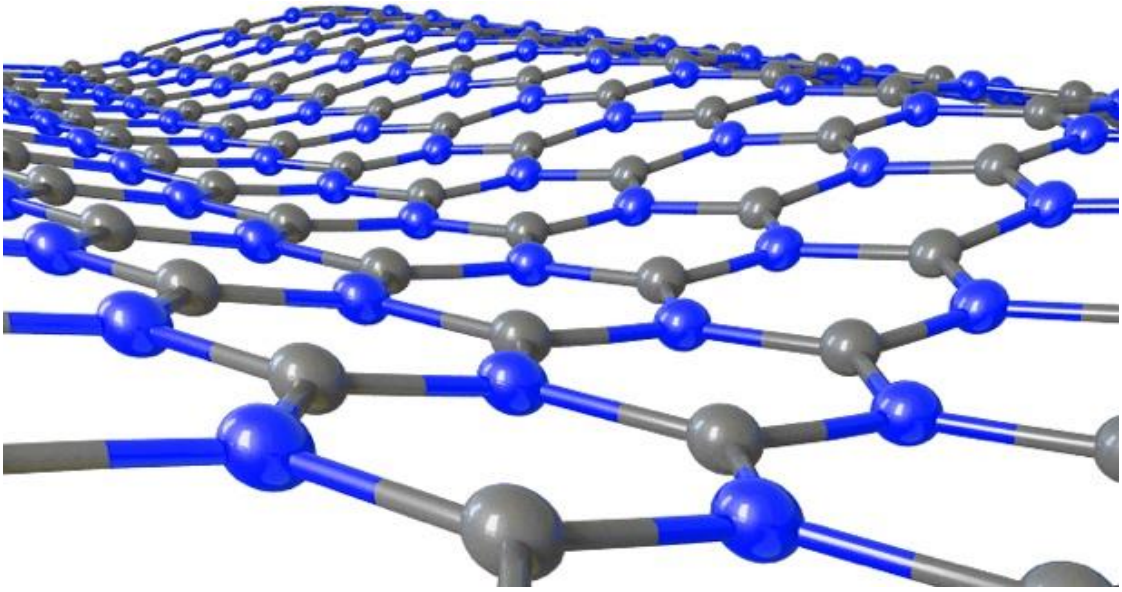

Fig. 1. Structure of Boron Nitride Sheet

BNNTs can be obtained simply by rolling Boron Nitride sheets as it is demonstrated in Figure 2. The rolling side of nanosheet determine the armchair, zigzag, and chiral structure of nanotube [34].

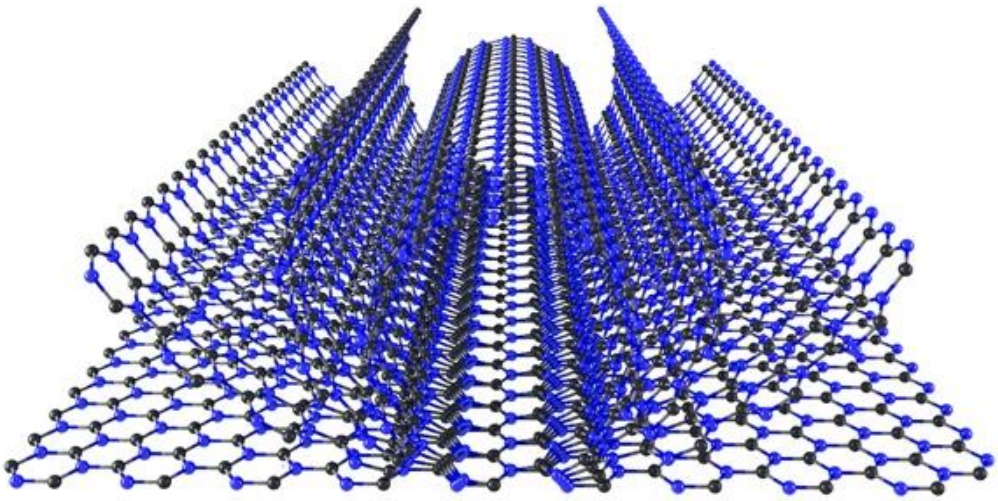

Fig. 2. Rolling Boron Nitride sheet to obtain Boron Nitride Nanotube

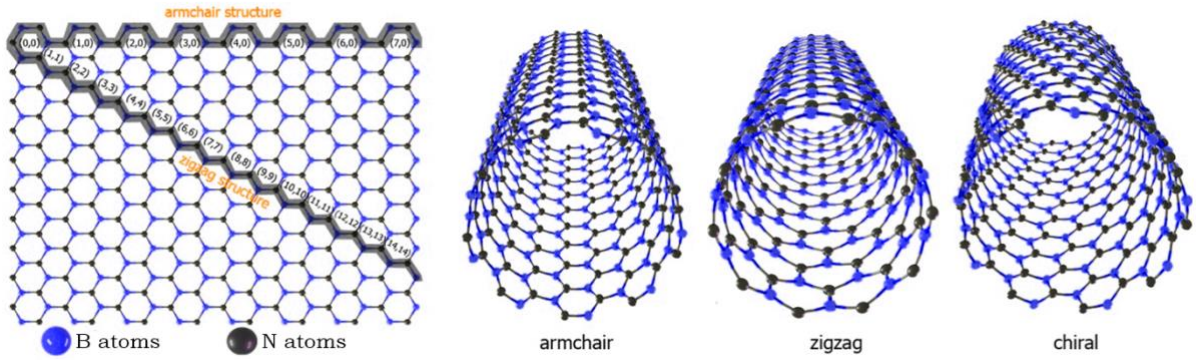

Fig. 3. Armchair, zigzag, and chiral Boron Nitride Nanotube

As it can be seen from Fig. (3) (m, n) represent the zigzag and armchair atom numbers. The rolling side of nanosheet determine the structure of nanotube. Armchair, zigzag, and chiral nanotubes have different physical, mechanical, and electrical properties which are neglected in continuum mechanic. On the other hand, these different properties are taken into consideration in MD simulation methods.

3. Nonlocal Elasticity Theory for Nanotubes

Due to the size in nanometer scale in nanotubes, classical continuum mechanic theories perform insufficient in very small sized analyzes. In this paper, Eringen's nonlocal theory is used to take the size effect into consideration [35]. The nonlocal constitutive formulation is [36]

$$[1-(e_0a)^2\nabla^2]\sigma_{ij} = C_{ijkl} \tag{1}$$

Where σ_{ij} represent the nonlocal stress tensor, $C_{ijkl}(x')$ is the classical (Cauchy) or local stress tensor at any x' point in the body. e_0a is the nonlocal parameter constant which depends on the material used in a range. Displacement components of a Euler-Bernoulli beam theory can be represented as

$$u_1(x,z) = -z\frac{\mathrm{d}w(x)}{\mathrm{d}x} \tag{2}$$

$$u_2(x,z) = 0 \tag{3}$$

$$u_3(x,z) = w(x) \tag{4}$$

In above equations u_1, u_2, u_3 are the $x-$, $y-$ and $z-$ of the displacement vector components for x,y,z axes respectively. w is the transverse displacements. The strain-displacement equations can be stated as [37]

$$\varepsilon_{11} = \frac{du}{dx} = -z\frac{d^2w}{dx^2}\ ,\ \varepsilon_{22} = \varepsilon_{33} = \varepsilon_{12} = \varepsilon_{13} = \varepsilon_{23} = 0 \tag{5}$$

In Eq.(5) ε_{11} represent the axial strain. The stress-strain equations can be expressed as

$$\sigma_{11} = -Ez\frac{d^2w}{dx^2}\ ,\ \sigma_{22} = \sigma_{33} = \tau_{12} = \tau_{13} = \tau_{23} = 0 \tag{6}$$

According to Eqs. (2-4), the nonlocal stress-strain equations

$$\sigma_{11} - \mu\frac{d^2\sigma_{11}}{dx^2} = E\varepsilon_{11},\ \sigma_{22} = 0,\ \sigma_{33} = 0 \ \text{ and } \ \tau_{12} = \tau_{21} = 0,\ \tau_{13} = \tau_{31} = 0,\ \tau_{23} = \tau_{32} = 0 \tag{7}$$

Minimum total potential energy principle is used to derive governing equations.

$$\delta\prod = \delta U - \delta W = 0 \tag{8}$$

$$\delta U = \int_0^L\int_A \left(\sigma_{11}\delta\varepsilon_{11}\right)dAdx = \int_0^L\int_A \left(\sigma_{11}\left(-z\frac{d^2\delta w}{dx^2}\right)\right)dAdx \tag{9}$$

Where δU is strain energy. The work can expressed as follows:

$$\delta W = \int_0^L \left(P\frac{dw}{dx}\delta\frac{dw}{dx} + qw(x)\right)dx \tag{10}$$

$$\int_0^L \left(-M \frac{d^2 \delta w}{dx^2} \right) dx - \int_0^L \left(P \frac{dw}{dx} \delta \frac{dw}{dx} + qw(x) \right) dx = 0 \tag{11}$$

Where P is axial force. The buckling equation and boundary conditions can be expressed as

$$\delta \mathrm{w} : \frac{dw}{dx} \left(P \frac{dw}{dx} \right) - q = \frac{d^2 M}{dx^2} \tag{12}$$

$$\frac{dM}{dx} - P \frac{dw}{dx} = 0 \quad \text{and} \quad M = 0 \tag{13}$$

$$M - \mu \frac{d^2 M}{dx^2} = -EI \frac{d^2 w}{dx^2} \tag{14}$$

Substituting Eq. (12) into Eq. (14), the moment resultant can be obtained as follows

$$M = \mu \left(\frac{d}{dx} \left(P \frac{dw}{dx} \right) - q \right) - EI \frac{d^2 w}{dx^2} \tag{15}$$

$$\delta \mathrm{w} : \frac{d^2}{dx^2} \left(-EI \frac{d^2 w}{dx^2} \right) + \mu \frac{d^2}{dx^2} \left(\frac{d}{dx} \left(P \frac{dw}{dx} \right) - q \right) + q - \frac{d}{dx} \left(P \frac{dw}{dx} \right) = 0 \tag{16}$$

Nonlocal boundary conditions are as follows [23]

$$\frac{d}{dx} \left(\mu \left(\frac{d}{dx} \left(P \frac{dw}{dx} \right) - q \right) - EI \frac{d^2 w}{dx^2} \right) - P \frac{dw}{dx} = 0 \tag{17}$$

$$\mu \left(\frac{d}{dx} \left(P \frac{dw}{dx} \right) - q \right) - EI \frac{d^2 w}{dx^2} = 0 \tag{18}$$

For a nanobeam resting on double parameter Pasternak foundation

$$p(x) = k_w w - k_p \frac{d^2 w}{dx^2} \tag{19}$$

In Eq. (19) k_w and k_p stand for double parameter foundation constants [38]. Subscript w and p represent Winkler and Pasternak respectively. By taking these two constant zero, the foundation effect would be neglected [39]. μ is the nonlocal parameter.

$$\left(-EI + P\mu - k_p \mu \right) \frac{d^4 w}{dx^2} + \left(k_w \mu - P + k_p \right) \frac{d^2 w}{dx^2} - k_w w = 0 \tag{20}$$

The critical buckling load for a nanobeam resting on two parameter foundation including nonlocal size effect can be stated as follows:

$$P(n)=\frac{(\overline{EI}-k_p\mu)\left(\frac{n\pi}{L}\right)^4+(k_w\mu+k_p)\left(\frac{n\pi}{L}\right)^2+k_w}{\mu\left(\frac{n\pi}{L}\right)^4+\left(\frac{n\pi}{L}\right)^2} \tag{21}$$

The real view and its continuum model of BNNT is demonstrated in Fig. 4. As it can be seen from the bottom of Fig. 4 the continuum model of BNNT have no structural details. Modeled structure can be seen as a standard tube. The effect of armchair, zigzag, or chiral structure can be defined to the model only by determining the material properties differently.

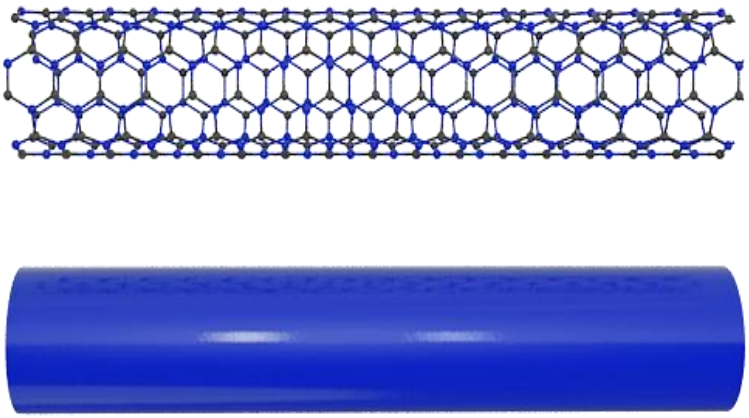

Fig. 4. Real view (top) and continuum model (bottom) of BNNT

4. Molecular Dynamics for Nanotubes

Zigzag, armchair, and chiral structures details of nanotube have key role on molecular dynamic simulation. The chiral indices of nanotube are represented as (m, n). In this paper the chiral structure of BNNT is analyzed. Modeling the structure for MD simulation was done using Visual Molecular Dynamics (VMD). After modeling the structure, obtained data is implemented to LAMMPS software [40]. LAMMPS is commonly used to simulate the molecular dynamics and perform interactions between objects. Hence Tersoff potential is used to model the intercommunication between atoms of BNNT structure [41-44].

$$2E=\sum_i \quad \sum_{j\neq 1} f_c(r_{ij}) \quad \left(f_T(r_{ij})+b_{ij}f_E(r_{ij})\right) \tag{22}$$

Where

$$f_T(r\ )=Ae^{(-\lambda_1 r)} \tag{23}$$

$$f_E(r\ )=-Be^{(-\lambda_2 r)} \tag{24}$$

$$f_C(r\ ) = \begin{cases} 1 & : r < R - D \\ 0.5 - 0.5sin\left(\frac{\pi}{2}\left(\frac{r-D}{D}\right)\right) & : R - D < r < R + D \\ 0 & : r > R + D \end{cases} \quad (25)$$

$$b_{ij} = \sqrt[2n]{\frac{1}{1+\beta^n \xi_{ij}^n}} \quad (26)$$

$$\xi_{ij} = \sum_{k \neq i,j} f_C(r_{ij}) g(\theta_{ijk})\, e^{\lambda_3^m (r_{ij} - r_{ik})^m} \quad (27)$$

$$g(\theta) = \gamma_{ijk}\left(1 + \frac{c^2}{d^2} - \frac{c^2}{d^2 + (cos\theta - cos\theta_0)^2}\right) \quad (28)$$

In above equations i,j and k represent the atom numbers, θ is the angle between atoms, r is the distance between Boron and Nitrogen atoms. Moreover, f_T act in place of a two-body term, f_C represent cutoff term while f_E stand for three-body interactions.

4. Numerical Results

In this section the comparative buckling analysis of BNNT using Eringen's nonlocal elasticity theory and MD simulation is presented. Zigzag (5,5) BNNT is examined with 400 atoms. The length and diameter of nanotube is variable with ratio from 0 to 0.1. Size dependent continuum mechanic results in harmony with our previous studies [45-56] and MD simulation results.

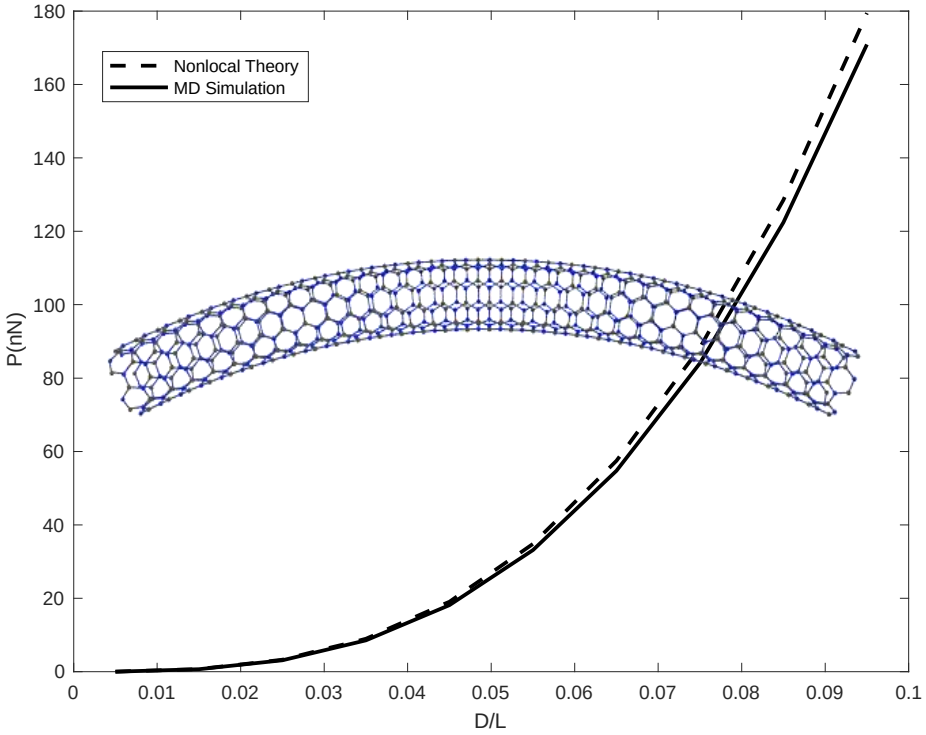

Fig. 5. Critical buckling load of BNNT

As it is seen from Figure 5, the critical buckling load of BNNT rise with increase in diameter to length ratio. The buckled form of BNNT is demonstrated in Fig. (5). As the critical buckling load is investigated, mode number n is equal to 1.

5. Conclusions

Boron Nitride Nanotube (BNNT) come forward in the great variety of nanotubes with higher mechanical resistance, oxidation resistance, hardness, corrosion resistance, durability in high temperature, piezoelectric and pyroelectric. The critical buckling load of Boron Nitride Nanotube is investigated using two different methods. Eringen's nonlocal elasticity theory is employed to obtain size-dependent critical buckling loads. LAMMPS software is used to simulate molecular dynamics. The length and diameter of nanotube is selected with ratio from 0 to 0.1. For lower D/L ratio, the critical buckling load stay low while the critical buckling load get dramatically higher for high D/L ratio. To conclude, MD simulation perform better in case of stability comparing to size-effective continuum mechanic as MD simulation has the opportunity to model and simulate imperfect nanotubes with different properties.

References

[1] Iijima, S., Helical microtubules of graphitic carbon. *Nature*, 354(6348), 56, 1991.

[2] Demir, C., Mercan, K., Numanoglu, H.M., Civalek, O., Bending Response of Nanobeams Resting on Elastic Foundation. *Journal of Applied and Computational Mechanics*, 4(2), 105-114, 2018.

[3] Mercan, K., Civalek, O., DSC method for buckling analysis of boron nitride nanotube (BNNT) surrounded by an elastic matrix. *Composite Structures*, 143, 300-309, 2016.

[4] Mercan, K., Civalek, Ö., Buckling analysis of Silicon carbide nanotubes (SiCNTs) with surface effect and nonlocal elasticity using the method of HDQ. *Composites Part B: Engineering*, 114, 34-45, 2017.

[5] Numanoglu, H.M., Mercan, K., Civalek, O., Finite element model and size-dependent stability analysis of boron nitride and silicon carbide nanowires/nanotubes. *Scientia Iranica*, 26(4), 2079-2099, 2019.

[6] Ferreira, T.H., Faria, J.A.Q.A., Gonzalez, I.J., Outon, L.E.F., Macedo, W.A.A., Gomes, D.A., Sousa, E.M.B., BNNT/Fe3O4 System as an Efficient Tool for Magnetohyperthermia Therapy. *Journal of Nanoscience and Nanotechnology*, 18(10), 6746-6755, 2018.

[7] Khaleghian, M., Azarakhshi, F., Quantum Mechanical Investigation of Geometrical Structure and Dynamic Behavior of h-BNNT (9,9-5) and h-AlNNT (9,9-5)Single-Walled Nanotubes: NBO Analysis. *Letters in Organic Chemistry*, 16(9), 705-717, 2019.

[8] Vedaei, S.S., Nadimi, E., Gas sensing properties of CNT-BNNT-CNT nanostructures: A first principles study. *Applied Surface Science*, 470, 933-942, 2019.

[9] Ashraf, M.A., Liu, Z., Najafi, M., DFT Study of CN Oxidation (CN+1/2O(2) -> OCN) on the Surfaces of Chromium-Doped Nanotubes (Cr-CNT (8, 0) and Cr-BNNT (8,0)). *Russian Journal of Physical Chemistry B*, 14(2), 217-221, 2020.

[10] Li, Y., Chen, P.J., Zhang, C., Peng, J., Gao, F., Liu, H., Molecular dynamics simulation on the buckling of single-layer MoS2 sheet with defects under uniaxial compression. *Computational Materials Science*, 162, 116-123, 2019.

[11] Yang, B., Li, M.D., Wang, J.Y., Zhang, J.C., Liao, D.M., Yue, Y.N., Critical fracture properties of puckered and buckled arsenenes by molecular dynamics simulations. *Physical Chemistry Chemical Physics*, 21(23), 12372-12379, 2019.

[12] Jiang, S.P., Wu, H.L., Kou, L.Z., Tang, C., Wang, C.Y., Chen, C.F., Buckling of blue phosphorus nanotubes under axial compression: Insights from molecular dynamics simulations. *Journal of Applied Physics*, 127(1), 2020.

[13] Ajori, S., Boroushak, S.H., Hassani, R., Ansari, R., A molecular dynamics study on the buckling behavior of x-graphyne based single- and multi-walled nanotubes. *Computational Materials Science*, 191, 2021.

[14] Zhang, J., Zhou, J.L., Buckling of boron nanotubes under axial compression: Insights from molecular mechanics and continuum mechanics. *Physica E-Low-Dimensional Systems & Nanostructures*, 127, 2021.

[15] Mercan, K., Emsen, E., Civalek, O., Effect of silicon dioxide substrate on buckling behavior of Zinc Oxide nanotubes via size-dependent continuum theories. *Composite Structures*, 218, 130-141, 2019.

[16] Arefi, M., Firouzeh, S., Bidgoli, E.M.R., Civalek, O., Analysis of porous micro -plates reinforced with FG-GNPs based on Reddy plate theory. *Composite Structures*, 247, 2020.

[17] Dastjerdi, S., Akgoz, B., Civalek, O., On the effect of viscoelasticity on behavior of gyroscopes. *International Journal of Engineering Science*, 149, 2020.

[18] Yayli, M.Ö., Torsional vibration analysis of nanorods with elastic torsional restraints using non-local elasticity theory. *Micro & Nano Letters*, 13(5), 595-599, 2018.

[19] Yayli, M.O., Cercevik, A.E., Axial vibration analysis of cracked nanorods with arbitrary boundary conditions. *Journal of Vibroengineering*, 17(6), 2907-2921, 2015.

[20] Civalek, O., Uzun, B., Yayli, M.O., Stability analysis of nanobeams placed in electromagnetic field using a finite element method. *Arabian Journal of Geosciences*, 13(21), 2020.

[21] Uzun, B., Yaylı, M.Ö., Nonlocal vibration analysis of Ti-6Al-4V/ZrO2 functionally graded nanobeam on elastic matrix. *Arabian Journal of Geosciences*, 13(4), 155, 2020.

[22] Uzun, B., Yayli, M.O., Deliktas, B., Free vibration of FG nanobeam using a finite-element method. *Micro & Nano Letters*, 15(1), 35-40, 2020.

[23] Mercan, K., Numanoglu, H.M., Akgoz, B., Demir, C., Civalek, O., Higher-order continuum theories for buckling response of silicon carbide nanowires (SiCNWs) on elastic matrix. *Archive of Applied Mechanics*, 87(11), 1797-1814, 2017.

[24] Civalek, Ö., Kiracioglu, O., Free vibration analysis of Timoshenko beams by DSC method. *International Journal for Numerical Methods in Biomedical Engineering*, 26(12), 1890-1898, 2010.

[25] Demir, C., Mercan, K., Civalek, O., Determination of critical buckling loads of isotropic, FGM and laminated truncated conical panel. *Composites Part B-Engineering*, 94, 1-10, 2016.

[26] Ersoy, H., Mercan, K., Civalek, O., Frequencies of FGM shells and annular plates by the methods of discrete singular convolution and differential quadrature methods. *Composite Structures*, 183, 7-20, 2018.

[27] Mercan, K., Baltacioglu, A.K., Civalek, O., Free vibration of laminated and FGM/CNT composites annular thick plates with shear deformation by discrete singular convolution method. *Composite Structures*, 186, 139-153, 2018.

[28] Mercan, K., Ebrahimi, F., Civalek, O., Vibration of angle-ply laminated composite circular and annular plates. *Steel and Composite Structures*, 34(1), 141-154, 2020.

[29] Mercan, K., Demir, Ç., Civalek, Ö., Vibration analysis of FG cylindrical shells with power-law index using discrete singular convolution technique. *Curved and Layered Structures*, 3(1), 2016.

[30] Hadji, L., Avcar, M., Civalek, Ö., An analytical solution for the free vibration of FG nanoplates. *Journal of the Brazilian Society of Mechanical Sciences and Engineering*, 43(9), 418, 2021.

[31] Civalek, O., Avcar, M., Free vibration and buckling analyses of CNT reinforced laminated non-rectangular plates by discrete singular convolution method. *Engineering with Computers*, 2020.

[32] Avcar, M., Hadji, L., Civalek, Ö., Natural frequency analysis of sigmoid functionally graded sandwich beams in the framework of high order shear deformation theory. *Composite Structures*, 276, 114564, 2021.

[33] Hadji, L., Avcar, M., Nonlocal free vibration analysis of porous FG nanobeams using hyperbolic shear deformation beam theory. *Advances in Nano Research*, 10(3), 281-293, 2021.

[34] Rubio, A., Corkill, J.L., Cohen, M.L., Theory of graphitic boron nitride nanotubes. *Physical Review B*, 49(7), 5081-5084, 1994.

[35] Eringen, A.C., On Differential-Equations of Nonlocal Elasticity and Solutions of Screw Dislocation and Surface-Waves. *Journal of Applied Physics*, 54(9), 4703-4710, 1983.

[36] Asghari, M., Kahrobaiyan, M.H., Ahmadian, M.T., A nonlinear Timoshenko beam formulation based on the modified couple stress theory. *International Journal of Engineering Science*, 48(12), 1749-1761, 2010.

[37] Akbas, S.D., Mercan, K., Civalek, O., Post-buckling analysis of aorta artery under axial compression loads. *Advances in Nano Research*, 8(3), 255-264, 2020.

[38] Uzun, B., Civalek, Ö., Yaylı, M.Ö., Vibration of FG nano-sized beams embedded in Winkler elastic foundation and with various boundary conditions. *Mechanics Based Design of Structures and Machines*, 1-20, 2020.

[39] Demir, C., Akgoz, B., Erdinc, M.C., Mercan, K., Civalek, O., Free vibration analysis of graphene sheets on elastic matrix. *Journal of the Faculty of Engineering and Architecture of Gazi University*, 32(2), 551-562, 2017.

[40] Thompson, A.P., Aktulga, H.M., Berger, R., Bolintineanu, D.S., Brown, W.M., Crozier, P.S., in 't Veld, P.J., Kohlmeyer, A., Moore, S.G., Nguyen, T.D., Shan, R., Stevens, M.J., Tranchida, J., Trott, C., Plimpton, S.J., LAMMPS - a flexible simulation tool for particle-based materials modeling at the atomic, meso, and continuum scales. *Computer Physics Communications*, 271, 108171, 2022.

[41] Sevik, C., Kinaci, A., Haskins, J.B., Cagin, T., Characterization of thermal transport in low-dimensional boron nitride nanostructures. *Physical Review B*, 84(8), 2011.

[42] Tersoff, J., Modeling solid-state chemistry: Interatomic potentials for multicomponent systems. *Physical Review B*, 39(8), 5566-5568, 1989.

[43] Zeighampour, H., Beni, Y., Electromechanical buckling analysis of boron nitride nanotube using molecular dynamic simulation. *Chinese Journal of Physics*, 67, 212-221, 2020.

[44] Zeighampour, H., Beni, Y.T., Buckling analysis of boron nitride nanotube with and without defect using molecular dynamic simulation. *Molecular Simulation*, 46(4), 279-288, 2020.

[45] Mercan, K., Demir, Ç., Akgöz, B., Civalek, Ö., Coordinate Transformation for Sector and Annular Sector Shaped Graphene Sheets on Silicone Matrix, *International Journal of Engineering and Applied Sciences*, 7(2), 56-73, 2015.

[46] Mercan, K. , Civalek, Ö., Buckling Analysis of Silicon Carbide Nanotubes (SiCNTs), *International Journal of Engineering and Applied Sciences*, 8(2), 101-108, 2016.

[47] Emsen, E., Mercan, K., Akgöz, B., Civalek, Ö., Modal analysis of tapered beam-column embedded in winkler elastic foundation, *International Journal of Engineering and Applied Sciences*, 7(1), 1-11, 2015.

[48] Akgöz, B. , Mercan, K. , Demir, Ç., Civalek, Ö., Static Analysis of Beams on Elastic Foundation by the Method of Discrete Singular Convolution, *International Journal of Engineering and Applied Sciences*, 8(3), 67-73, 2016.

[49] Mercan, K., Akgöz, B., Demir, Ç., Civalek, Ö., Frequencies Values of Orthotropic Composite Circular and Annular Plates, *International Journal of Engineering and Applied Sciences*, 9(2), 55-65, 2017.

[50] Numanoglu, H.M. , Mercan, K., Civalek, Ö., Frequency and Mode Shapes of Au Nanowires Using the Continuous Beam Models, *International Journal of Engineering and Applied Sciences*, 9 (1) , 55-61, 2017.

[51] Civalek, O., Numanoglu, H.M., Mercan, K., Finite Element Model and Size Dependent Stability Analysis of Boron Nitride and Silicon Carbide Nanowires/Nanotubes, *Scientia Iranica*, 26(Issue 4: Special Issue Dedicated to Professor Abolhassan Vafai), 2079-2099. 2019.

[52] Mercan, K., A Comparative Buckling Analysis of Silicon Carbide Nanotube and Boron Nitride Nanotube, *International Journal of Engineering and Applied Sciences*, 8(4) , 99-107, 2016.

[53] Mercan, K., Demir, Ç., Ersoy, H., Civalek, Ö., The effects of thickness on frequency values for rotating circular shells, *International Journal of Engineering and Applied Sciences*, 8(1), 26-37, 2016.

[54] Mercan, K., Civalek, Ö., Modal Analysis of Micro and Nanowires Using Finite Element Softwares, *International Journal of Engineering and Applied Sciences*, 10(4), 291-304, 2019.

[55] Mercan, K., Civalek, Ö., Comparison of small scale effect theories for buckling analysis of nanobeams, *International Journal of Engineering and Applied Sciences*, 9(3) , 87-97, 2017.

[56] Mercan, K., Aydoğdu, İ., Civalek, Ö., Discrete Singular Convolution and Differential Quadrature Method for Buckling Analysis of Laminated Composite Plates, *International Journal of Engineering and Applied Sciences* , 8(4) , 66-74, 2016.